NBS TECHNICAL NOTE 1050

U.S. DEPARTMENT OF COMMERCE / National Bureau of Standards

Backscatter Signature Simulations

NBS TECHNICAL PUBLICATIONS

PERIODICALS

JOURNAL OF RESEARCH—The Journal of Research of the National Bureau of Standards reports NBS research and development in those disciplines of the physical and engineering sciences in which the Bureau is active. These include physics, chemistry, engineering, mathematics, and computer sciences. Papers cover a broad range of subjects, with major emphasis on measurement methodology and the basic technology underlying standardization. Also included from time to time are survey articles on topics closely related to the Bureau's technical and scientific programs. As a special service to subscribers each issue contains complete citations to all recent Bureau publications in both NBS and non-NBS media. Issued six times a year. Annual subscription: domestic $16; foreign $20. Single copy, $3.75 domestic; $4.70 foreign.

NOTE: The Journal was formerly published in two sections: Section A "Physics and Chemistry" and Section B "Mathematical Sciences."

DIMENSIONS/NBS—This monthly magazine is published to inform scientists, engineers, business and industry leaders, teachers, students, and consumers of the latest advances in science and technology, with primary emphasis on work at NBS. The magazine highlights and reviews such issues as energy research, fire protection, building technology, metric conversion, pollution abatement, health and safety, and consumer product performance. In addition, it reports the results of Bureau programs in measurement standards and techniques, properties of matter and materials, engineering standards and services, instrumentation, and automatic data processing. Annual subscription: domestic $11; foreign $13.75.

NONPERIODICALS

Monographs—Major contributions to the technical literature on various subjects related to the Bureau's scientific and technical activities.

Handbooks—Recommended codes of engineering and industrial practice (including safety codes) developed in cooperation with interested industries, professional organizations, and regulatory bodies.

Special Publications—Include proceedings of conferences sponsored by NBS, NBS annual reports, and other special publications appropriate to this grouping such as wall charts, pocket cards, and bibliographies.

Applied Mathematics Series—Mathematical tables, manuals, and studies of special interest to physicists, engineers, chemists, biologists, mathematicians, computer programmers, and others engaged in scientific and technical work.

National Standard Reference Data Series—Provides quantitative data on the physical and chemical properties of materials, compiled from the world's literature and critically evaluated. Developed under a worldwide program coordinated by NBS under the authority of the National Standard Data Act (Public Law 90-396).

NOTE: The principal publication outlet for the foregoing data is the Journal of Physical and Chemical Reference Data (JPCRD) published quarterly for NBS by the American Chemical Society (ACS) and the American Institute of Physics (AIP). Subscriptions, reprints, and supplements available from ACS, 1155 Sixteenth St., NW, Washington, DC 20056.

Building Science Series—Disseminates technical information developed at the Bureau on building materials, components, systems, and whole structures. The series presents research results, test methods, and performance criteria related to the structural and environmental functions and the durability and safety characteristics of building elements and systems.

Technical Notes—Studies or reports which are complete in themselves but restrictive in their treatment of a subject. Analogous to monographs but not so comprehensive in scope or definitive in treatment of the subject area. Often serve as a vehicle for final reports of work performed at NBS under the sponsorship of other government agencies.

Voluntary Product Standards—Developed under procedures published by the Department of Commerce in Part 10, Title 15, of the Code of Federal Regulations. The standards establish nationally recognized requirements for products, and provide all concerned interests with a basis for common understanding of the characteristics of the products. NBS administers this program as a supplement to the activities of the private sector standardizing organizations.

Consumer Information Series—Practical information, based on NBS research and experience, covering areas of interest to the consumer. Easily understandable language and illustrations provide useful background knowledge for shopping in today's technological marketplace.

Order the **above** *NBS publications from: Superintendent of Documents, Government Printing Office, Washington, DC 20402.*

Order the **following** *NBS publications—FIPS and NBSIR's—from the National Technical Information Services, Springfield, VA 22161.*

Federal Information Processing Standards Publications (FIPS PUB)—Publications in this series collectively constitute the Federal Information Processing Standards Register. The Register serves as the official source of information in the Federal Government regarding standards issued by NBS pursuant to the Federal Property and Administrative Services Act of 1949 as amended, Public Law 89-306 (79 Stat. 1127), and as implemented by Executive Order 11717 (38 FR 12315, dated May 11, 1973) and Part 6 of Title 15 CFR (Code of Federal Regulations).

NBS Interagency Reports (NBSIR)—A special series of interim or final reports on work performed by NBS for outside sponsors (both government and non-government). In general, initial distribution is handled by the sponsor; public distribution is by the National Technical Information Services, Springfield, VA 22161, in paper copy or microfiche form.

Backscatter Signature Simulations

NBS technical note

B.L. Danielson

Electromagnetic Technology Division
National Engineering Laboratory
National Bureau of Standards
Boulder, Colorado 80303

Issued December 1981

Sponsored by:

Communications Systems Center
U.S. Army Communications R&D Command
Fort Monmouth, New Jersey 07703

U.S. DEPARTMENT OF COMMERCE, Malcolm Baldrige, Secretary

NATIONAL BUREAU OF STANDARDS, Ernest Ambler, Director

National Bureau of Standards Technical Note 1050
Nat. Bur. Stand. (U.S.), Tech. Note 1050, 100 pages (December 1981)
CODEN: NBTNAE

U.S. GOVERNMENT PRINTING OFFICE
WASHINGTON: 1981

CONTENTS

Table 1.

List of Symbols, Nomenclature, and Units

Symbol	Nomenclature	Units
A	Rayleigh scattering coefficient	$m^{-1}\mu m^{+4}$
B	Absorption coefficient	m^{-1}
$C(\lambda)$	Wavelength dependent absorption	m^{-1}
D	Smallest resolvable defect separation in time	s
ERW	Equivalent rectangular width	s
F	Capture fraction	
FWHM	Full width half maximum	s
G_1	Actual splice loss in forward direction	dB
G_2	Actual splice loss in backward direction	dB
i	Detector current	A
j	$\sqrt{-1}$	
k	Number of points in model	
L	Smallest resolvable defect separation in distance	m
log	Logarithm to base 10	
M_1	Measured backscatter loss in forward direction	dB
M_2	Measured backscatter loss in backward direction	dB
$\langle M \rangle$	Mean measured splice loss	dB
n	Summation index	
NA	Numerical aperture	
P(N)	Probability of occurrence of amplitude N	
SNR	Signal-to-noise ratio	
t	Time	s
v_g	Group velocity	ms^{-1}
W	Pulse width	s
x	Distance along a fiber	m
α_s	Rayleigh scattering loss coefficient	m^{-1}
α_T	Total loss coefficient	m^{-1}
ΔT	Time delay	s
θ	Half vertex angle of fiber output radiation	
λ	Wavelength	um
σ	RMS width of a Gaussian pulse	s
Φ	Power	W
ω	Angular frequency	s^{-1}

Backscatter Signature Simulations

B. L. Danielson*
National Bureau of Standards
Boulder, Colorado 80303

This report presents a collection of computer-generated backscatter signatures which represent realistic replicas of signals that can be encountered in optical time-domain reflectometer (OTDR) systems. Emphasis is placed on illustrating the appearance of backscatter signatures originating from localized and distributed imperfections which are superimposed on an otherwise uniform optical fiber. The details of these signatures are shown to be a function of the particular type of fiber perturbation, experimental parameters, and data reduction methods. This compilation of simulated responses is intended to facilitate the correct interpretation of OTDR signals as well as to point out sources of error which can arise in the characterization of optical fibers using backscatter techniques.

Key words: backscattering; backscatter signatures; optical fiber scattering; optical time-domain reflectometer; OTDR.

1. Introduction

As early as 1972, Kapron, Maurer, and Teter [1] pointed out the possibilities of using the Rayleigh backscattering in optical fibers for fiber characterization purposes. It remained to Barnoski and Jensen [2], in 1976, to implement these ideas in a practical device. The result is the optical time-domain reflectometer which has gained acceptance as one of the most versatile instruments used in optical fiber metrology. Here a short pulse of optical radiation is launched into the fiber and, as the pulse propagates along the length of tne waveguide, light is continuously scattered from variations in the index of refraction as well as flaws and other perturbations. A small amount of this light is trapped as guided radiation in the backward direction. This light signal, as a function of time, is characteristic of the fiber under test and is referred to as the backscatter signature, from which much useful information may be extracted. In a recent review article, Rourke [3] has enumerated some of the many applications areas in which the backscatter method has demonstrated its utility. The most important applications are in fiber parameter estimation, principally with regard to length, defect location and identification, attenuation, core diameter fluctuations, splice loss, and, to a lesser extent, pulse broadening. Probably the most significant advantages of this measurement technique are that it is nondestructive and can be used with only one end of the fiber accessible. However, OTDR methods are not without their limitations. Occasionally, the interpretation of the structure observed on the signatures is not completely straightforward, or even unambiguous. In addition, the accuracy and reliabilty of backscatter data often suffers in comparison with other measurement techniques.

*Electromagnetic Technology Division, National Engineering Laboratory.

This report presents a number of simulated signatures which have been generated on a digital computer. They are intended to represent the backscatter response of a number of types of defects and irregularities which can occur in fiber waveguides. There are two main motivations for presenting these detailed simulations. The first arises from a hope that the examples will aid in interpreting signatures from fiber anomalies. A second reason has to do with the fact that OTDR methods are an attractive candidate for use in standard test procedures, acceptance testing, and quality control applications. Since the qualitative as well as quantitative nature of the signature depends on the details of the experimental conditions and display techniques, these examples may help minimize parameter measurement errors and possibly promote a consensus concerning the most desirable format for OTDR data in specific applications areas.

2. OTDR Signatures: A Modeling of the Backscatter Process

2.1 Theoretical Background

Consider a fiber whose transmission properties, for a given set of launch conditions, are constant (i.e., not a function of length) and the same in both forward and reverse directions. Under these conditions, the OTDR signal $\Phi(t)$ at the detector, and as a function of time, can be shown to be [4,5]

$$\Phi(t) = 0.5\ \Phi_o W\ v_g\ \alpha_s F\ \exp\ [-\alpha_t v_g\ t], \qquad (2\text{-}1)$$

where Φ_o is the peak power injected into the fiber, W is the time duration of that probe pulse, v_g its group velocity, α_s the Rayleigh scattering coefficient, F the capture fraction, and α_t the total attenuation coefficient. This backscatter response is due largely to Rayleigh scattering[1] which has an angular dependence of $(1+\cos^2\theta)$, with θ the angle of scattering relative to the fiber axis, and a wavelength dependence of λ^{-4}. This type of scattering originates in dopant-concentration fluctuations and index of refraction variations which occur on a scale small compared to a wavelength. For most fibers encountered in practice, in addition to the background signal given in eq (2-1), there will be backscatter contributions due to reflection, scattering and/or absorption arising from imperfections in our assumed uniform fiber. In the following text, many examples will be seen of the influence of these defects and nonuniformities on the backscatter response. The specific nature of the signatures due to non-Rayleigh components is a function of many variables involving fiber parameters and experimental conditions. These include the type of fiber perturbation and its location, wavelength of operation, probe pulse shape and duration, and output graphics, among others.

[1] Brillouin scattering has the same angular and wavelength dependence as Rayleigh scattering, but ony about 13 percent of its magnitude in optical fibers [6]. Raman scattering is negligible. Nonlinear processes [7] can be a concern, especially in single-mode fibers, but will not be considered here.

Some of the signatures included in this report are nothing more than the convolution of the impulse response of the fiber h(t) with the probe pulse shape f(t). The backscatter response in this case is

$$\Phi(t) = \int_0^\infty f(t-\tau)h(\tau)d\tau). \qquad (2\text{-}2)$$

In writing this equation, we assume that the fiber-defect system is linear, shift-invariant, and causal [8].

2.2 Discrete Model

Computer codes have been developed for this work which generate a simulated backscatter signal for sample fibers possessing many different types of perturbations. The phenomenological model on which these codes are based is applicable to multimode fibers, and has been described in detail elsewhere [9]. For the present application, we have divided the fiber into 512 elements, each of which is characterized by six bulk parameters: forward and reverse absorption loss, forward and reverse scattering loss, and forward and reverse capture fractions. For a discrete model such as this, the appropriate approximation to a delta function probe pulse is the "delta sequence" which is one point in time duration and of unit amplitude. The corresponding analogy to the backscatter impulse response is referred to as the delta response. In this report we will, however, make no distinction between impulse response and delta response since the signatures will differ in an obvious way.

In all of the cases considered here, we have ignored pulse broadening due to fiber dispersion. This is a good approximation for graded-index fibers and the pulse durations encountered in most OTDR systems.

The discrete analogy to the convolution integral given in eq (2-2) is

$$\Phi(n) = \sum_{k=0}^{n} f(n-k)\ h(k), \qquad (2\text{-}3)$$

where n and k refer to points in the range 0 to 511.

2.3 Display Techniques

There are three main types of graphic displays used in signature analysis. The ordinate of the X-Y plot can be a variable proportional to the (1) direct detector output, (2) logarithm of the detector output, or (3) differential logarithm of the detector output. The abscissa can be either time or distance along the fiber axis. In this report we will choose time as the appropriate variable as this is the experimental observable. The linear display, $\Phi(t)$ versus t, requires the least signal analysis and may be observed directly on an oscilloscope. Semilogarithmic plots, 10 log $[\Phi(t)/\Phi(0)]$ simplify the estimation of fiber attenuation and make obvious losses which are length dependent. This tcchnique does require additional experimental equipment which, in the analog case at least, must be calibrated. The differential method, also referred to as the "two-point" or "two-channel" technique, was originated by Conduit et al. [10,11,12]. This approach can yield the local attenuation

directly and, when used in data acquisition, has several experimental advantages, including insensitivity to pulse-to-pulse laser power variations and long term drifts. It also requires a minicomputer for data analysis. The quantity which is plotted as a function of time, $10 \log[\Phi(t_1)/\Phi(t_1-\Delta T)]$ is proportional to the differential loss between points corresponding to times t_1 and $t_1-\Delta T$, where ΔT is an adjustable, but constant, time delay. In a digital sense, this reduces to the derivative of the logarithm if the delay ΔT is taken to be small compared with system resolution. In the differential signals to follow we have taken the delay ΔT to be positive so that increasing loss appears as a negative-going signal. This convention was adopted to facilitate comparisons with the semilogarithmic display. It should be noted that this differs slightly from the definitions given by Conduit et al. Also, those authors chose ΔT to maximize the signal-to-noise ratio (SNR) in their data acquisition system. However, in systems where the data are processed by a digital computer, the final display may be chosen independently of the format of the input data. It may be desirable here to select ΔT for the most convenient and edifying output graphics. We will examine some of these possibilities later.

3. Signature Examples

In this section we will illustrate the dependence of some backscatter signatures on various fiber properties as well as experimental conditions and graphic displays. The fiber properties include length-dependent Rayleigh scattering, and the presence of fiber defects both localized and distributed over lengths comparable to the physical length of the probe pulse. Among the experimental parameters we will give examples of the effect of probe pulse width and shape, wavelength, and noise.

For purposes of illustration we will consider three types of probe pulse shape. The first is the impulse response (delta response) mentioned earlier. The second is the rectangular probe pulse of unit height and duration W. This type of pulse demonstrates the effect of a fast leading edge on the backscatter response. The third type of pulse is Gaussian shaped, also with unity maximum amplitude and a duration specified in terms of an equivalent rectangular width (ERW). The ERW of any pulse g(t) is defined by the equation

$$\mathrm{ERW} = \frac{\int_{-\infty}^{+\infty} g(t)\, dt}{[g(t)]_{max}}, \qquad (3\text{-}1)$$

where $[g(t)]_{max}$ is the maximum value of g(t) and is presumed to be single-valued. If the pulse is normalized so that its maximum amplitude is one, then ERW=W, and the energy (area) is the same as the corresponding rectangular pulse of unit amplitude. This convention was chosen since, from eq (2-1), the magnitude of the backscatter signal is, to a first approximation, proportional to W. If g(t) is assumed to be Gaussian, then W is approximately a factor of 2.5 times the rms value (sigma). This is illustrated in figure 3-1. The Gaussian pulse has an ERW of W=51 time units, and a sigma of 51/2.5 time units. The energy is the same for both pulses.

3.1 Point Defects: Effect of Probe Pulse Width and Shape

We will now consider the evolution of some point-defect signatures for the probe pulses enumerated above.

3.1.1 Scatter-Like Point Defects

A scatter-like defect is defined here to be a perturbation whose impulse response shows an increase in backscatter signal, due to scattering or a reflection, which is greater than the subsequent signal decrease [13]. Changes in the fibers' capture fraction (numerical aperture or index of refraction) can also produce a scatter-like response. Since scatter is a form of loss, there will always be an absorption component, however small, associated with this type of defect. An air line in the fiber, due to a bubble in the preform, may give rise to this type of signature. Occasionally, splices, connectors, and couplers may exhibit this type of response also. Figures 3-2 to 3-16 illustrate a uniform fiber possessing a single scattering defect whose signature is determined by various combinations of probe pulse width and shape. In all cases, the ordinate gives a realistic indication of the magnitude of the backscatter response relative to the impulse response. Variations in the signature are given as follows:

1. Figure 3-2. The impulse response for a scatter-like imperfection. Logarithmic display. This signature is the archetype for the entire sequence in this section.
2. Figure 3-3. Scatter-like imperfection; Gaussian probe pulse; equivalent rectangular width 5 time units. Logarithmic display.
3. Figure 3-4. Scatter-like imperfection; Gaussian probe pulse; equivalent rectangular width 10 time units. Logarithmic display.
4. Figure 3-5. Scatter-like imperfection; Gaussian probe pulse; equivalent rectangular width 20 time units. Logarithmic display.
5. Figure 3-6. Scatter-like imperfection; Gaussian probe pulse; equivalent rectangular width 30 time units. Logarithmic display.
6. Figure 3-7. Scatter-like imperfection; Gaussian probe pulse; equivalent rectangular width 40 time units. Logarithmic display.
7. Figure 3-8. Scatter-like imperfection; Gaussian probe pulse; equivalent rectangular width 50 time units. Logarithmic display.
8. Figure 3-9. Scatter-like imperfection; Gaussian probe pulse; equivalent rectangular width 100 time units. Logarithmic display.
9. Figure 3-10. Scatter-like imperfection; rectangular probe pulse of width 5 time units. Logarithmic display.
10. Figure 3-11. Scatter-like imperfection; rectangular probe pulse of width 10 time units. Logarithmic display.
11. Figure 3-12. Scatter-like imperfection; rectangular probe pulse of width 20 time units. Logarithmic display.
12. Figure 3-13. Scatter-like imperfection; rectangular probe pulse of width 30 time units. Logarithmic display.

13. Figure 3-14. Scatter-like imperfection; rectangular probe pulse of width 40 time units. Logarithmic display.
14. Figure 3-15. Scatter-like imperfection; rectangular probe pulse of width 50 time units. Logarithmic display.
15. Figure 3-16. Scatter-like imperfection; rectangular probe pulse of width 100 time units. Logarithmic display.

3.1.2 Absorption-Like Point Defects

An absorption-like defect is defined for our purposes to be a perturbation whose impulse response shows a decrease in backscatter signal which is greater in absolute magnitude than any preceding associated scattering feature [13]. Most imperfections fall under this classification. Included particles, splices, couplers, microbends, macrobends, and various scattering processes which scatter radiation largely in the forward direction can produce absorption-like signatures. Figures 3-17 to 3-31 illustrate a uniform fiber possessing a single absorption defect whose signature is determined by various combinations of probe pulse width and shape. As before, the ordinate gives a realistic indication of the magnitude of the backscatter response relative to the impulse response. Variations in the signature are given as follows:

1. Figure 3-17. The impulse response for an absorption-like imperfection. Logarithmic display. This signature is the archetype for the entire sequence in this section.
2. Figure 3-18. Absorption-like imperfection; Gaussian probe pulse; equivalent rectangular width 5 time units. Logarithmic display.
3. Figure 3-19. Absorption-like imperfection; Gaussian probe pulse; equivalent rectangular width 10 time units. Logarithmic display.
4. Figure 3-20. Absorption-like imperfection; Gaussian probe pulse; equivalent rectangular width 20 time units. Logarithmic display.
5. Figure 3-21. Absorption-like imperfection; Gaussian probe pulse; equivalent rectangular width 30 time units. Logarithmic display.
6. Figure 3-22. Absorption-like imperfection; Gaussian probe pulse; equivalent rectangular width 40 time units. Logarithmic display.
7. Figure 3-23. Absorption-like imperfection; Gaussian probe pulse; equivalent rectangular width 50 time units. Logarithmic display.
8. Figure 3-24. Absorption-like imperfection; Gaussian probe pulse; equivalent rectangular width 100 time units. Logarithmic display.
9. Figure 3-25. Absorption-like imperfection; rectangular probe pulse of width 5 time units.
10. Figure 3-26. Absorption-like imperfection; rectangular probe pulse of width 10 time units. Logarithmic display.
11. Figure 3-27. Absorption-like imperfection; rectangular probe pulse of width 20 time units. Logarithmic display.

12. Figure 3-28. Absorption-like imperfection; rectangular probe pulse of width 30 time units. Logarithmic display.
13. Figure 3-29. Absorption-like imperfection; rectangular probe pulse of width 40 time units. Logarithmic display.
14. Figure 3-30. Absorption-like imperfection; rectangular probe pulse of width 50 time units. Logarithmic display.
15. Figure 3-31. Absorption-like imperfection; rectangular probe pulse of width 100 time units. Logarithmic display.

3.1.3 Composite Point Defects

A composite defect is defined as a perturbation whose impulse response shows features which are both scatter-like and absorption-like in nature, that is, they exhibit a pronounced increase in backscatter signal followed by a pronounced decrease in signal level. As long as the defects produce small power losses, the resulting signature will be, to a good approximation in our model, an additive superposition of the features due to the individual scatter and absorption components. The composite-type defect therefore produces a signature whose features can be inferred from the examples detailed in the previous two sections. We will give an example of such an imperfection in the following series. Here we simulate a fault which has a rather large scatter cross section, but associated with this is a much smaller capture fraction than shown in section 3.1.1. This could happen, for example, at a flaw which scatters radiation largely in the forward direction. Variations in the composite signature are given as follows:

1. Figure 3-32. The impulse response for a composite imperfection. Logarithmic display. This signature is the archetype for the entire sequence in this section.
2. Figure 3-33. Composite imperfection; Gaussian probe pulse; equivalent rectangular width 5 time units. Logarithmic display.
3. Figure 3-34. Composite imperfection; Gaussian probe pulse; equivalent rectangular width 10 time units. Logarithmic display.
4. Figure 3-35. Composite imperfection; Gaussian probe pulse; equivalent rectangular width 20 time units. Logarithmic display.
5. Figure 3-36. Composite imperfection; Gaussian probe pulse; equivalent rectangular width 30 time units. Logarithmic display.
6. Figure 3-37. Composite imperfection; Gaussian probe pulse; equivalent rectangular width 40 time units. Logarithmic display.
7. Figure 3-38. Composite imperfection; Gaussian probe pulse; equivalent rectangular width 50 time units. Logarithmic display.
8. Figure 3-39. Composite imperfection; Gaussian probe pulse; equivalent rectangular width 100 time units. Logarithmic display.
9. Figure 3-40. Composite imperfection; rectangular probe pulse of width 5 time units.
10. Figure 3-41. Composite imperfection; rectangular probe pulse of width 10 time units. Logarithmic display.

11. Figure 3-42. Composite imperfection; rectangular probe pulse of width 20 time units. Logarithmic display.
12. Figure 3-43. Composite imperfection; rectangular probe pulse of width 30 time units. Logarithmic display.
13. Figure 3-44. Composite imperfection; rectangular probe pulse of width 40 time units. Logarithmic display.
14. Figure 3-45. Composite imperfection; rectangular probe pulse of width 50 time units. Logarithmic display.
15. Figure 3-46. Composite imperfection; rectangular probe pulse of width 100 time units. Logarithmic display.

Figures 3-47 to 3-48 illustrate the effect of varying the delay ΔT in the differential display 10 log $[\Phi(t_1)/D(t_1-\Delta T)]$. We have chosen the response of figure 3-10 as the archetype for this series (Gaussian probe pulse of equivalent rectangular width 10 time units). Changing the time delay ΔT from one time unit to 100 time units generates the following sequence:

1. Figure 3-47. Composite imperfection; Gaussian probe pulse; equivalent rectangular width 10 time units; delay 1 time unit. Differential display.
2. Figure 3-48. Composite imperfection; Gaussian probe pulse; equivalent rectangular width 10 time units; delay 2 time units. Differential display.
3. Figure 3-49. Composite imperfection; Gaussian probe pulse; equivalent rectangular width 10 time units; delay 5 time units. Differential display.
4. Figure 3-50. Composite imperfection; Gaussian probe pulse; equivalent rectangular width 10 time units; delay 10 time units. Differential display.
5. Figure 3-51. Composite imperfection; Gaussian probe pulse; equivalent rectangular width 10 time units; delay 15 time units. Differential display.
6. Figure 3-52. Composite imperfection; Gaussian probe pulse; equivalent rectangular width 10 time units; delay 20 time units. Differential display.
7. Figure 3-53. Composite imperfection; Gaussian probe pulse; equivalent rectangular width 10 time units; delay 25 time units. Differential display.
8. Figure 3-54. Composite imperfection; Gaussian probe pulse; equivalent rectangular width 10 time units; delay 30 time units. Differential display.
9. Figure 3-55. Composite imperfection; Gaussian probe pulse; equivalent rectangular width 10 time units; delay 35 time units. Differential display.
10. Figure 3-56. Composite imperfection; Gaussian probe pulse equivalent rectangular width 10 time units; delay 40 time units. Differential display.
11. Figure 3-57. Composite imperfection; Gaussian probe pulse equivalent rectangular width 20 time units; delay 50 time units. Differential display.
12. Figure 3-58. Composite imperfection; Gaussian probe pulse equivalent rectangular width 30 time units; delay 60 time units. Differential display.

13. Figure 3-59. Composite imperfection; Gaussian probe pulse equivalent rectangular width 40 time units; delay 100 time units. Differential display.

3.1.4 Discussion of Point Defect Signatures

From a perusal of the foregoing signature examples we may draw the following conclusions:

1. The magnitude of the distributed Rayleigh component is approximately proportional to the energy in the probe pulse. This may also be seen from eq (2-1). In our examples the probe pulse always had a maximum amplitude of one, so that the backscatter signal is approximately proportional to the ERW.
2. The magnitudes of the scatter-like signatures do not increase with probe pulse duration the way the Rayleigh signature does; rather, this defect structure tends to broaden out and the contrast becomes washed-out. This wash-out phenomenon is due to the fundamentally different reflection properties of discrete and distributed systems when irradiated with finite-width optical pulses. Reflection from localized regions returns a basically unaltered pulse in the backward direction. Reflection from extended regions involves a convolution process of the probe pulse with the scattering medium. Therefore, scatter-like signatures will have a strong functional dependence on the probe pulse ERW.
3. Absorption-like defects provide a signature from which the loss (determined from the step signal decrease) can always be inferred even at probe pulse widths that completely wash-out a scatter-like signature under similar conditions. The main effect of increasing the probe pulse width in this case is to cause a relative decrease in the higher frequency components of the signature.
4. There are always transient effects at t=0, at the end of the fiber and at discontinuities, which are apparent signatures from finite width pulses. These transients appear over time intervals approximately equal to the probe pulse duration. Problems in signature interpretation can occur if the defect response occurs in this nonequilibrium region.
5. Another transient effect which appears with increasing probe pulse duration is the apparent time-shift in the appearance of the most prominant defect signature features. This is due to the fact that the time scale in our examples is "triggered" at the 10 percent amplitude of the probe pulse. With the rectangular input pulse the location of the defect is still given correctly by the leading edge of the defect signature.
6. The precision associated with the visual location of a defect is determined more by the rise time of the probe pulse than its duration.
7. Signatures arising from point defects will have recognizable time durations approximately the same as the input pulse.
8. When the log differential display is used, a convenient criterion for maximizing the signal while avoiding signature ambiguities is to set the probe pulse ERW $\approx$ Delay.

That is, $W \simeq \Delta T$. This produces a signature which closely resembles the derivative of the semilogarithmic plots.

3.2 Extended Defects

If a fiber possesses regions of anomalous properties which occur on a length scale less than or comparable to the physical length of the probe pulse in the fiber, the resulting backscatter response will differ in a qualitative way from that due to point defects. Here, the time dependence of the returned signal is determined by a convolution integral involving the probe pulse and the scattering region. In general, the backscatter signature will be broadened when compared with the input probe pulse duration. As an example of this, we consider a distributed scattering region centered at x_o in the fiber, and extending over a length surrounding x_o in a roll-off characteristic of a Gaussian function with an rms width (sigma) equal to σ_x. That is, the backscatter response from a delta function input pulse is

$$h(t) = \exp[-(t-t_0)^2/2\sigma_1^2], \tag{3-2}$$

where

$$\sigma_1 = 2\sigma_x/v_g \tag{3-3}$$

and

$$t_0 = 2x_o/v_g, \tag{3-4}$$

with v_g the group velocity of a pulse in the fiber. If now the probe pulse is changed to a Gaussian pulse itself, or

$$f(t) = \exp[-t^2/2\sigma_2^2], \tag{3-5}$$

then the resulting backscatter response can be shown to be yet another Gaussian-shaped pulse proportional to

$$\Phi(t) = \exp\,[-(t-t_0)^2/2\sigma_3^2], \tag{3-6}$$

whose width is determined from the relation

$$\sigma_3 = (\sigma_1^2 + \sigma_2^2)^{1/2}. \tag{3-7}$$

As a further example, consider a region Δx of a fiber with a high, but constant, scattering loss, the fiber itself having negligible loss. The impulse response from this type of imperfection will appear as in figure 3-60, where $2\Delta X/v_g = 100$ time units. If now the probe pulse is rectangular in shape, the signature will resemble a truncated pyramid, as in

figure 3-61, with increased amplitude as expected. Note that the backscattered pulse width measured at the full width half maximum (FWHM) will be the same as that of the impulse response. This is true for all probe pulse widths $W \leq 2\Delta X/v_g$. In figure 3-62 the probe pulse is equal in duration to the impulse response (100 time units). For probe pulses of duration greater than the impulse response we again get the truncated-pyramid shape as in figure 3-63. Here W = 150 time units. The measured FWHM of the signature for $W \leq 2\ \Delta X/vg$ will be equal to W.

3.3 Symmetry and Length-Dependent Effects

It has been shown elsewhere [9] that errors are introduced in backscatter-derived attenuation determinations, and signature interpretations can become troublesome, if either of two types of fiber anomalies occur. One source of error originates in distributed fiber properties (scattering, absorption, numerical aperture, diameter) which are a function of length; the second relates to the lack of fiber symmetry with respect to the forward and reverse directions of propagation of radiation. We will refer to a fiber as uniform if its loss and/or transmission properties denoted by $\alpha_i(\vec{x})$ (appropriate to the mode volume under consideration) are invariant to a displacement along the fiber axis $\vec{x} + \vec{x}'$; i.e., $\alpha_i(\vec{x}) = \alpha_i(\vec{x} + \vec{x}')$. In a similar vein, reciprocity is used in the sense of invariance to reversal of the propagation direction, i.e., $\alpha_i(\vec{x}) = \alpha_i(-\vec{x})$. These properties may be intrinsic to the fiber, such as numerical aperture changes, or may be due to mode coupling effects occurring in multimode fibers in either the probe pulse or the backscattered radiation. Mode conversion in conjunction with differential modal attenuation causes the radiation to propagate in an environment which is length dependent and possibly nonreciprocal as well. Figure 3-64 illustrates several types of nonuniform and nonreciprocal behavior which can occur in fibers either on a local (at splices or couplers) or distributed basis. Figures 3-64 (a), (b), and (c) represent splices between dissimilar fibers. Figure 3-64 (d) illustrates schematically the case where the forward travelling probe pulse is launched into a set of low order modes. These modes can, and often do, have lower average losses than the higher order modes. The Rayleigh backscatter, on the other hand, is approximately isotropic, and this excites a different set of modes including the higher order, more lossy, modes represented by the ray B in the figure. The average loss in the two directions can be significantly different, as much as 1 dB/km with some fibers. We will now give several examples of signature distortion when nonuniform and nonreciprocal fiber properties are encountered.

The series of figures 3-65 to 3-67 illustrate the condition where the capture fraction F increases toward the remote end by 50 percent (this is equivalent to a 22 percent increase in numerical aperture). Figure 3-65 shows the capture fraction dependence on fiber length (in arbitrary units). The resulting signature appears in figure 3-66. A slight negative curvature[2] can be detected in the logarithmic plot. This curvature is more apparent in the plot of residuals in figure 3-66. The residuals are taken to be

[2]The usual definition of positive curvature implies that as one moves along the curve toward larger times, the path tends to move generally in a counterclockwise direction.

Residual (dB) = Actual Attenuation (dB) - Predicted Attenuation (dB) (3-8)

where the predicted attenuation is given by a linear least-squares fit. When the same fiber is reversed end for end, the resulting signature and residuals are illustrated in figures 3-68 and 3-69, respectively. Rather surprisingly, the curvature of both figures is the same. The measured attenuation is different, as expected [9].

A similar series for scattering loss is given in figures 3-70 to 3-74. Figure 3-70 shows the functional dependence of scattering loss in the forward direction; the scattering loss increases 20 percent from one end to the other. Figure 3-71 shows the resulting signature and figure 3-72 the corresponding residuals. Figures 3-73 and 3-74 illustrate the changes observed when the fiber is reversed end for end. The curvature undergoes a sign change in contrast to the previous example (figures 3-68 and 3-69).

The final series represents the case for absorption loss, figures 3-75 to 3-79. Figure 3-75 shows the functional dependence of absorption loss in the forward direction; the absorption loss increases 50 percent from one end to the other. Figure 3-76 shows the resulting signature and figure 3-77 the residuals. Figures 3-78 and 3-79 illustrate the changes observed when the fiber is reversed end for end.

It can be seen that, in all cases, the sign of the curvature of the semilog plot and the residuals is the same. However, the interpretation of this curvature is ambiguous. A negative curvature may be due to either scattering loss or absorption loss increasing toward the remote end, or to numerical aperture changes. The positive curvature may be identified with either absorption loss or scattering loss decreasing toward the far end.

Splices and couplers in fiber links are probably the most important examples of situations which can exhibit symmetry and length-dependent anomalies. An extreme example of an unsymmetric splice is displayed in figures 3-80 and 3-81, representing the signature from opposite ends of the fiber. In figure 3-80, the near-end fiber (#1, represented by $t < 200$) has 50 percent greater scattering loss than the far-end fiber (#2, $t \geq 200$). In this case, there is zero loss at the splice but nevertheless the signature exhibits the normal type step response indicating a loss. On reversing the fiber end-for-end the signature in figure 3-81 results. There is apparent "gain" at the splice. Several authors have analyzed problems of this sort [9,14-17], and also effects of this nature have been observed experimentally [17,18]. It can be shown that the measured splice loss M_1 (determined from the magnitude of the step in the backscatter signature) in the forward direction is

$$M_1 = \frac{G_1+G_2}{2} + 5 \log \left(\frac{\alpha_{s1}F_1}{\alpha_{s2}F_2}\right) \quad \text{(dB)}, \tag{3-9}$$

where G_1 and G_2 are the actual splice losses (in dB) in the forward and reverse directions respectively, and α_s represents the scattering loss and F the capture fractions of the two fibers 1 and 2, as before. The corresponding measured splice loss M_2 from the opposite end is

$$M_2 = \frac{G_1+G_2}{M} - 5\log\left(\frac{\alpha_{a1}F_1}{\alpha_{s2}F_2}\right) \quad \text{(dB)}, \tag{3-10}$$

It can be seen that the mean measured splice loss from both ends <M> is

$$\langle M\rangle = \frac{(M_1+M_2)}{2} = \frac{(G_1+G_2)}{2} \quad \text{(dB)}, \tag{3-11}$$

i.e., the correct value of the splice loss averaged in both directions. Only round-trip splice loss can be determined exactly using the backscatter technique. In almost all cases, what is really desired is an estimate of the one-way splice loss. In this case, we can say with certainty only that the one-way splice loss G_1 lies in the region $0 \leq G_1 \leq 2\langle M\rangle$. Estimating G_1 by identifying its value with <M> therefore can involve a potential error of magnitude ± <M> (100 percent error). It is not possible to obtain bounded estimates of G_1 from backscatter measurements made from one end of the fiber only, unless the quantity $(\alpha_{s1}F_1/\alpha_{s2}F_2)$ is known. However, if necessary, this quantity may be determined from independent measurements on both fibers prior to the splicing operation [17]. With $5\log(\alpha_{s1}F_1/\alpha_{s2}F_2)$ a known quantity, we may then estimate G_1 when only one end of the spliced fiber is available. This can be done by using eq (3-9) and assuming $G_1=G_2$. The maximum error involved in estimating F_1 in this way will be $\pm[M_1-5\log(\alpha_{s1}F_1/\alpha_{s2}F_2)]$.

3.4 DiVita Technique

In the previous section it was shown that making backscatter measurements from both ends of the fiber can eliminate certain types of errors in signature interpretation. DiVita and Rossi [19] have generalized this approach to provide a means for separating the distributed loss of the fiber from the backscatter contributions due to any imperfections. We will give an example of the power of this approach. The backscatter signals from either end of the fiber are taken to be $w_f(x)$ and $w_b(x)$. In both cases, the distance x is measured from the same end face. The separation of the distributed loss from local perturbations can be made by defining the following two quantities:

$$I(x) = (w_f(x)\ w_b(x))^{1/2} = \text{const.}\ F(x)\ \alpha_s(x) \tag{3-12}$$

$$D(x) = (w_f(x)/w_b(x))^{1/2} = \text{const.}\ \exp\{-2\int_0^x \alpha_T(x')dx'\}. \tag{3-13}$$

Here the capture fraction F(x) and scattering coefficient $\alpha_s(x)$ are functions of the distance from the fiber end. The power decay, from which the attenuation is obtained, is given by D(x) and local perturbations, as a function of distance, by I(x). Ambiguities in signature interpretation are thus removed at the expense of requiring measurements from both ends of the fiber.

As an example of this technique, we apply eqs (3-12) and (3-13) to the situation demonstrated previously in figures 3-80 and 3-81. The resulting log power loss D(t) is shown in

figure 3-82. This shows clearly that there is no loss at the splice and that the attenuation of both fibers is different. The attenuation value of each segment may be inferred from the log scale though this has not been expressed in dB here. The perturbation parameter I(t) in figure 3-83 also shows the dependence of the (in this case) scattering coefficients α_s, but the vertical scale is arbitrary.

3.5 Wavelength Dependence

A convenient expression for resolving the total background loss of a fiber into its component parts is given by [20]

$$\alpha(\lambda) = \frac{A}{\lambda^4} + B + \sum c_i(\lambda). \qquad (3\text{-}14)$$

In this expression, $\alpha(\lambda)$ is the total loss at wavelength λ, A is the Rayleigh scattering coefficient, B is the excess loss term having no wavelength dependence, and $C_i(\lambda)$ is the i'th contribution to a wavelength dependent absorption. Absorption due to OH radicals is usually the most important of these. Curve fitting the attenuation of many sample fibers to eq (3-14) has demonstrated that Rayleigh scattering is the dominant loss term at 850 nm, even in fairly high loss fibers. On the other hand, many localized imperfections will have defect signatures that are largely independent of wavelength. Also, backscatter structure due to diameter fluctuations appears to be nearly constant [10]. From eqs (2-1) and (3-14) it is apparent that the magnitude of the background Rayleigh signature will vary as the inverse fourth power of the wavelength.[3] For this reason, the qualitative nature of most backscatter signatures containing localized defects will change with wavelength in a predictable way. Two examples are shown in figures 3-84 and 3-85. These correspond to fibers whose loss consists entirely of Rayleigh scattering and whose composite defect is wavelength independent. The ordinate in both cases indicates relative scattering levels for wavelengths of 800 and 900 nm. It can be seen that the t=0 scattering level is higher in the 800 nm case by a factor of $(800/900)^{-4}$ or about 2 dB, but the slope at t = 0 is greater. Also, the features of the defect signature are altered somewhat even though the defect parameters are unchanged.

3.6 Noise Considerations

Up to this point we have considered the effect that various fiber perturbations can have on the backscatter response of a uniform fiber. Experimental influences incidental to the data acquisition process may also cause distortions in the backscatter signature. We will consider one example of this.

The major limitation of OTDR techniques is the limited dynamic range over which adequate SNR may be obtained. The fact that backscatter signals are inherently very small[4]

[3]The backscatter levels will also depend on the capture fraction F which is proportional to the square of the fiber's numerical aperture. This quantity is, however, not strongly dependent on wavelength. See, for example, reference [21].

[4]A fairly representative backscatter power level is about -50 dB down from the peak power of the forward propagating probe pulse at the same point in the fiber [13].

means that system noise is almost always a concern. Thermal noise, background radiation, fluctuations in the carrier multiplication process in the avalanche photodiode, and laser diode power fluctuations can contribute significant amounts of noise in OTDR systems. As an illustration of signature distortion caused by noise, we have modeled a backscatter response which contains additive Gaussian detector noise. The noise in this case has a dc average value of zero and the probability P(N) that the amplitude will have a value between N and N+ ΔN is given by

$$P(N) = \frac{1}{\sigma_n (2\pi)^{1/2}} \int_N^{N+\Delta N} \exp\left(-\frac{n^2}{2\sigma_n^2}\right) dn, \qquad (3\text{-}15)$$

where σ_n is the rms noise current amplitude. The amplitudes in eq (3-15) are determined by Monte-Carlo methods. For our purposes, the electrical SNR can be defined to be

$$SNR = 20 \log \left(\frac{i_s}{\sigma_n}\right) \quad (dB). \qquad (3\text{-}16)$$

Here i'_s is the detector signal current equal in magnitude to the optical backscatter power. Figure 3-86 indicates the appearance of a segment of the noisy backscatter signal with a SNR of 10 at the midpoint of the scan. The same data are presented in figure 3-87 on a semi-logarithmic plot. It is clear from the display that the log scale tends to skew the average values toward higher loss values. That is, logarithmic scales are nonlinear, and positive-going noise excursions do not affect the signature to the same extent as corresponding negative-going excursions. A least-squares fit or other type of averaging in the log space will therefore contain a bias when low SNRs are encountered. The remedy is simple: Averaging noisy signals in the logarithmic domain should be avoided.

3.7 Point Defects in Close Proximity: The Resolution Question

Backscatter signatures of localized defects in close association present special problems. One is the uncertainty in interpretation of the resultant structure which is often observed in the signature. Another question which arises is related to the probe pulse characteristics which are required to completely resolve and identify the defects. As we shall see, the signatures can be rather complex under certain conditions, being a function of the properties of the defect in question, the magnitude of the backscatter signal generated, as well as the probe pulse width, shape, and type of graphic display.

Although in principle the distributed Rayleigh signature can be separated out from the contribution of the imperfections, we have usually not pursued that approach here. The rationale is that, experimentally, one always observes the background and perturbations together and interpretations must always be made in this type of nexus.

We assume that the resolution is determined exclusively by the probe pulse. That is, that fiber dispersion is negligible, and the response of the APD and data-processing electronics does not contribute appreciably to the shape of the defect signatures.

By resolution we mean the ability of the OTDR system to distinguish between defects which are in close proximity in the fiber. The smallest spacing between point scatterers, L, that can just be resolved is usually taken to be [22]

$$L = \frac{v_g W}{2}, \tag{3-17}$$

where, as before, v_g is the group velocity and W the pulse duration of the assumed rectangular probe pulse.[5] More correctly, this is referred to as the "limit of spatial resolution" rather than "resolution", although often these terms are used interchangeably. In the following sections we will illustrate the appearance of some signatures from closely spaced imperfections under excitation by various types of probe pulses. Since the signatures are plotted as a function of time rather than distance, the resolution criterion corresponding to eq (3-17) is

$$D = W, \tag{3-18}$$

where D is the temporal spacing of the defects in the impulse response.

3.7.1 Resolution of Scatter-Like Defects

The signatures in figures 3-88 to 3-120 are based on two adjacent point scatterers separated by ten (arbitrary) time units. These defects occur at t=200 and t=210. Variations in the signature are given as follows:

1. Figure 3-88. The impulse response for two scatter-like imperfections. Logarithmic display. This signature is the archetype for the entire sequence in this section.
2. Figure 3-89. Scatter-like imperfections; Gaussian probe pulse; equivalent rectangular width 5 time units. Logarithmic display.
3. Figure 3-90. Scatter-like imperfections; Gaussian probe pulse; equivalent rectangular width 9 time units. Logarithmic display.
4. Figure 3-91. Scatter-like imperfections; Gaussian probe pulse; equivalent rectangular width 10 time units. Logarithmic display. This pulse width corresponds to the resolution criterion given in eq (3-17). Comparison with figure 3-90 shows that small changes in probe pulse width are quite significant in distinguishing these defects.
5. Figure 3-92. Scatter-like imperfections; Gaussian probe pulse; equivalent rectangular width 15 time units. Logarithmic display. The two defects are now completely unresolved. Also there is an apparent shift in location.
6. Figure 3-93. Scatter-like imperfections; Gaussian probe pulse; equivalent rectangular width 20 time units. Logarithmic display.

[5] This criterion is also used in radar applications where it is called the "radar resolution cell" [23].

7. Figure 3-94. Scatter-like imperfections; Gaussian probe pulse; equivalent rectangular width 25 time units. Logarithmic display.
8. Figure 3-95. The impulse response for two scatter-like imperfections. Linear display. Compare with figure 3-98.
9. Figure 3-96. Scatter-like imperfections; Gaussian probe pulse; equivalent rectangular width 5 time units. Linear display. It can be seen in this and the following figures that there is no great difference in the linear and logarithmic displays, at least for this demonstration.
10. Figure 3-97. Scatter-like imperfections; Gaussian probe pulse of width 9 time units. Linear display.
11. Figure 3-98. Scatter-like imperfections; Gaussian probe pulse; equivalent rectangular width 10 time units. Linear display.
12. Figure 3-99. Scatter-like imperfections; Gaussian probe pulse; equivalent rectangular width 15 time units. Linear display.
13. Figure 3-100. Scatter-like imperfections; Gaussian probe pulse; equivalent rectangular width 20 time units. Linear display.
14. Figure 3-101. Scatter-like imperfections; Gaussian probe pulse; equivalent rectangular width 25 time units. Linear display.
15. Figure 3-102. Scatter-like imperfections; rectangular probe pulse of width 5 time units. Logarithmic display.
16. Figure 3-103. Scatter-like imperfections; rectangular probe pulse of width 9 time units. Logarithmic display. The defects are still completely resolved.
17. Figure 3-104. Scatter-like imperfections; rectangular probe pulse of width 10 time units. Logarithmic display. The presence of two defects is observed only with difficulty.
18. Figure 3-105. Scatter-like imperfections; rectangular probe pulse of width 15 time units. Logarithmic display. Note the structure due to pulse overlap.
19. Figure 3-106. Scatter-like imperfections; rectangular probe pulse of width 20 time units. Logarithmic display.
20. Figure 3-107. Scatter-like imperfections; rectangular probe pulse of width 25 time units. Logarithmic display.
21. Figure 3-108. Scatter-like imperfections; rectangular probe pulse of width 5 time units. Linear display.
22. Figure 3-109. Scatter-like imperfections; rectangular probe pulse of width 9 time units. Linear display.
23. Figure 3-110. Scatter-like imperfections; rectangular probe pulse of width 10 time units. Linear display.
24. Figure 3-111. Scatter-like imperfections; rectangular probe pulse of width 15 time units. Linear display.
25. Figure 3-112. Scatter-like imperfections; rectangular probe pulse of width 20 time units. Linear display.

26. Figure 3-113. Scatter-like imperfections; rectangular probe pulse of width 25 time units. Linear display.

Figures 3-114 to 3-120 represent a few selected signatures plotted according to the differential technique. All are logarithmic displays.

1. Figure 3-114. The impulse response for two scatter-like imperfections. Differential display. This signature is the archetype for the sequence in following examples.
2. Figure 3-115. Scatter-like imperfections; Gaussian probe pulse; equivalent rectangular width 5 time units; delay 5 time units. Differential display. Note the transient at t=0; this is characteristic of all differential displays.
3. Figure 3-116. Scatter-like imperfections; Gaussian probe pulse; equivalent rectangular width; delay 5 time units. Differential display. The interpretation here is ambiguous.
4. Figure 3-117. Scatter-like imperfections; equivalent rectangular width 10 time units; delay 10 time units. Differential display. The two defects are completely unresolved here.
5. Figure 3-118. Scatter-like imperfections; rectangular probe pulse of width 5 time units; delay 5 time units. Differential display.
6. Figure 3-119. Scatter-like imperfections; rectangular probe pulse of width 10 time units; delay 5 time units. Differential display.
7. Figure 3-120. Scatter-like imperfections; rectangular probe pulse of width 10 time units; delay 10 time units. Differential display. The two defects are again completely unresolved.

3.7.2 Resolution of Absorption-Like Defects

The signatures in figures 3-121 to 3-139 are based on two adjacent absorbing defects separated by ten (arbitrary) time units. These defects occur at t=200 and t=210. Variations in the signature are given as follows:

1. Figure 3-121. The impulse response for two absorption-like imperfections. Logarithmic display. This signature is the archetype for the entire sequence in this section.
2. Figure 3-122. Absorption-like imperfections; Gaussian probe pulse; equivalent rectangular width 5 time units. Logarithmic display.
3. Figure 3-123. Absorption-like imperfections; Gaussian probe pulse; equivalent rectangular width 10 time units. Logarithmic display. The two defects are completely unresolved.
4. Figure 3-124. The impulse response for the two absorption-like imperfections. Linear display.
5. Figure 3-125. Absorption-like imperfections; Gaussian probe pulse; equivalent rectangular width 5 time units. Linear display.

6. Figure 3-126. Absorption-like imperfections; Gaussian probe pulse; equivalent rectangular width 10 time units. Linear display.
7. Figure 3-127. The impulse response for two absorption-like imperfections; delay 1 time unit. Differential display.
8. Figure 3-128. Absorption-like imperfections; Gaussian probe pulse; equivalent rectangular width 5 time units; delay 1 time unit. Differential display.
9. Figure 3-129. Absorption-like imperfections; Gaussian probe pulse; equivalent rectangular width 5 time units; delay 10 time units. Differential display. The defects are now completely unresolved.
10. Figure 3-130. Absorption-like imperfections; Gaussian probe pulse; equivalent rectangular width 10 time units; delay 5 time units. Differential display.
11. Figure 3-131. Absorption-like imperfections; Gaussian probe pulse; equivalent rectangular width 10 time units; delay 10 time units. Differential display.
12. Figure 3-132. Absorption-like imperfections; rectangular probe pulse of width 5 time units; delay 5 time units. Differential display.
13. Figure 3-133. Absorption-like imperfections; rectangular probe pulse of width 5 time units; delay 10 time units. Differential display.
14. Figure 3-134. Absorption-like imperfections; rectangular probe pulse of width 10 time units; delay 5 time units. Not only are the defects unresolved, but confusing structure arises with these parameters.
15. Figure 3-135. Absorption-like imperfections; rectangular probe pulse of width 10 time units; delay 10 time units. Differential display. The defects are completely unresolved in this case.
16. Figure 3-136. Absorption-like imperfections; rectangular probe pulse of width 5 time units. Logarithmic display.
17. Figure 3-137. Absorption-like imperfections; rectangular probe pulse of width 10 time units. Logarithmic display. The defects are completely unresolved in this case.
18. Figure 3-138. Absorption-like imperfections; rectangular probe pulse of width 5 time units. Linear display.
19. Figure 3-139. Absorption-like imperfections; rectangular probe pulse of width 10 time units. Linear display.

3.7.3 Resolution of Composite Defects

As mentioned in section 3.1.3, the scatter-like and absorption-like features of a composite-type defect will approximately add in the resultant signature. The effects of this type of imperfection can therefore be inferred from the foregoing material. Only one example will be given here. Figure 3-140 is the impulse response of two composite defects separated by 100 time units. The corresponding differential display for a Gaussian probe pulse having an equivalent rectangular width of 5 time units and delay of 5 time units is given in figure 3-141. It is seen that the defects are completely resolved in this case. In the next section we will propose the values shown here as a preferred resolution criterion.

3.7.4 Conclusions and Recommendations

The foregoing signature examples demonstrate the complexity of the backscatter response when defect responses appear with time separations comparable to the probe pulse width. The situation is complicated by the number of types of possible defect signatures, relative magnitude of the backscatter signals, launched pulse characteristics and graphic display techniques. For example, a comparison of the results of sections 3.7.1 and 3.7.2 indicate that scatter-like defects are often easier to resolve visually than absorption-like defects under similar experimental conditions. Also, it appears that the conventional definition of resolution given in eqs (3-17) and (3-18) is not really an adequate measure of the ability of the OTDR system to distinguish between all types of defects in close proximity. In some cases, e.g., figure 3-123, adjacent imperfections are completely unresolved using this criterion. We suggest a more conservative working definition of resolution might be more appropriate in backscatter applications. For example, in all examples considered here, the defects are distinct and the interpretation unambiguous if the resolution is defined to be different by a factor of two from eqs (3-17) and (3-18), or

$$L = v_g W, \tag{3-19}$$

and

$$D = 2W. \tag{3-20}$$

The criterion for the differential display, $\Delta T=W$, which is discussed previously seems to be satisfactory in this connection also.

4. Deconvolution

In this report we have emphasized that the only unique backscatter signature in the time domain, for a given fiber, is represented by that fiber's impulse response h(t). This, as has been noted, is the backscatter return due to a delta function probe pulse. If OTDR methods are to be used in fiber and cable inspection, acceptance testing, defect analysis or specifications, it is desirable to have signature displays which are independent of the details of the particular experimental apparatus generating the backscatter data. One approach is to adopt standard test conditions such as probe pulse shape and duration.[6] However, there are engineering tradeoffs between resolution and SNR, and special requirements may dictate the use of a particular probe pulse characteristic. Another possible stratagem for the production of uniform displays makes use of the method of deconvolution. Review articles by Jones [24] and Nahman [25] examine some of the difficulties and errors inherent in this approach. We will briefly review some of the salient points as they apply to backscatter signatures.

As noted previously, if h(t) represents the backscatter impulse response of a fiber, and the finite experimental input probe pulse is f(t), then the resulting distorted output

[6] An examination of the specifications of some eleven commercial OTDR systems indicated working probe pulse durations in the range of 4 to 130 ns.

backscatter response is given by the convolution integral in eq (2-2). Written in the usual simplified notation this becomes

$$\Phi(t) = f(t) * h(t). \tag{4-1}$$

For this relation to be valid we must have a linear, causal system where

$$h(t) = 0 \qquad t < 0. \tag{4-2}$$

The desired impulse response may be recovered from $\Phi(t)$ in eq (4-2) in either the time domain or the frequency domain using conventional techniques [24-29]. The main problem which arises in attempts to implement these convolution processes is the adverse, sometimes disastrous, effect of extraneous noise and mathematical approximations which occur in the analysis of real-world data. For example, the most straightforward deconvolution calculations are done in the frequency domain using discrete fast Fourier transformation (FFT) techniques. In the transform representation, eq (4-1) is given by the product relation

$$\Phi(j\omega) = F(j\omega) \cdot H(j\omega), \tag{4-3}$$

where $\Phi(j\omega)$, $F(j\omega)$ and $H(j\omega)$ are the discrete Fourier transforms of $\Phi(t)$, $f(t)$ and $h(t)$, also considered as discrete functions of k points. In this application, $H(j\omega)$ is sometimes referred to as the system function. Then, by a simple point-by-point division,

$$H(j\omega) = \frac{\Phi(j\omega)}{F(j\omega)}. \tag{4-4}$$

The desired impulse response $h(t)$ is obtained by a discrete inverse FFT. However, the zeros of $\Phi(j\omega)$ and $F(j\omega)$ must occur at exactly the same points in the complex plane in order to avoid indeterminate results. Small amounts of noise, sampling errors, and errors in analog-to-digital conversion in the region of the zeros of $\Phi(j\omega)$ and $F(j\omega)$ can result in very large discrepancies in the resulting value of $H(j\omega)$. In certain extreme cases the calculated values of impulse response can be quite meaningless. There are a number of strategies for minimizing these errors which involve filtering in the frequency domain [25]. This data processing must, of course, be done with a digital computer. Nevertheless, with care, the desired impulse response may be approximated adequately using these deconvolution methods. Backscatter signatures presented in this manner will be unambiguous and will also eliminate the time shift errors observed in many of the examples shown in this report. Although somewhat elaborate data processing is required, this is definitely the preferred display technique.

This work was supported by the Communications Systems Center, U.S. Army Communications Command, Fort Monmouth, New Jersey 07703.

5. References

[1] Kapron, F. P.; Maurer, R. D.; Teter, M. P. Theory of backscattering effects in waveguides. Appl. Opt. 16(9):1352-1356; 1972 December.

[2] Barnoski, M. K.; Jensen, S. M. Fiber waveguides: a novel technique for investigating attenuation characteristics. Appl. Opt. 15(9):2112-2115; 1976 September.

[3] Rourke, M. D. An overview of optical time domain reflectometry. Proceedings American Ceramic Society Meeting on Physics of Fiber Optics; 1980 April 28-30; Chicago, IL.

[4] Personik, S. D. Photon probe--an optical time domain reflectometer. Bell Syst. Tech. J. 56(3):355-366; 1977 March.

[5] Neumann, E. G. Analysis of the backscattering method for testing optical fiber cables. AEÜ, Electron. and Commun. 34(4):157-160; 1980.

[6] Lin, Shih-Chun; Giallovenzi, T. G. Sensitivity analysis of the Sagnac effect optical fiber ring interferometer. Appl. Opt. 18(6):915-931; 1979 March 15.

[7] Stolen, R. H. Nonlinear properties of optical fibers. Chapter 5 in Optical fiber telecommunications. Miller, S. E.; Chynoweth, A. G., eds. New York, NY: Academic Press; 1979. 125-150.

[8] Papoulis, A. Signal analysis. New York: McGraw-Hill Book Co.; 1977. 431 p.

[9] Danielson, B. L. An assessment of the backscatter technique as a means for estimating loss in optical waveguides. Nat. Bur. Stand. (U.S.) Tech. Note 1018; 1980 February. 76 p.

[10] Conduit, A. J.; Payne, D. N.; Hartog, A. H. Optical fiber backscatter-loss signatures: identification of features and correlation with known defects using the two-channel technique. Proceedings 6th European Conference on Optical Communications; 1980 September 16-19; University of York, United Kingdom. 152-155.

[11] Conduit, A. J.; Hartog, A. H.; Payne, D. N. Spectral- and length-dependent losses in optical fibers investigated by a two-channel backscatter technique. Electron. Lett. 16(3):77-78; 1980 January 31.

[12] Conduit, A. J.; Hullett, J. L.; Hartog, A. H.; Payne, D. N. An optimised technique for backscatter attenuation measurements in optical fibers. Opt. and Quant. Electron. 12(2):169-178; 1980 March.

[13] Danielson, B. L. Backscatter measurements on optical fibers. Nat. Bur. Stand. (U.S.) Tech. Note 1034; 1981 February. 44 p.

[14] Costa, B.; Esposto, F.; D'Orio, C.; Morra, P. Splice loss evaluation by means of the backscattering technique. Electron. Lett. 15(18):550-551; 1979 August 30.

[15] Matthijsse, P.; DeBlok, C. M. Measurement of splice insertion loss using the backscattering method. Proceedings 5th European Conference on Optical Communications; 1979 September 17-19; Amsterdam, Netherlands. 9.5.1-9.5.4.

[16] LeBoutet, A. Contribution to splice loss evaluation by the backscattering technique: a statistical comparison with insertion loss data. Nat. Bur. Stand. (U.S.) Spec. Publ. 597; Technical Digest--Symposium on Optical Fiber Measurements; 1980 October. 77-84.

[17] Matthijsse, P.; DeBlok, C. M. Field measurement of splice loss applying the backscattering method. Electron. Lett. 15(24):795-797; 1979 November 22.

[18] Hillerich, B. On site location of optical fiber defects and evaluation of transmission loss. Proceedings 26th International Wire and Cable Symposium; 1977 November 15-17; Cherry Hill, NJ. 373-379.

[19] DiVita, P.; Rossi, U. Backscatter measurements in optical fibers: separation of power decay from imperfection contribution. Electron. Lett. 15(15):467-469; 1979 July 19.

[20] Inada, K. A new graphical method relating to optical fiber attenuation. Opt. Commun. 19(3):437-439; 1976 December.

[21] Sladen, F. M. E.; Payne, D. N.; Adams, M. J. Definitive profile-dispersion data for germania-doped silica fibres over an extended wavelength range; Electron. Lett. 15(15):469-470; 1979 July 19.

[22] Marcuse, Dietrich. Principles of optical fiber measurements. New York: Academic Press; 1981. 360 p.

[23] Bird, G. J. A. Radar precision and resolution. New York: John Wiley & Sons; 1974. 151 p.

[24] Jones, A. F.; Missel, D. L. The problem of error in deconvolution. J. Phys. A: Gen. Phys. 3:462-472; 1970.

[25] Nahman, N. S.; Guillaume, M. E. Deconvolution of time domain waveforms in the presence of noise. Nat. Bur. Stand. (U.S.) Tech. Note (to be published). 115 p.

[26] Silverman, H. F.; Pearson, A. E. On deconvolution using the discrete Fourier transform. IEEE Trans. Audio Electroacoust. 2(12):112-118; 1973 April.

[27] Hunt, B. R. Deconvolution of linear systems by constrained regression and its relationship to the Wiener theory. IEEE Trans. on Auto. Control 17(5):703-705; 1972 October.

[28] Riad, S. M. Optical fiber dispersion characterization study. NASA Contract #NAS 10-9455, Final Report; 1979 December.

[29] Riad, S. M. Optical fiber impulse response using frequency domain optimal compensation deconvolution. Proceedings Third International Fiber Optics and Communications Exposition; 1980 September 16-18; San Francisco, CA. 210-213.

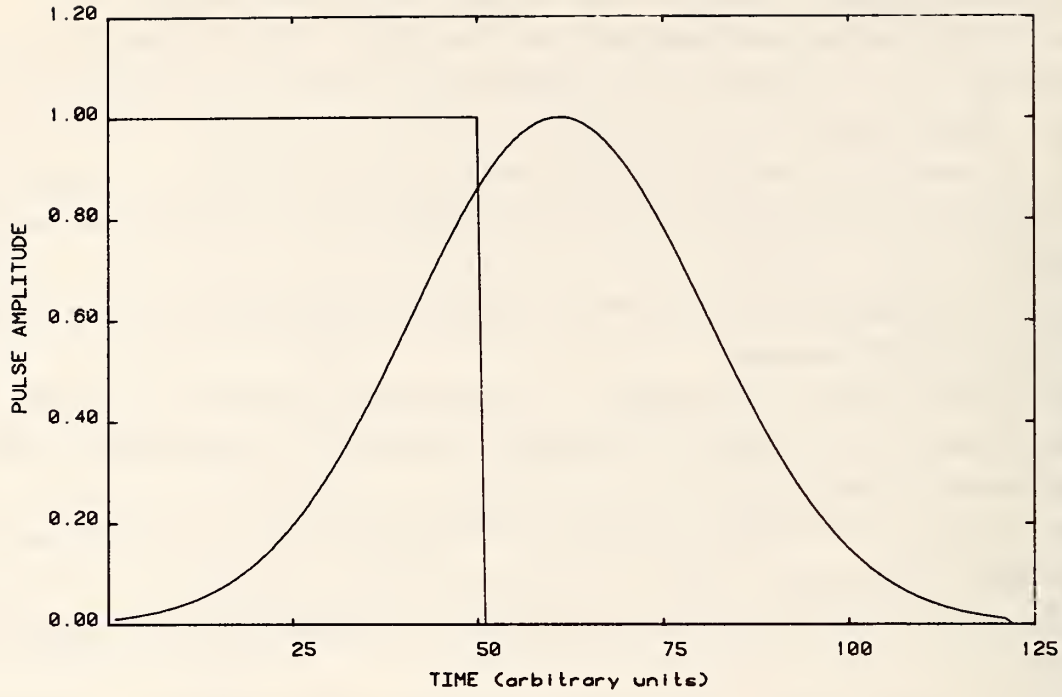

Figure 3-1. Illustration of the concept of equivalent rectangular width.

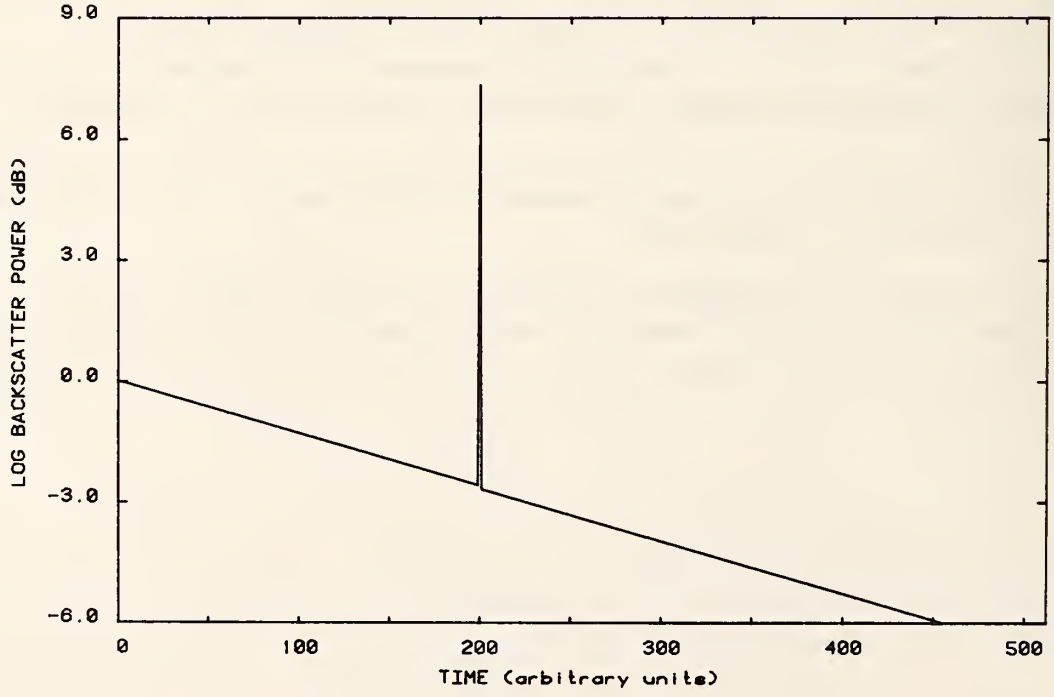

Figure 3-2. The impulse response for a scatter-like imperfection. Logarithmic display.

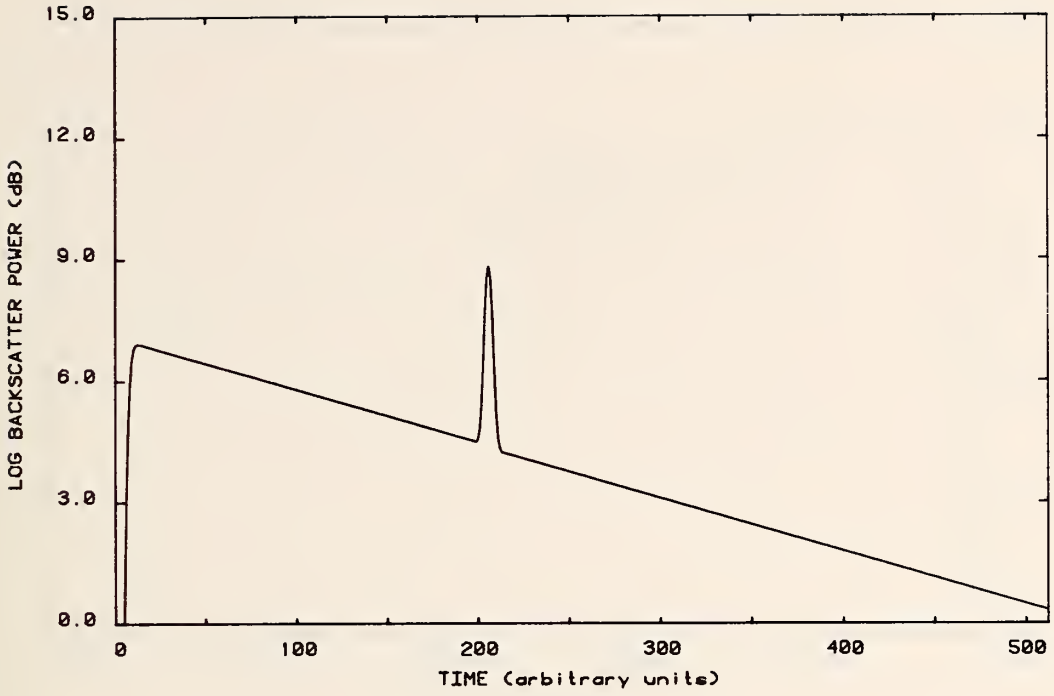

Figure 3-3. Scatter-like imperfection; Gaussian probe pulse; equivalent rectangular width 5 time units. Logarithmic display.

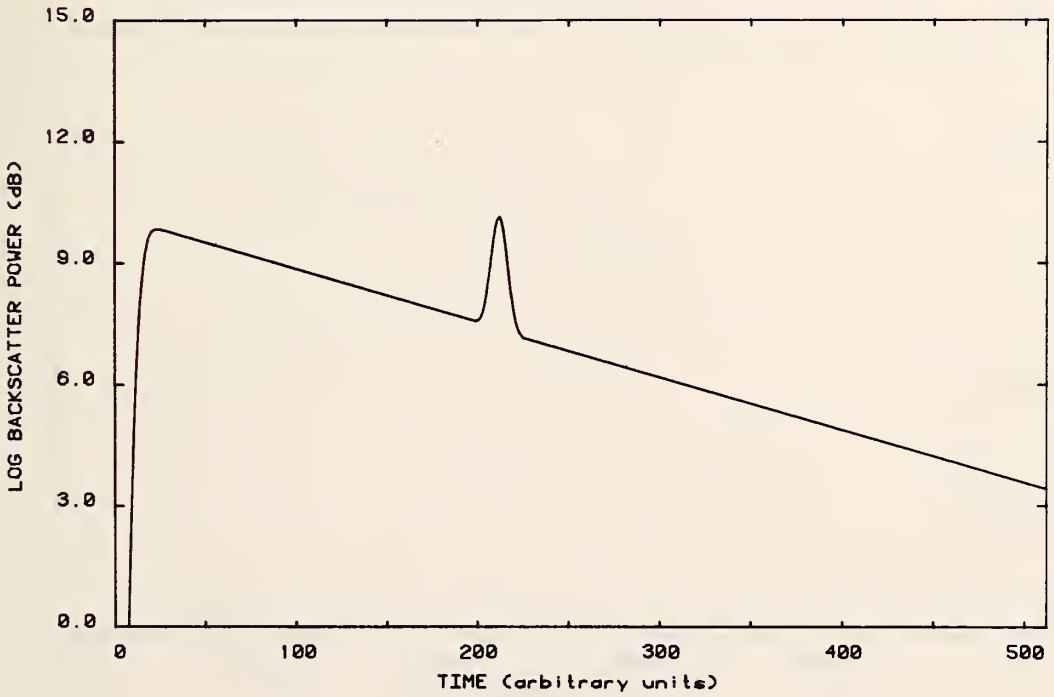

Figure 3-4. Scatter-like imperfection; Gaussian probe pulse; equivalent rectangular width 10 time units. Logarithmic display.

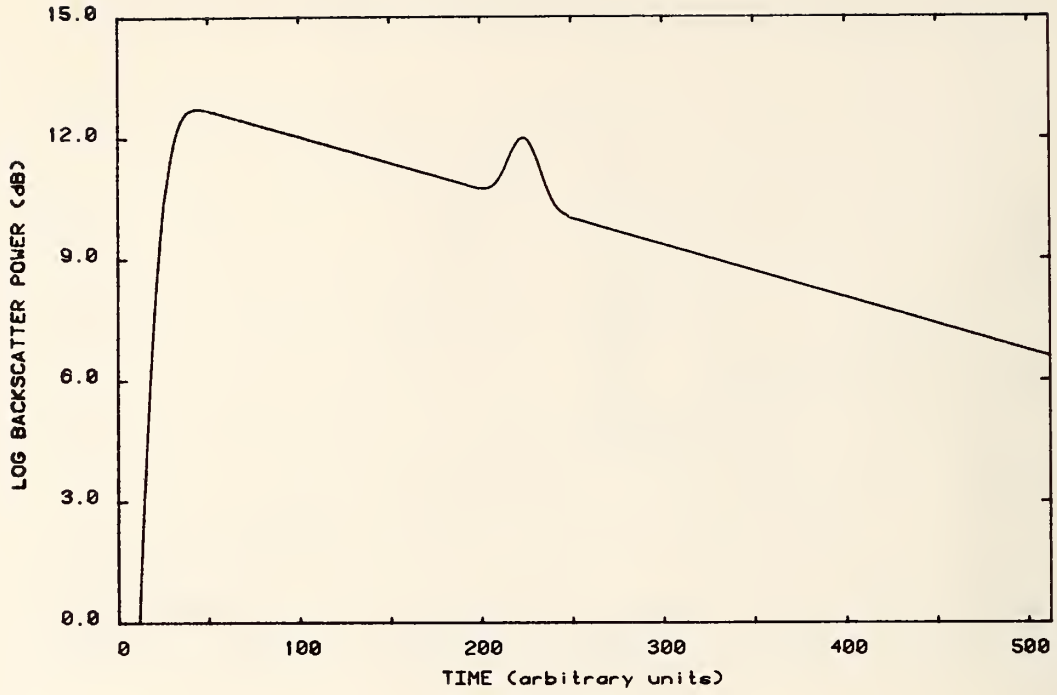

Figure 3-5. Scatter-like imperfection; Gaussian probe pulse; equivalent rectangular width 20 time units. Logarithmic display.

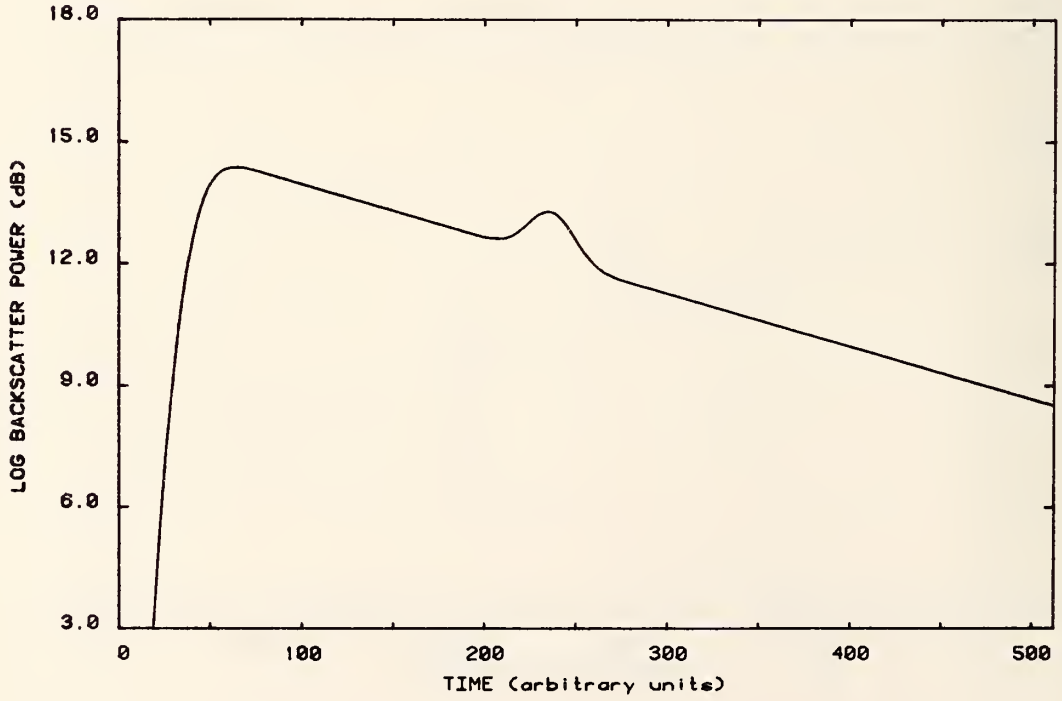

Figure 3-6. Scatter-like imperfection; Gaussian probe pulse; equivalent rectangular width 30 time units. Logarithmic display.

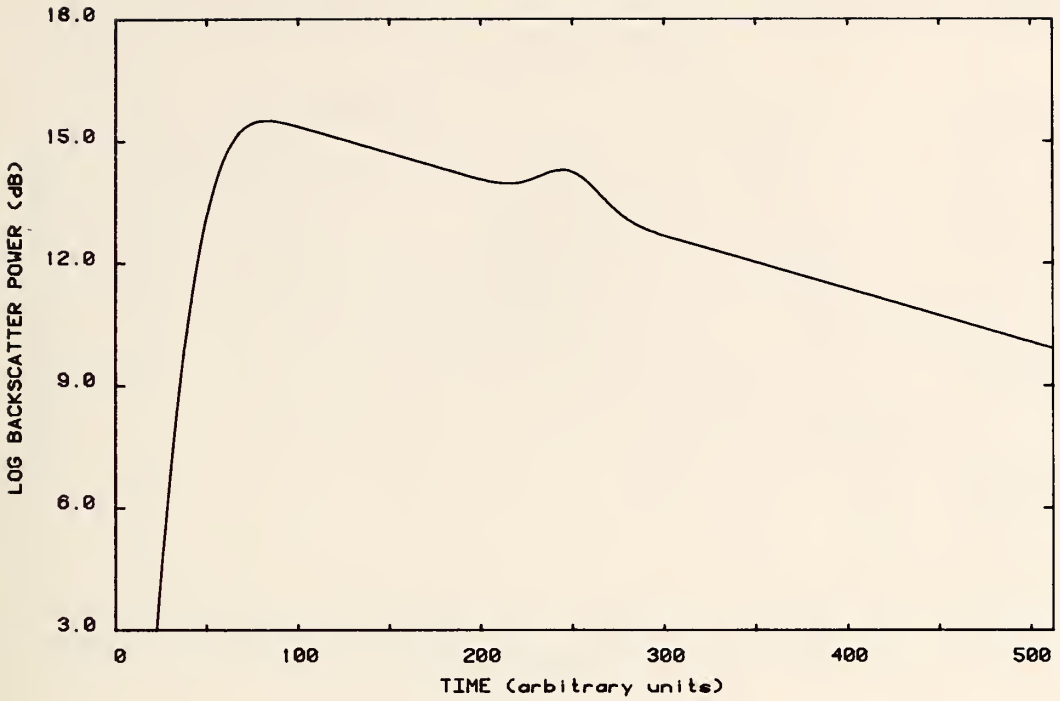

Figure 3-7. Scatter-like imperfection; Gaussian probe pulse; equivalent rectangular width 40 time units. Logarithmic display.

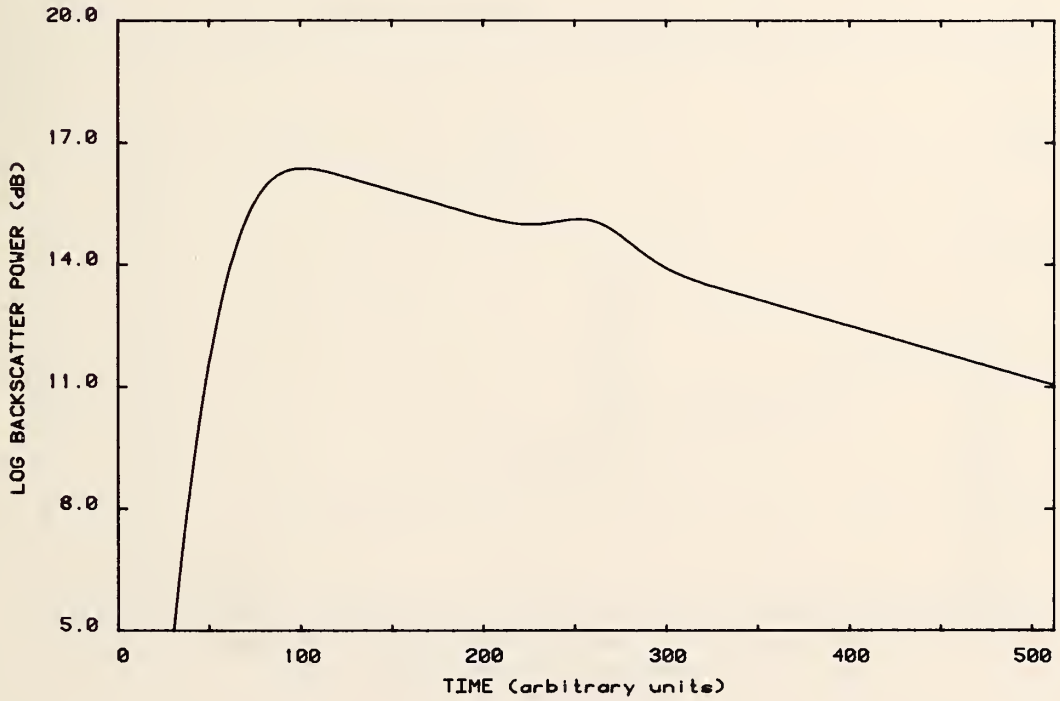

Figure 3-8. Scatter-like imperfection; Gaussian probe pulse; equivalent rectangular width 50 time units. Logarithmic display.

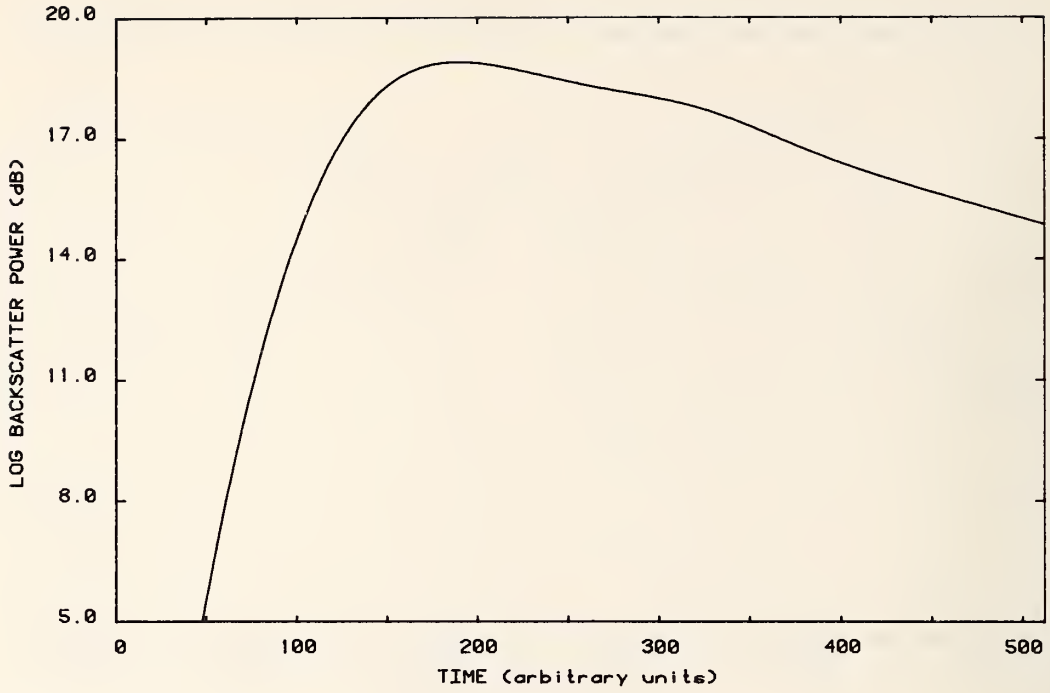

Figure 3-9. Scatter-like imperfection; Gaussian probe pulse; equivalent rectangular width 100 time units. Logarithmic display.

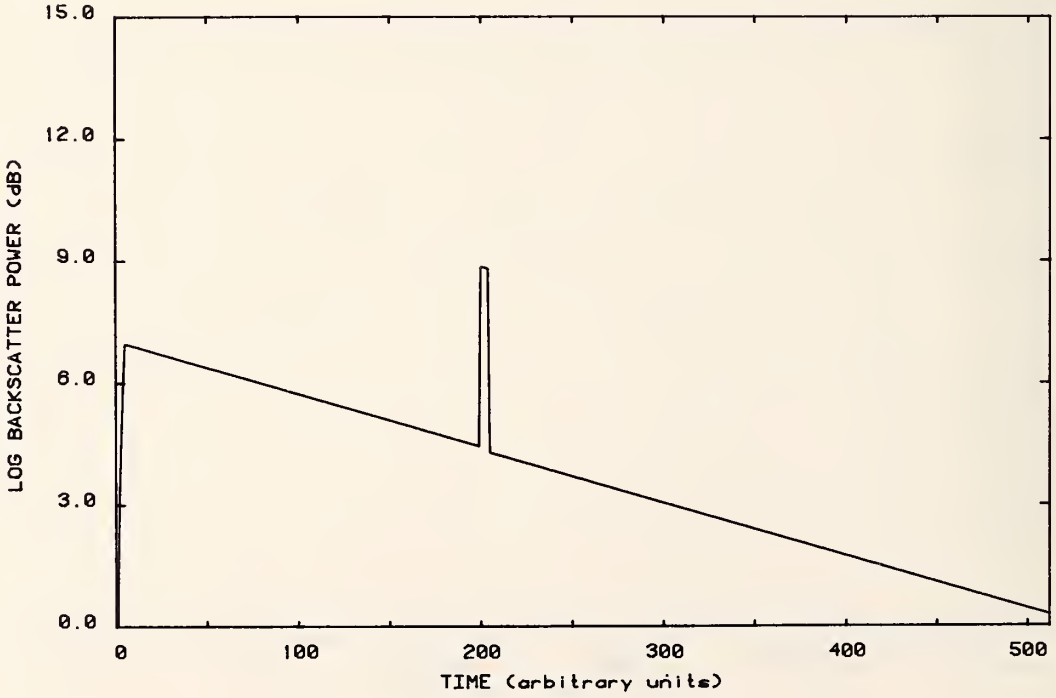

Figure 3-10. Scatter-like imperfection; rectangular probe pulse of width 5 time units. Logarithmic display.

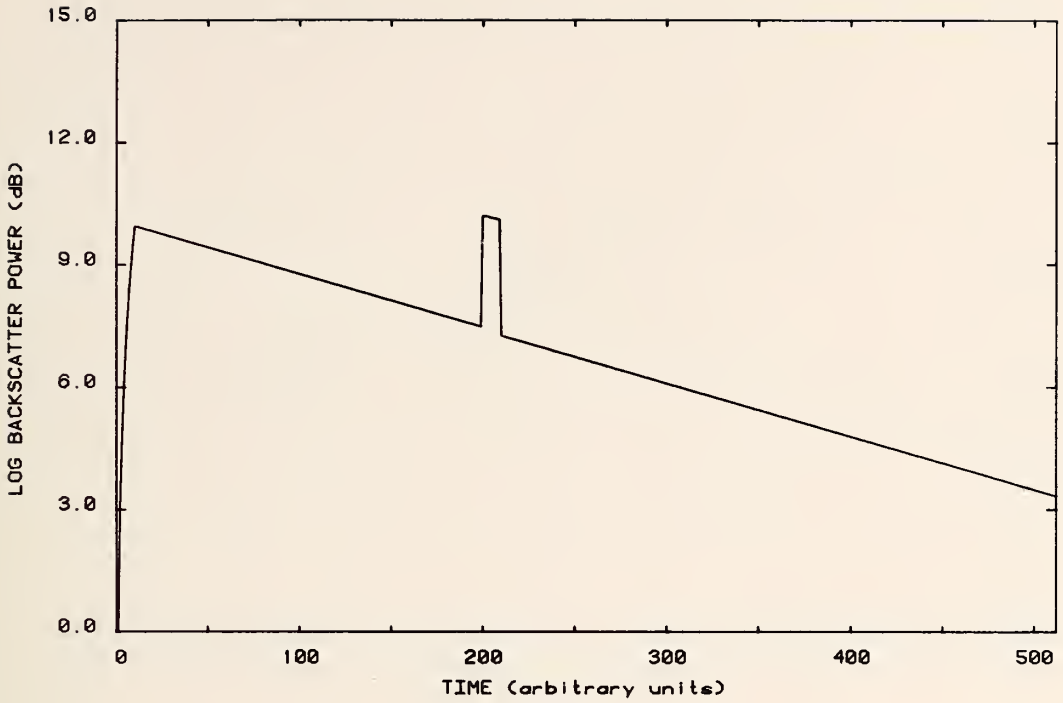

Figure 3-11. Scatter-like imperfection; rectangular probe pulse of width 10 time units. Logarithmic display.

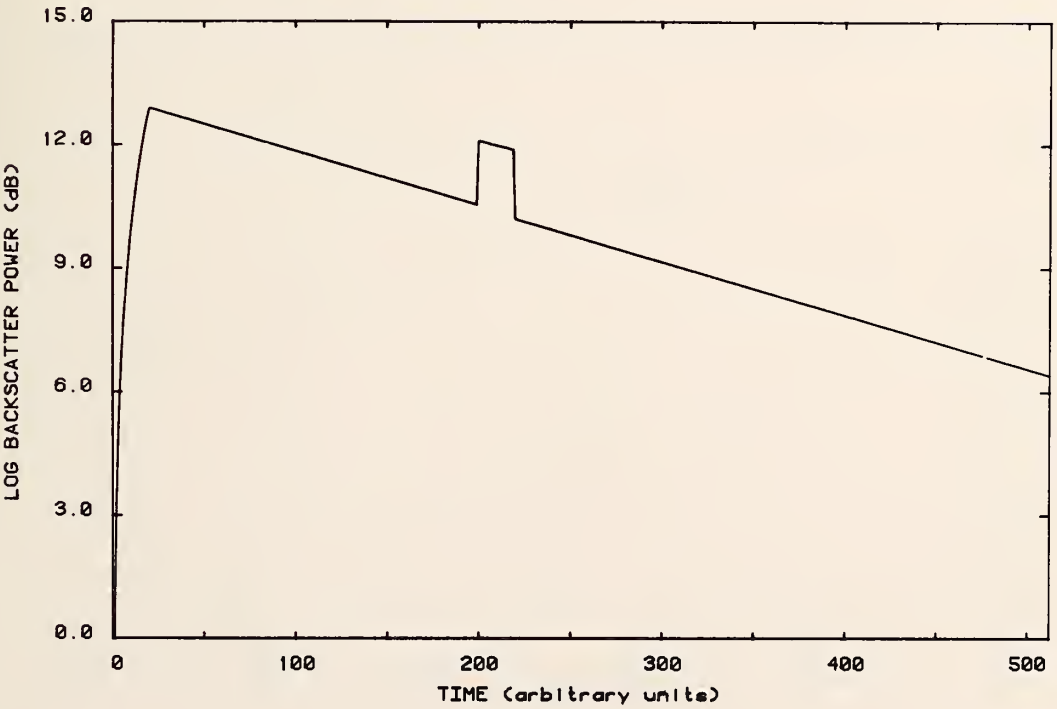

Figure 3-12. Scatter-like imperfection; rectangular probe pulse of width 20 time units. Logarithmic display.

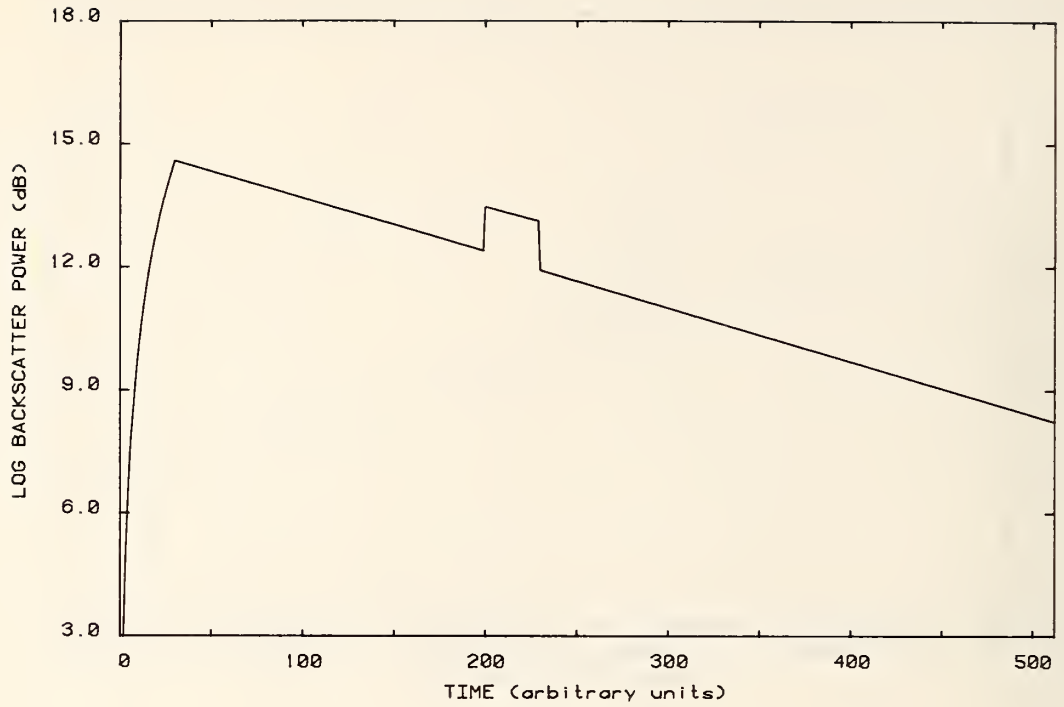

Figure 3-13. Scatter-like imperfection; rectangular probe pulse of width 30 time units. Logarithmic display.

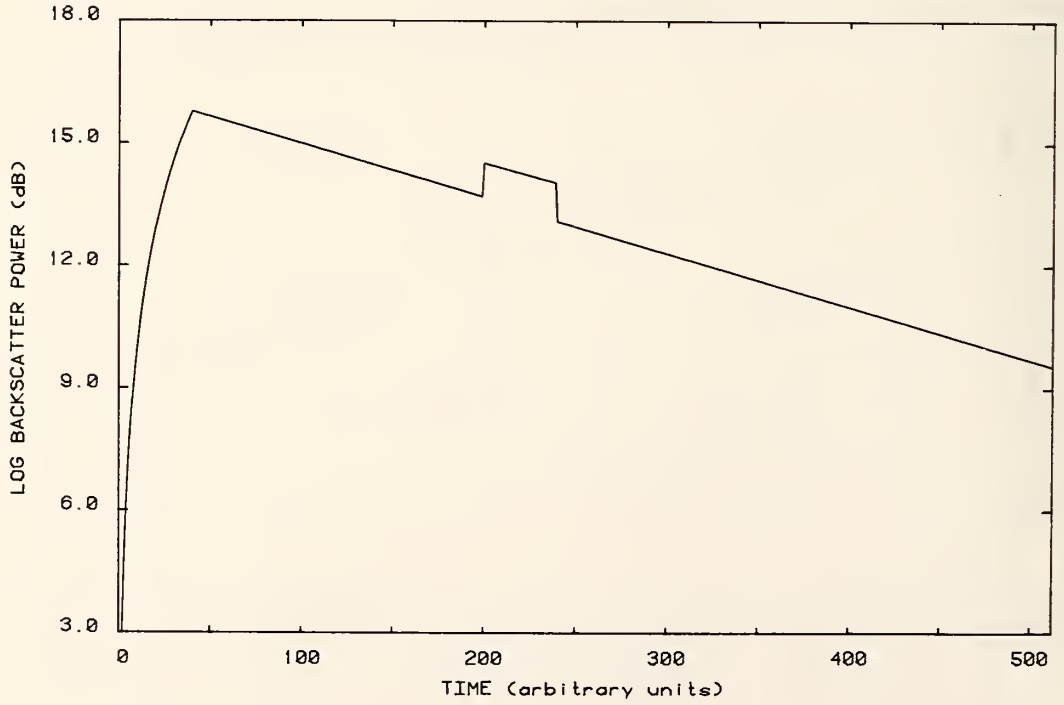

Figure 3-14. Scatter-like imperfection; rectangular probe pulse of width 40 time units. Logarithmic display.

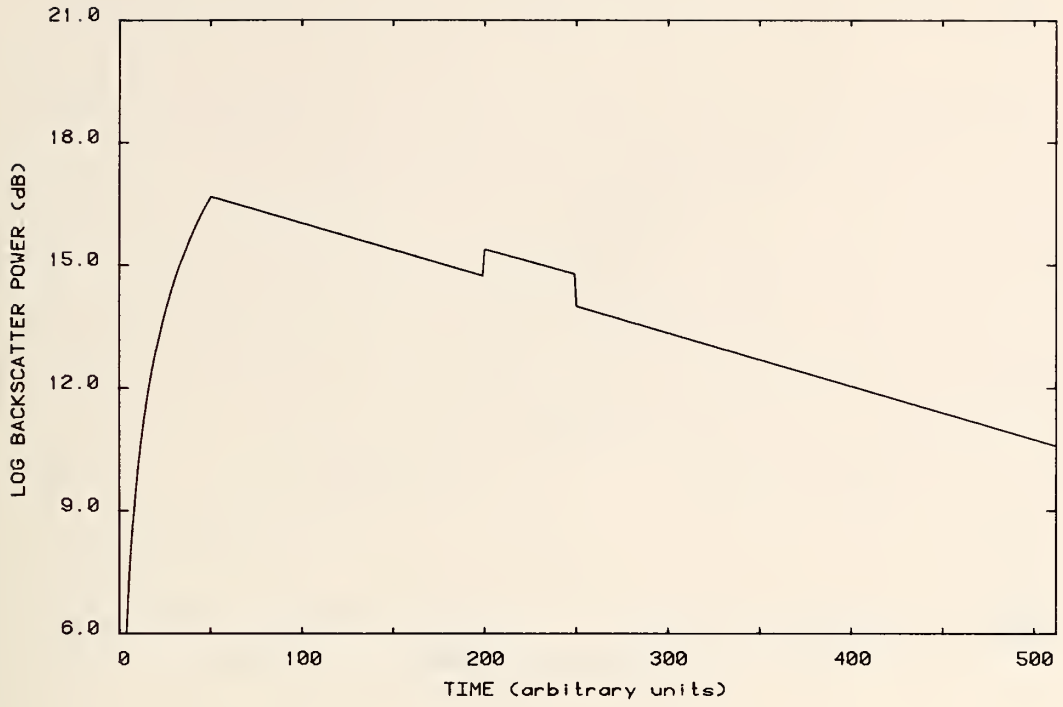

Figure 3-15. Scatter-like imperfection; rectangular probe pulse of width 50 time units. Logarithmic display.

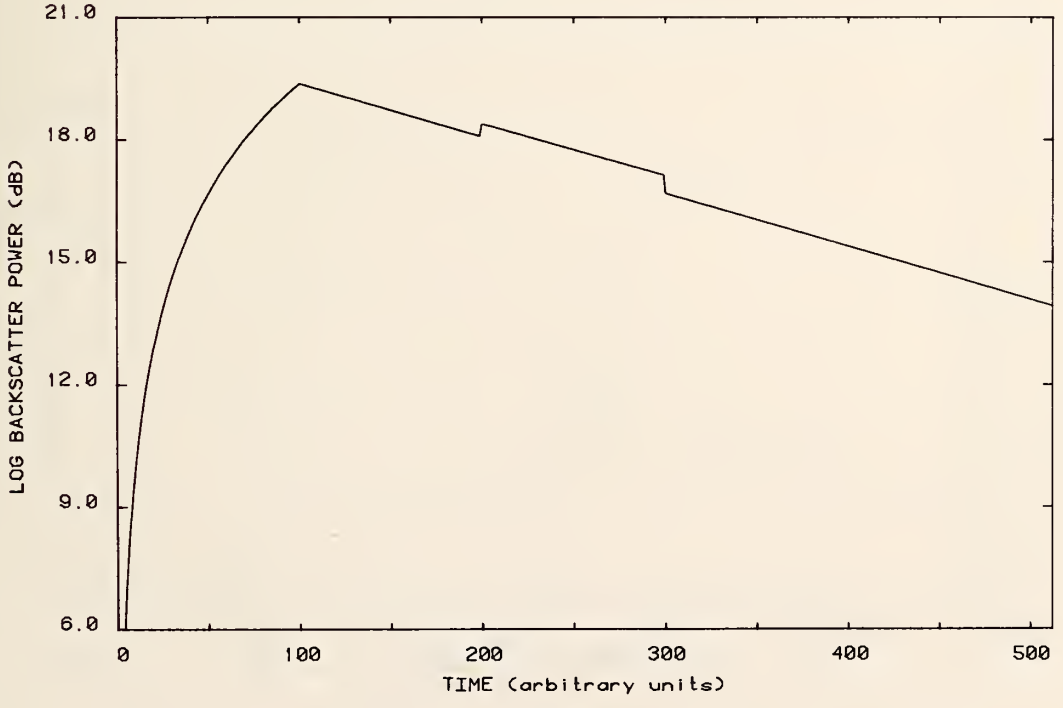

Figure 3-16. Scatter-like imperfection; rectangular probe pulse of width 100 time units. Logarithmic display.

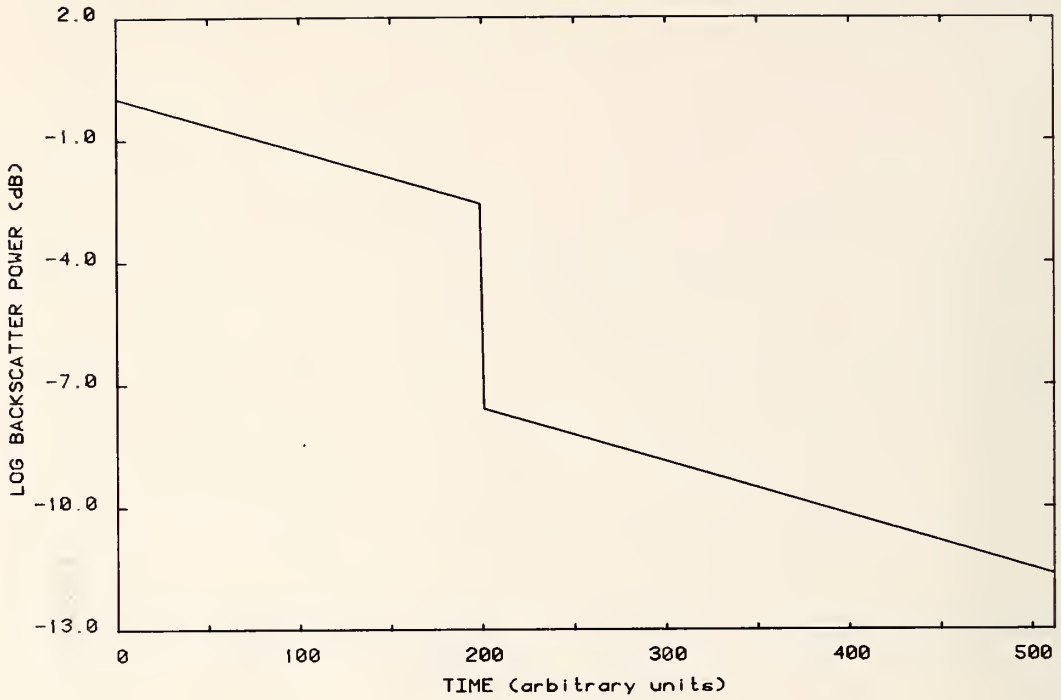

Figure 3-17. The impulse response for an absorption-like imperfection. Logarithmic display.

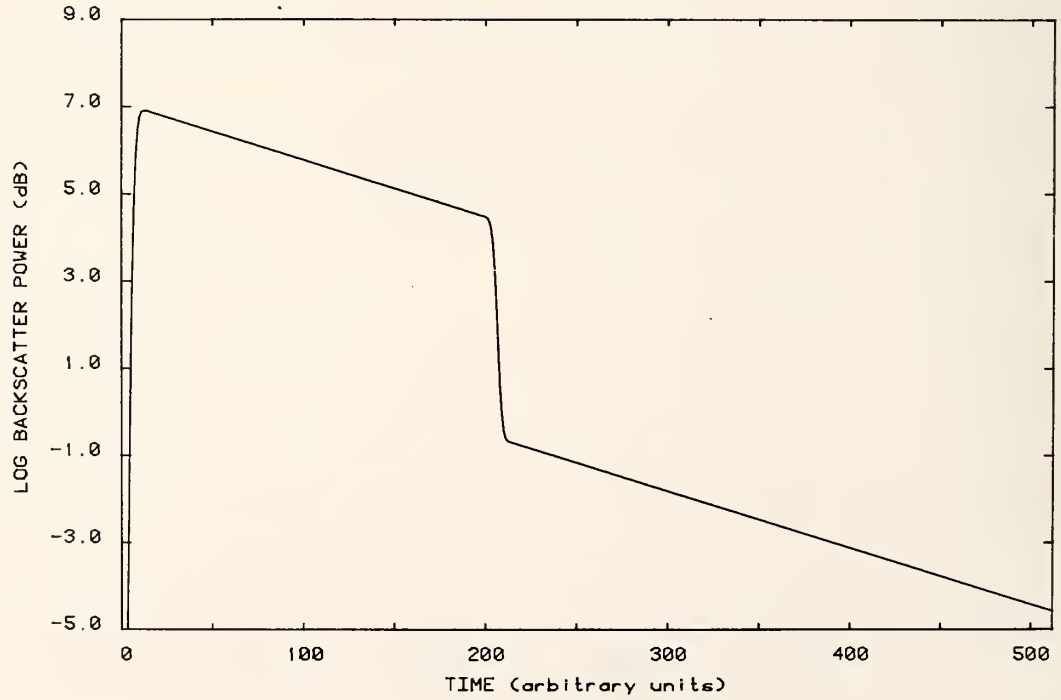

Figure 3-18. Absorption-like imperfection; Gaussian probe pulse; equivalent rectangular width 5 time units. Logarithmic display.

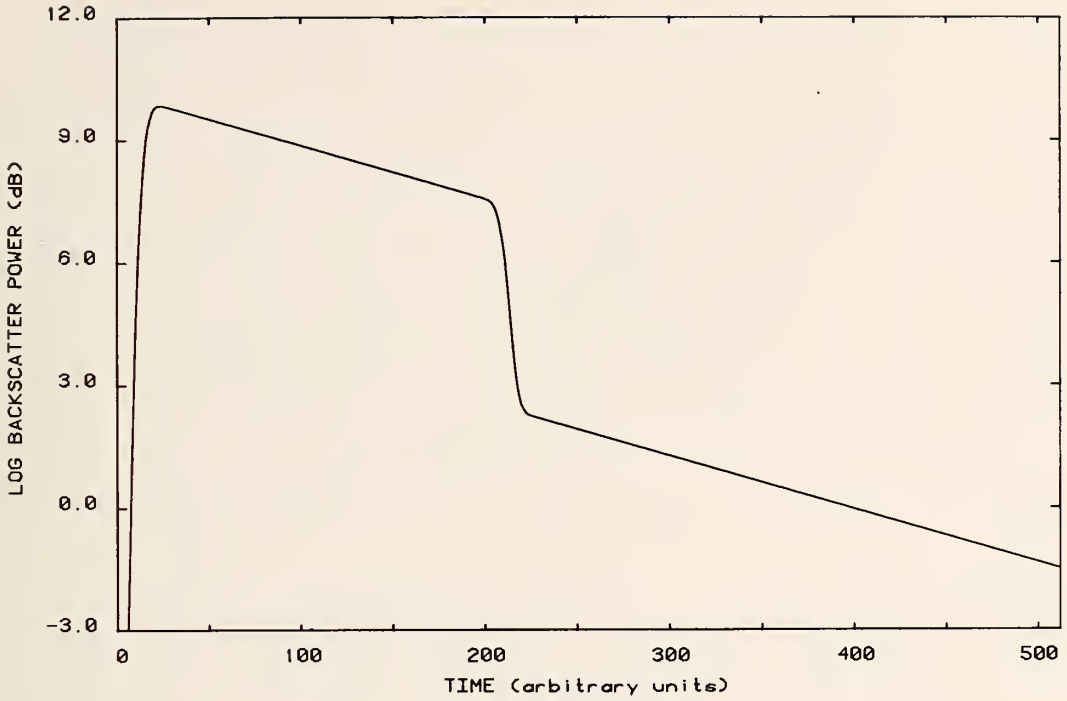

Figure 3-19. Absorption-like imperfection; Gaussian probe pulse; equivalent rectangular width 10 time units. Logarithmic display.

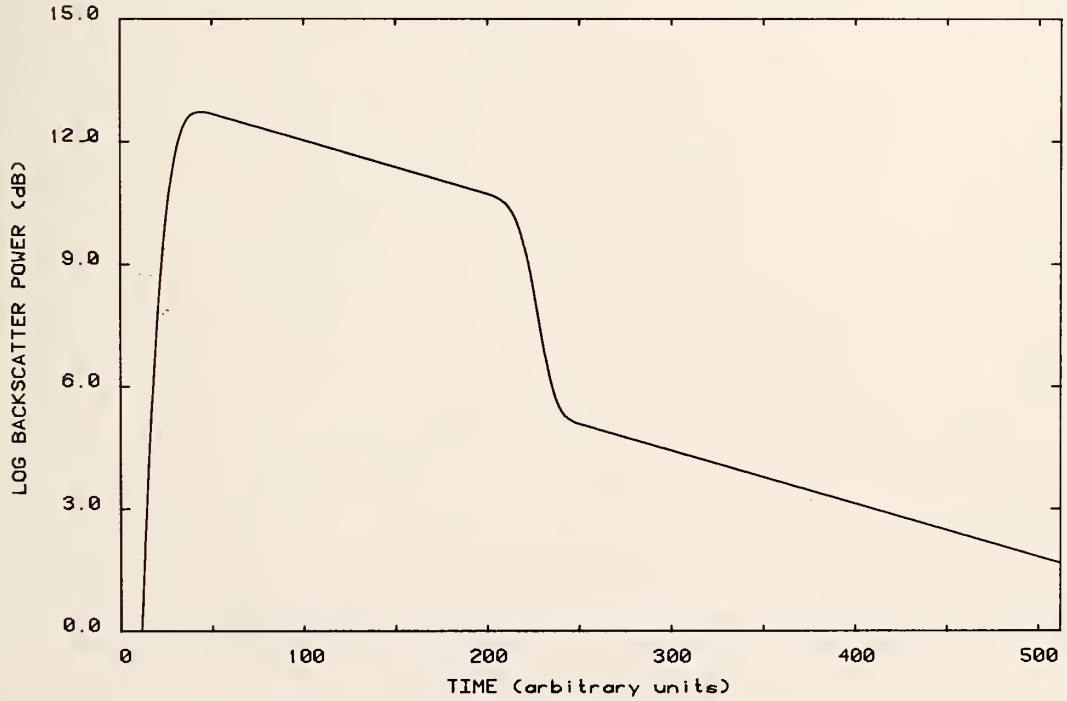

Figure 3-20. Absorption-like imperfection; Gaussian probe pulse; equivalent rectangular width 20 time units. Logarithmic display.

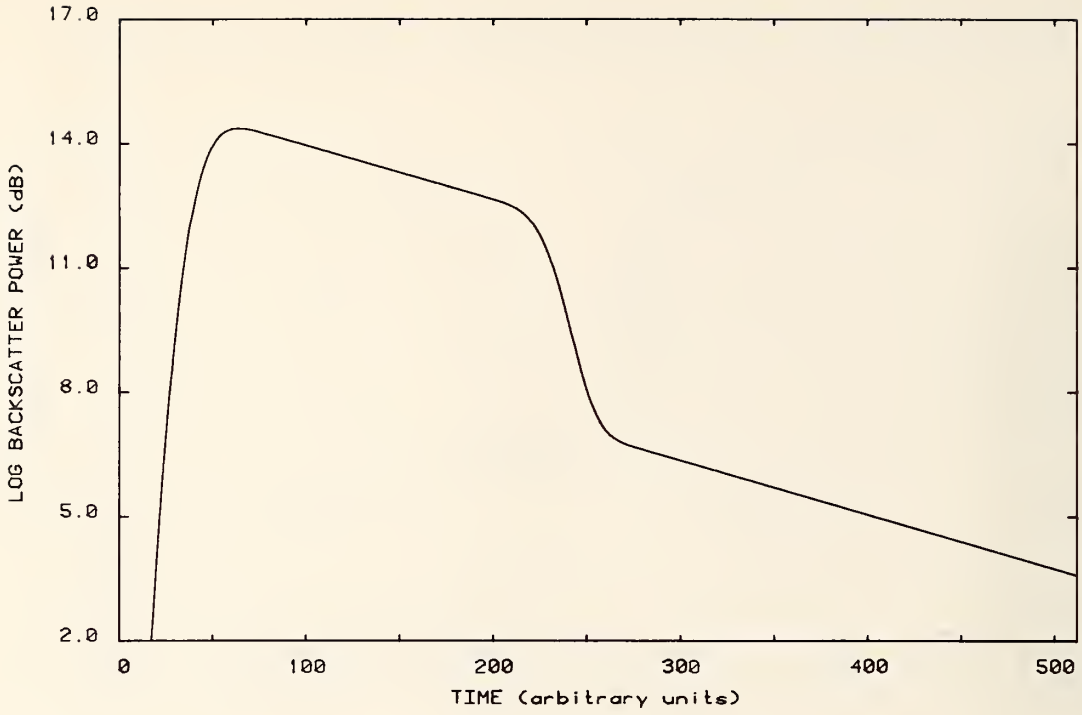

Figure 3-21. Absorption-like imperfection; Gaussian probe pulse; equivalent rectangular width 30 time units. Logarithmic display.

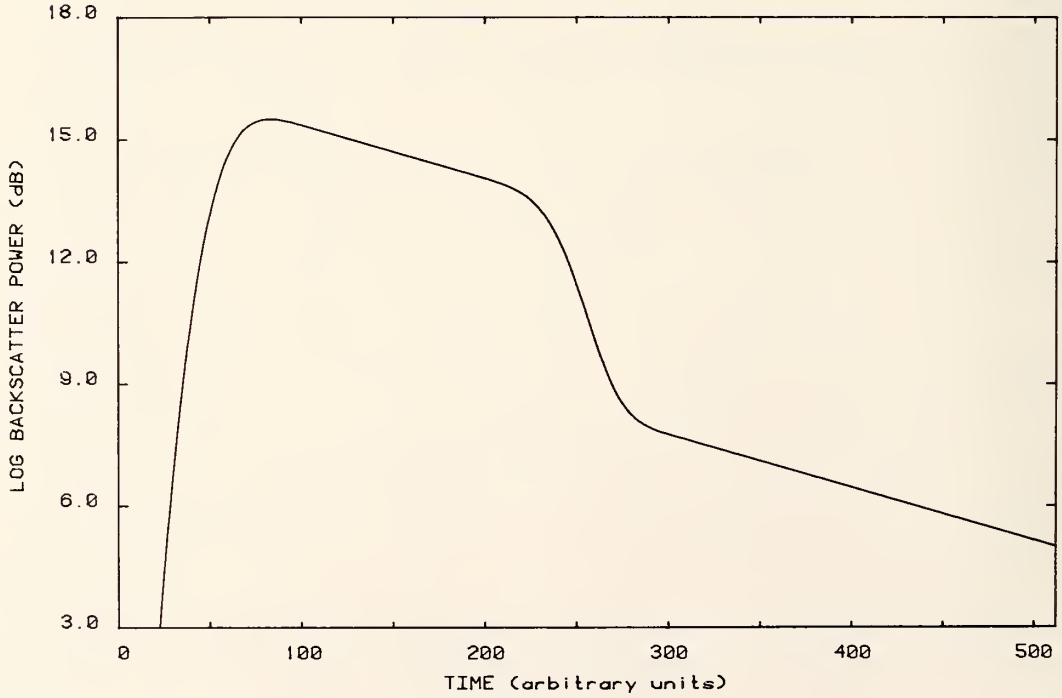

Figure 3-22. Absorption-like imperfection; Gaussian probe pulse; equivalent rectangular width 40 time units. Logarithmic display.

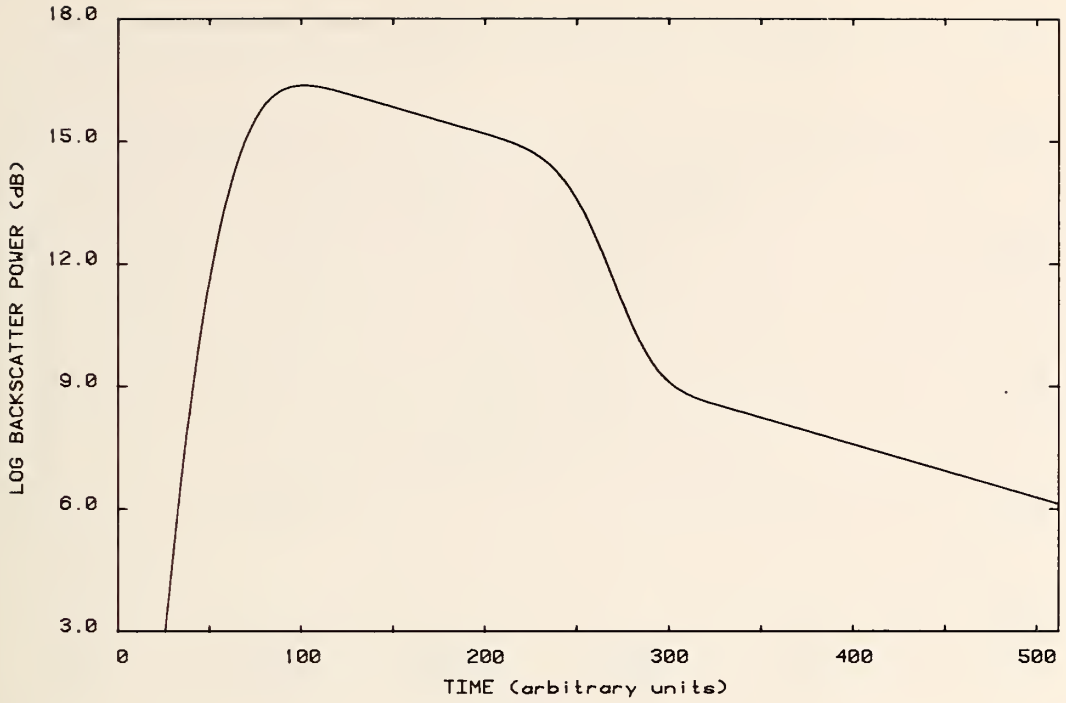

Figure 3-23. Absorption-like imperfection; Gaussian probe pulse; equivalent rectangular width 50 time units. Logarithmic display.

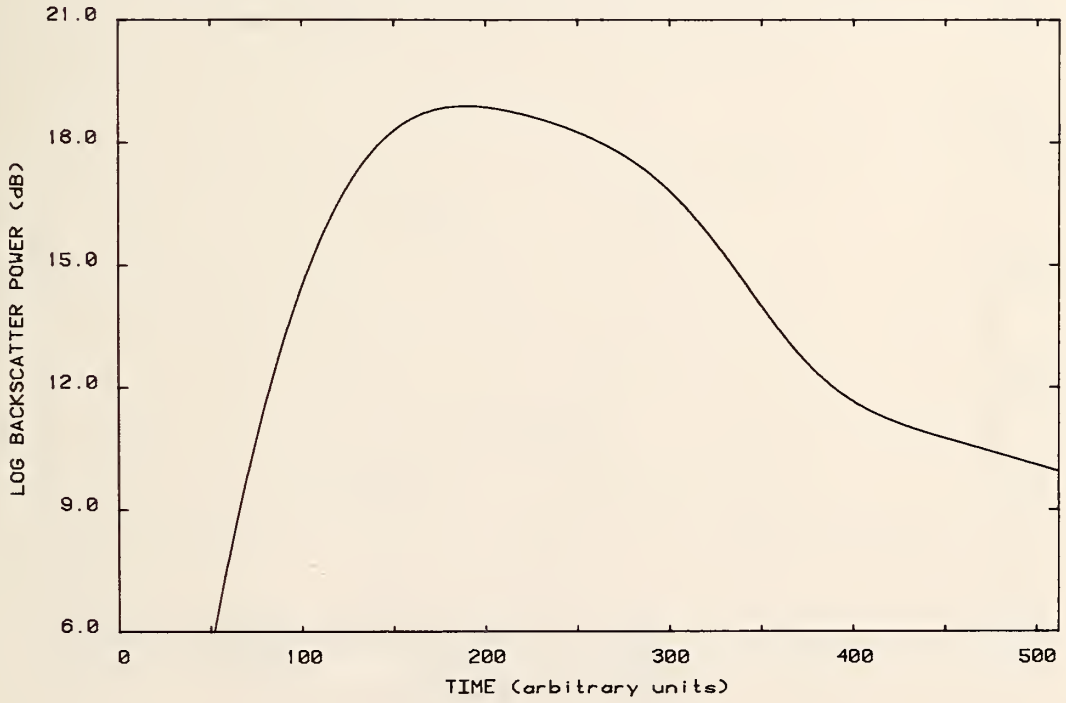

Figure 3-24. Absorption-like imperfection; Gaussian probe pulse; equivalent rectangular width 100 time units. Logarithmic display.

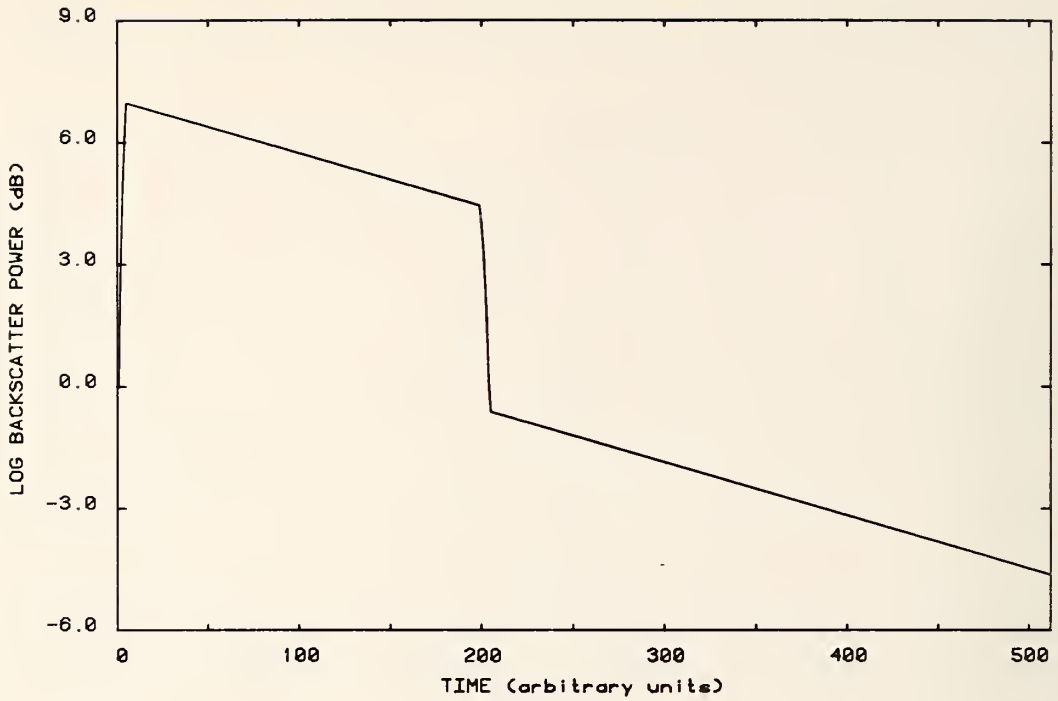

Figure 3-25. Absorption-like imperfection; rectangular probe pulse of width 5 time units.

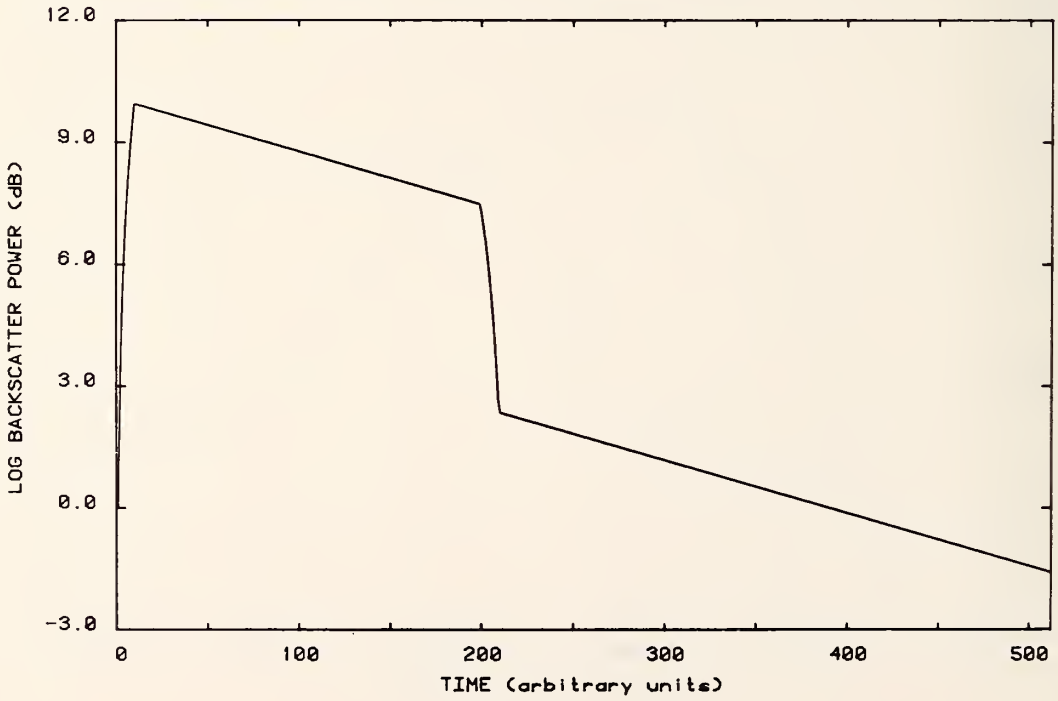

Figure 3-26. Absorption-like imperfection; rectangular probe pulse of width 10 time units. Logarithmic display.

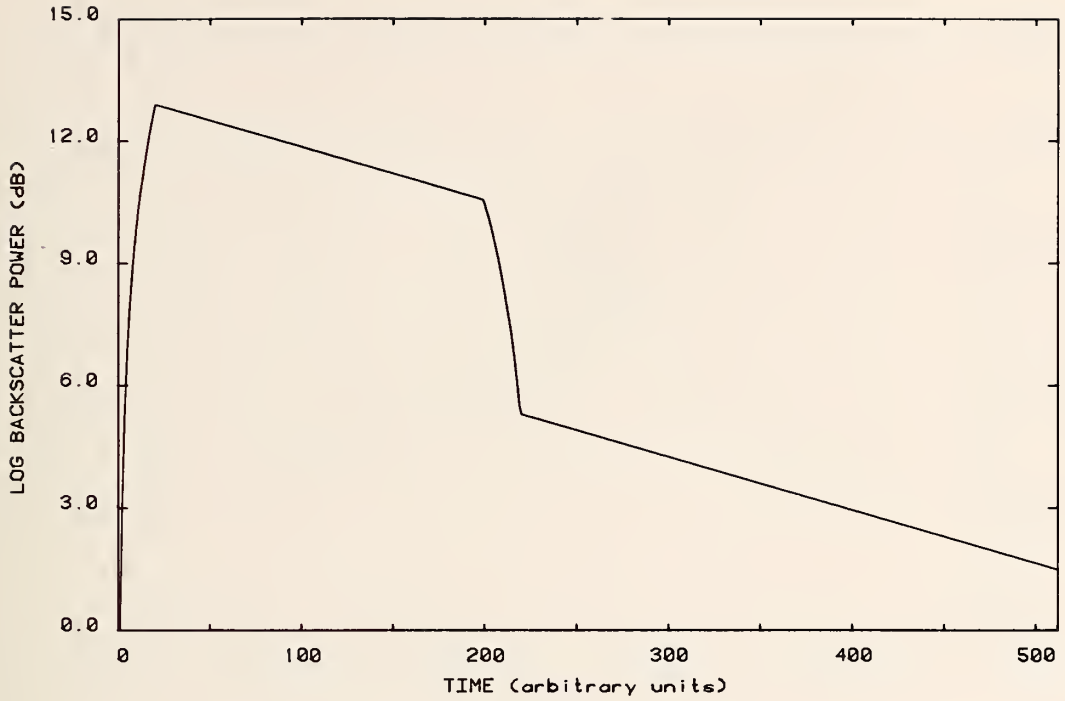

Figure 3-27. Absorption-like imperfection; rectangular probe pulse of width 20 time units. Logarithmic display.

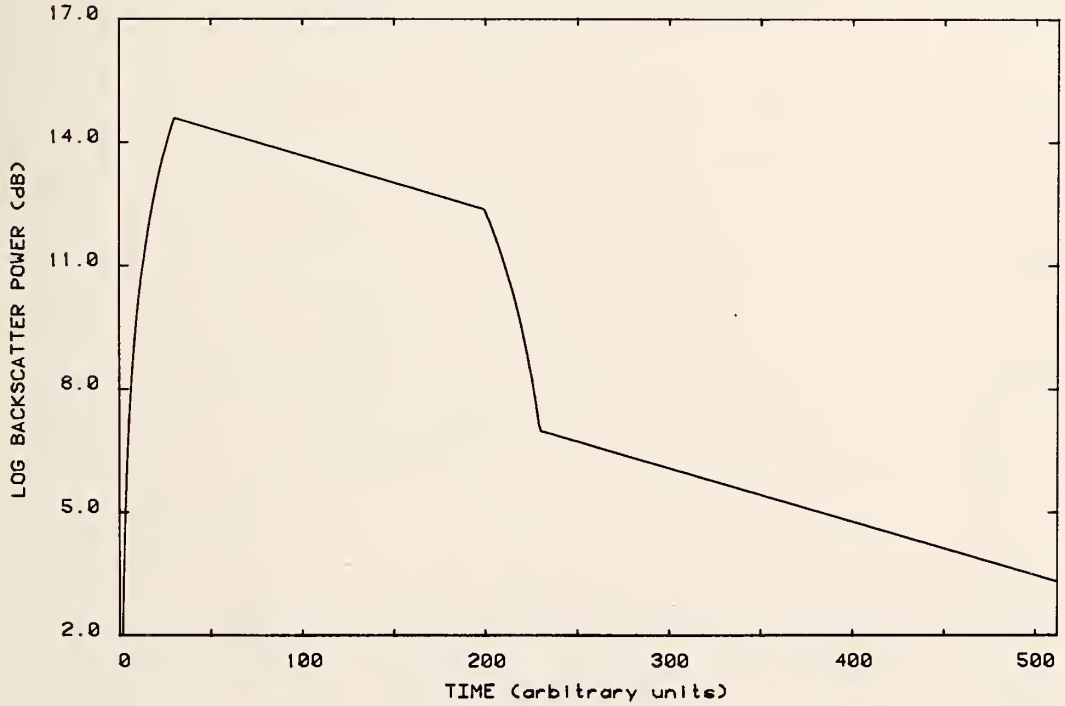

Figure 3-28. Absorption-like imperfection; rectangular probe pulse of width 30 time units. Logarithmic display.

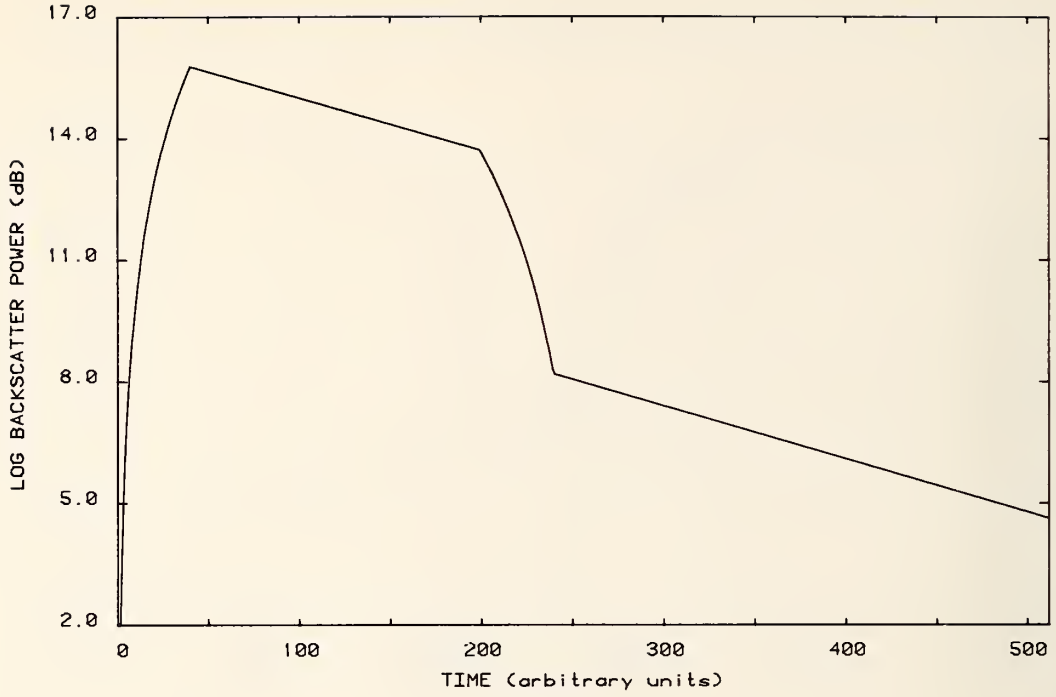

Figure 3-29. Absorption-like imperfection; rectangular probe pulse of width 40 time units. Logarithmic display.

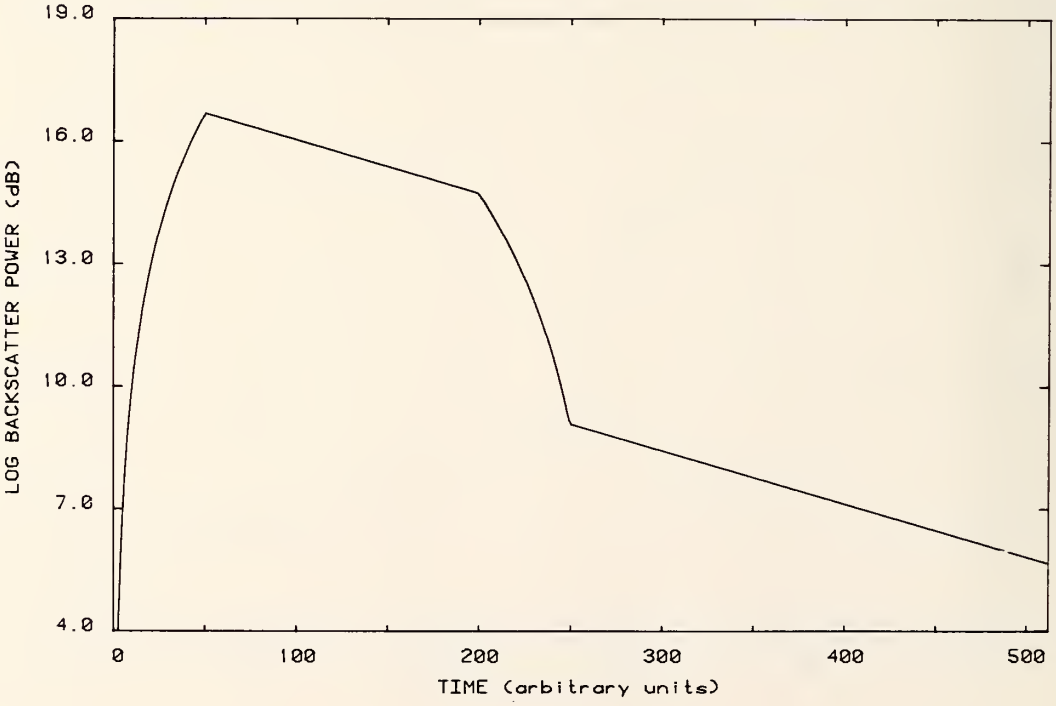

Figure 3-30. Absorption-like imperfection; rectangular probe pulse of width 50 time units. Logarithmic display.

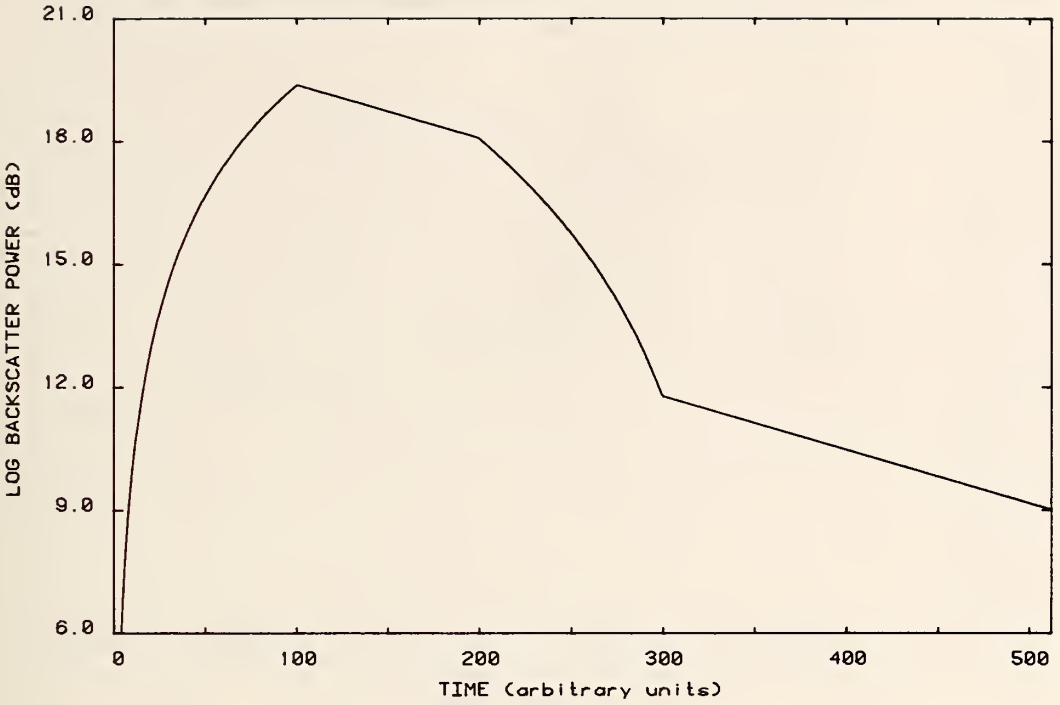

Figure 3-31. Absorption-like imperfection; rectangular probe pulse of width 100 time units. Logarithmic display.

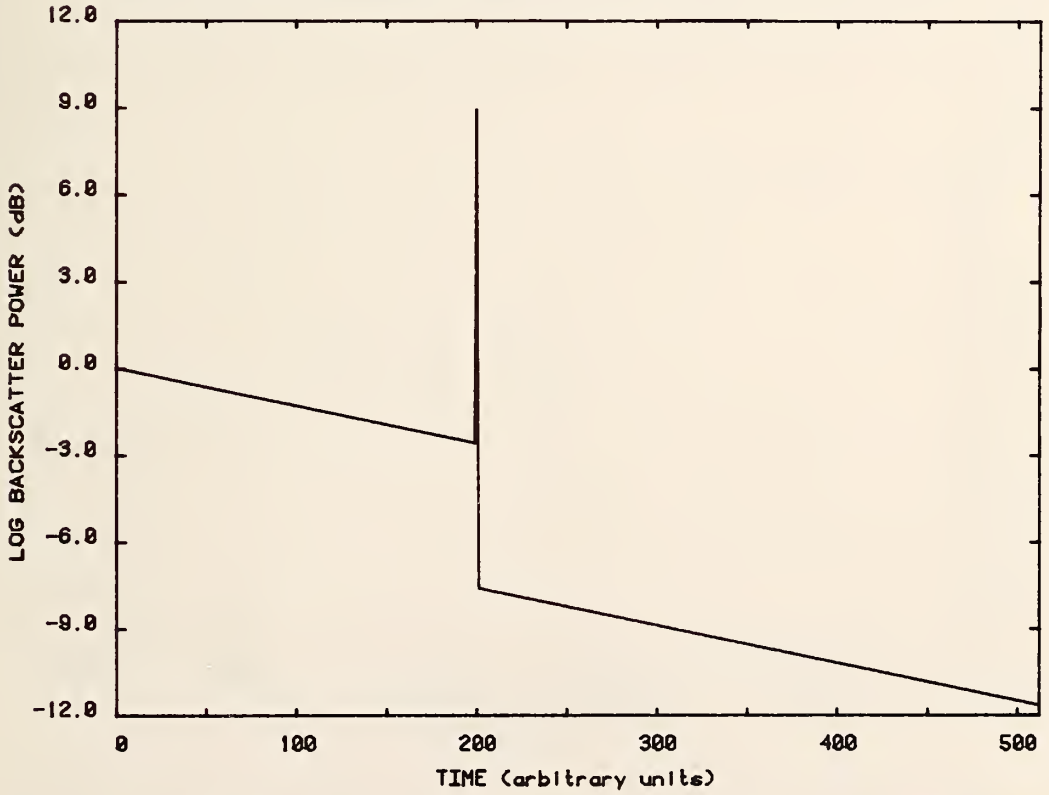

Figure 3-32. The impulse response for a composite imperfection. Logarithmic display.

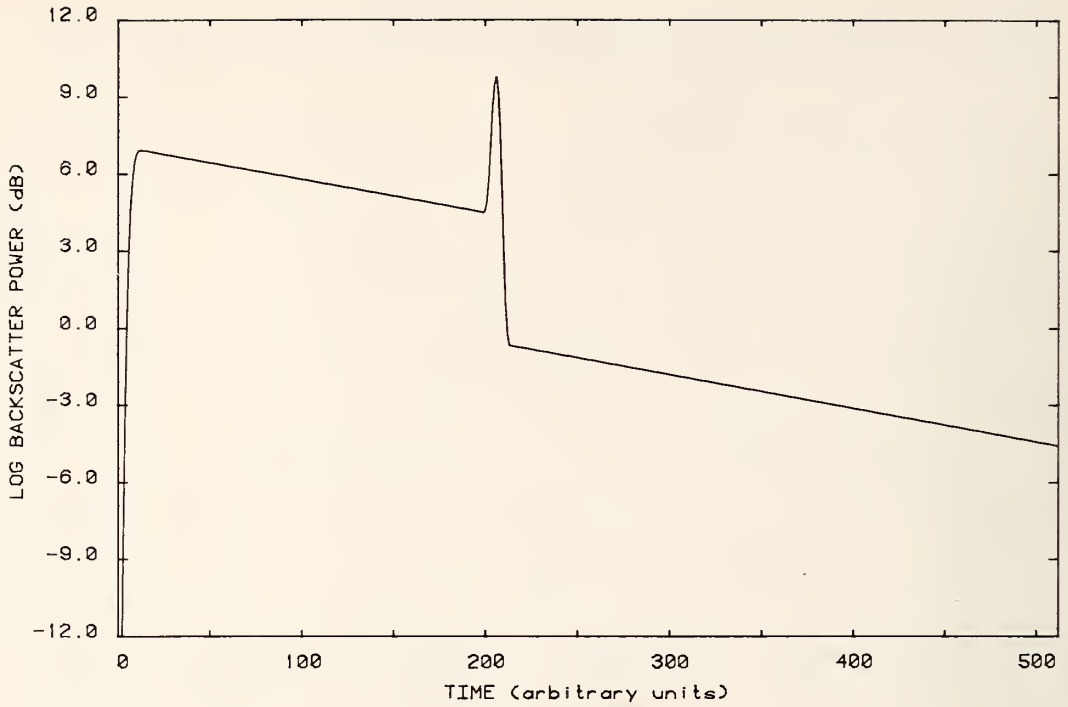

Figure 3-33. Composite imperfection; Gaussian probe pulse; equivalent rectangular width 5 time units. Logarithmic display.

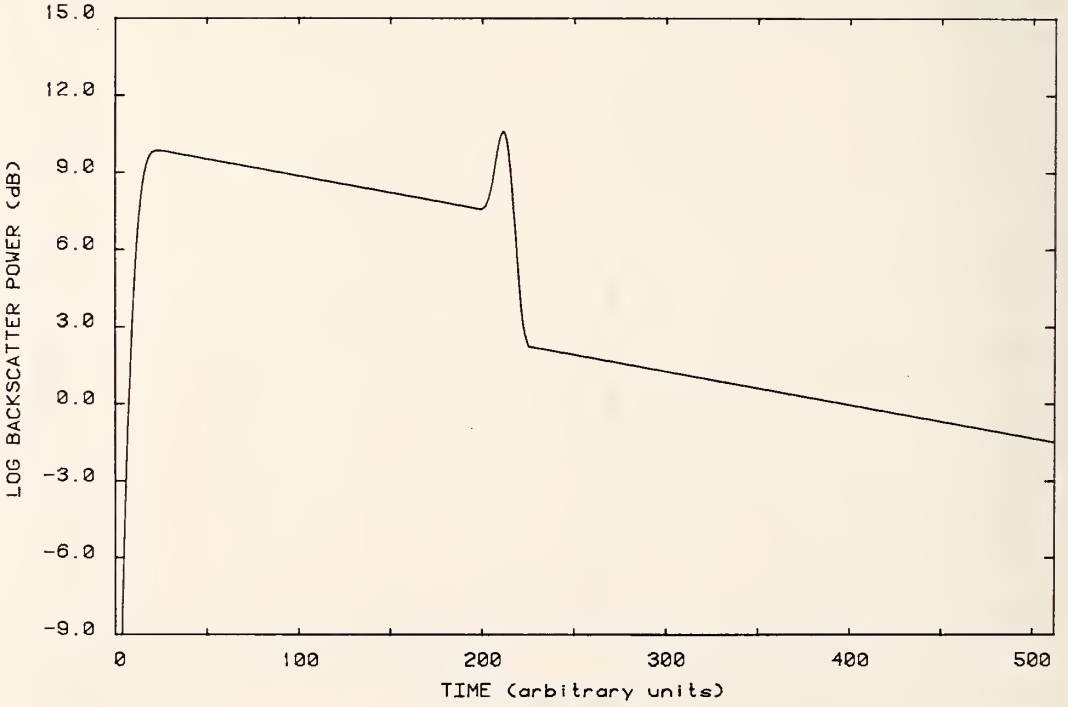

Figure 3-34. Composite imperfection; Gaussian probe pulse; equivalent rectangular width 10 time units. Logarithmic display.

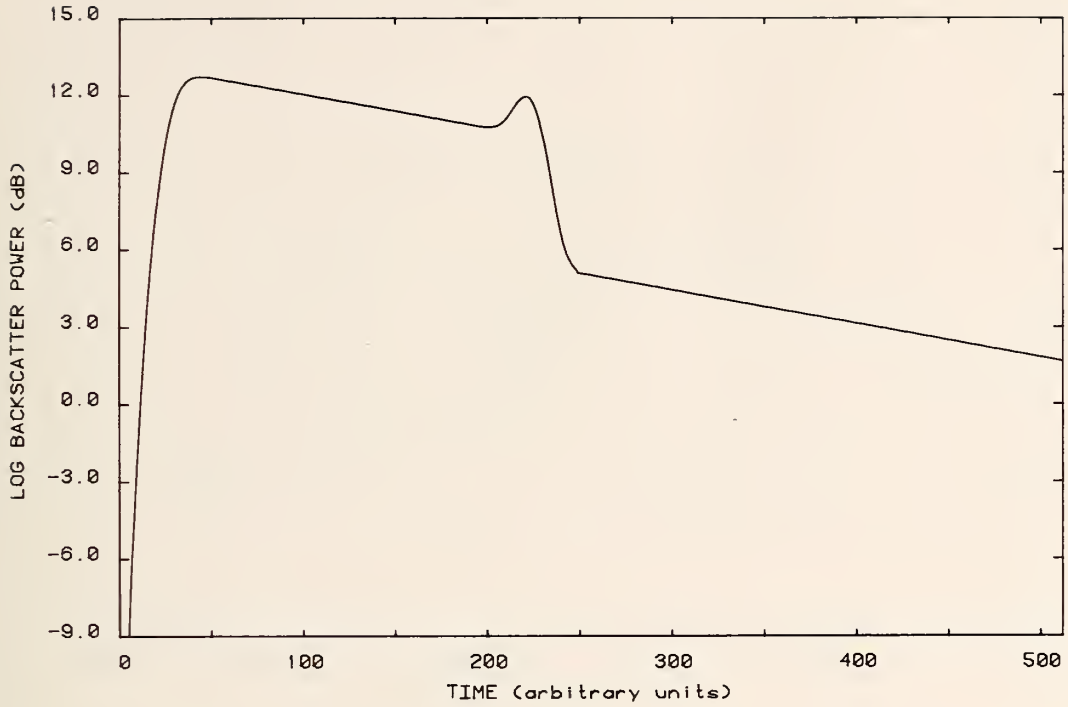

Figure 3-35. Composite imperfection; Gaussian probe pulse; equivalent rectangular width 20 time units. Logarithmic display.

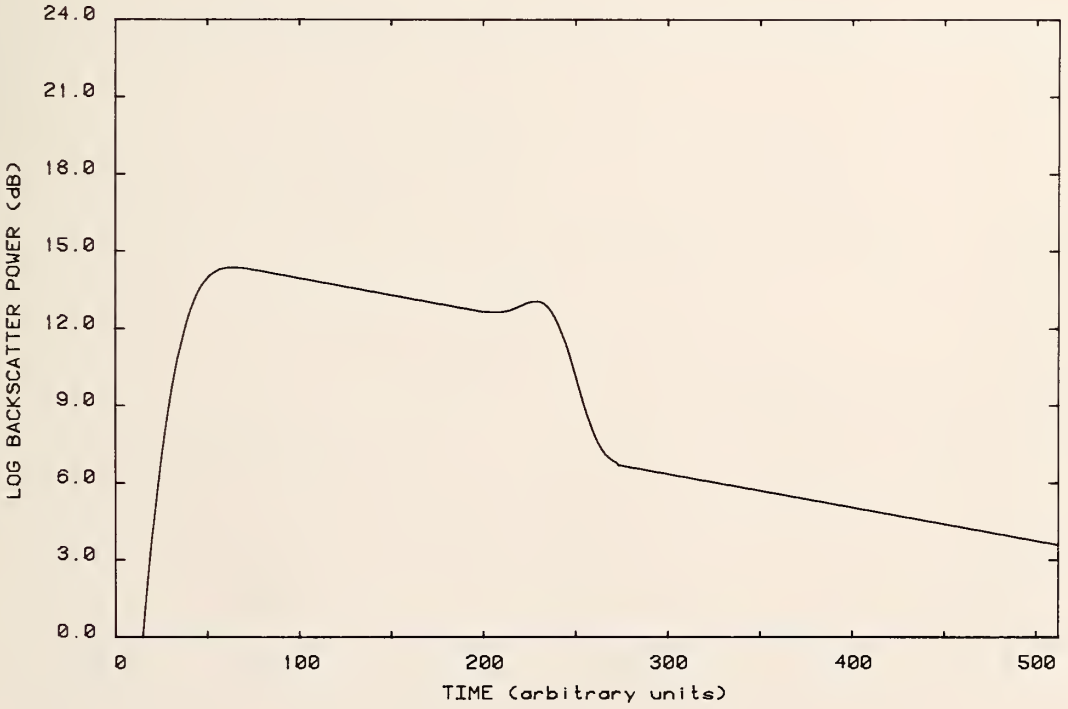

Figure 3-36. Composite imperfection; Gaussian probe pulse; equivalent rectangular width 30 time units. Logarithmic display.

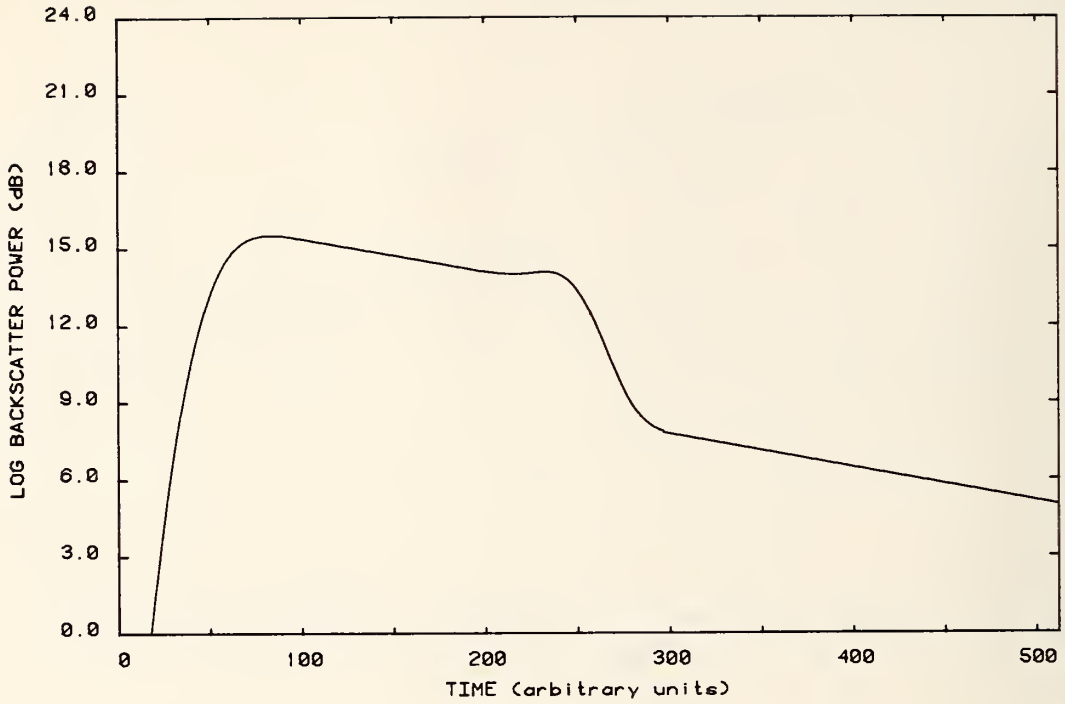

Figure 3-37. Composite imperfection; Gaussian probe pulse; equivalent rectangular width 40 time units. Logarithmic display.

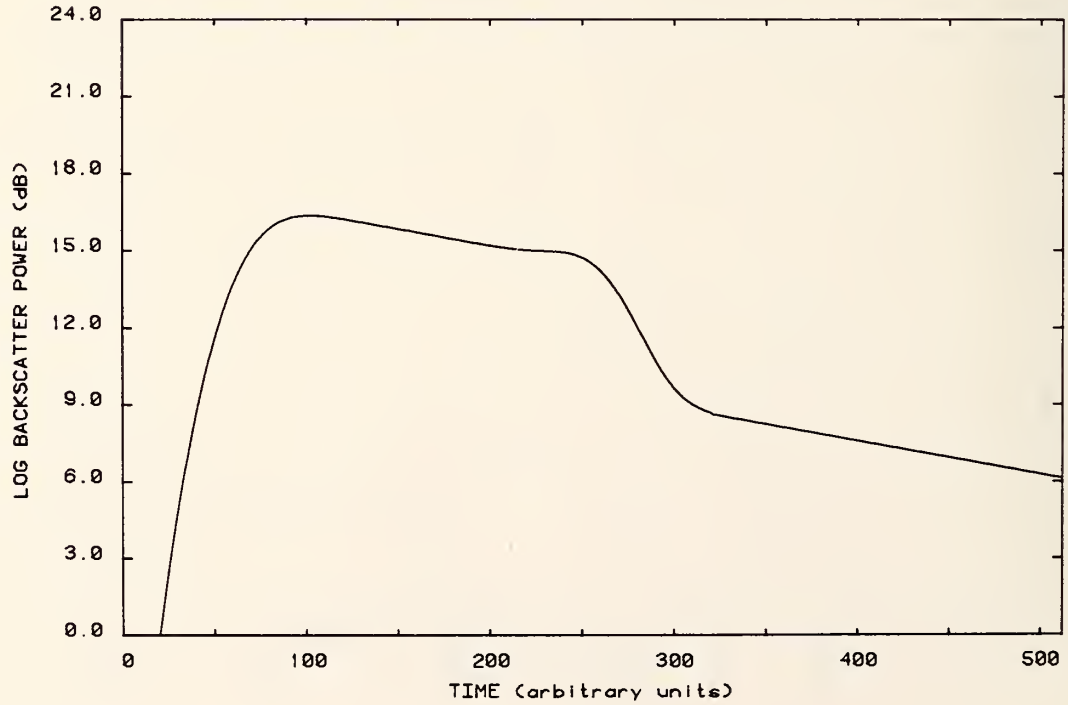

Figure 3-38. Composite imperfection; Gaussian probe pulse; equivalent rectangular width 50 time units. Logarithmic display.

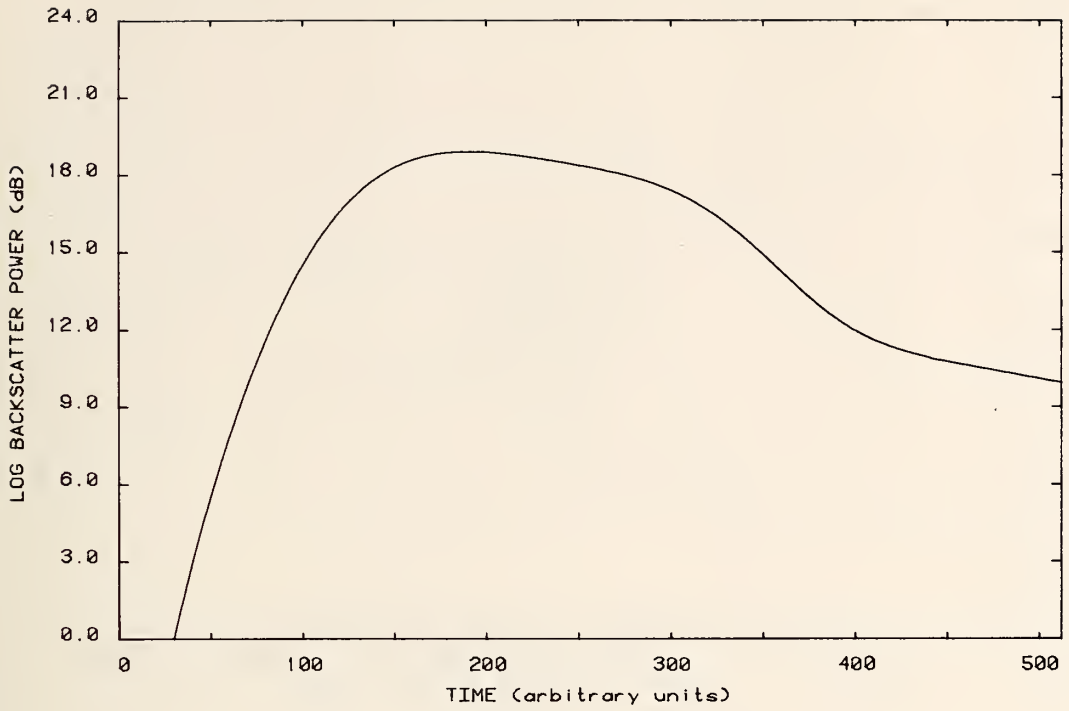

Figure 3-39. Composite imperfection; Gaussian probe pulse; equivalent rectangular width 100 time units. Logarithmic display.

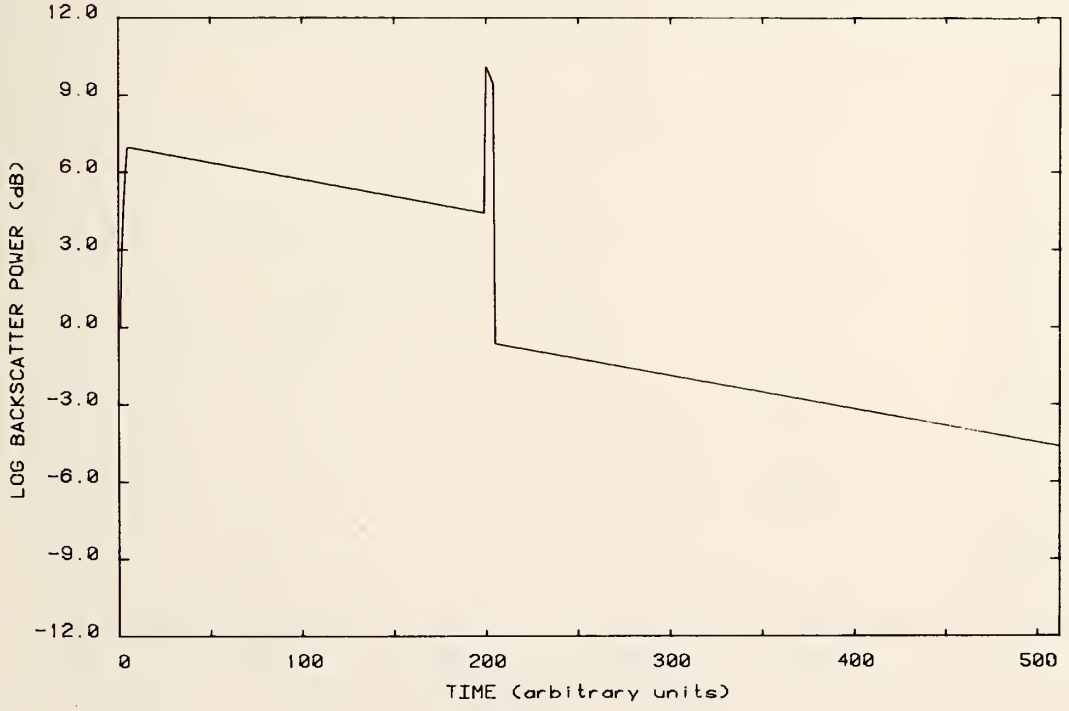

Figure 3-40. Composite imperfection; rectangular probe pulse of width 5 time units. Logarithmic display.

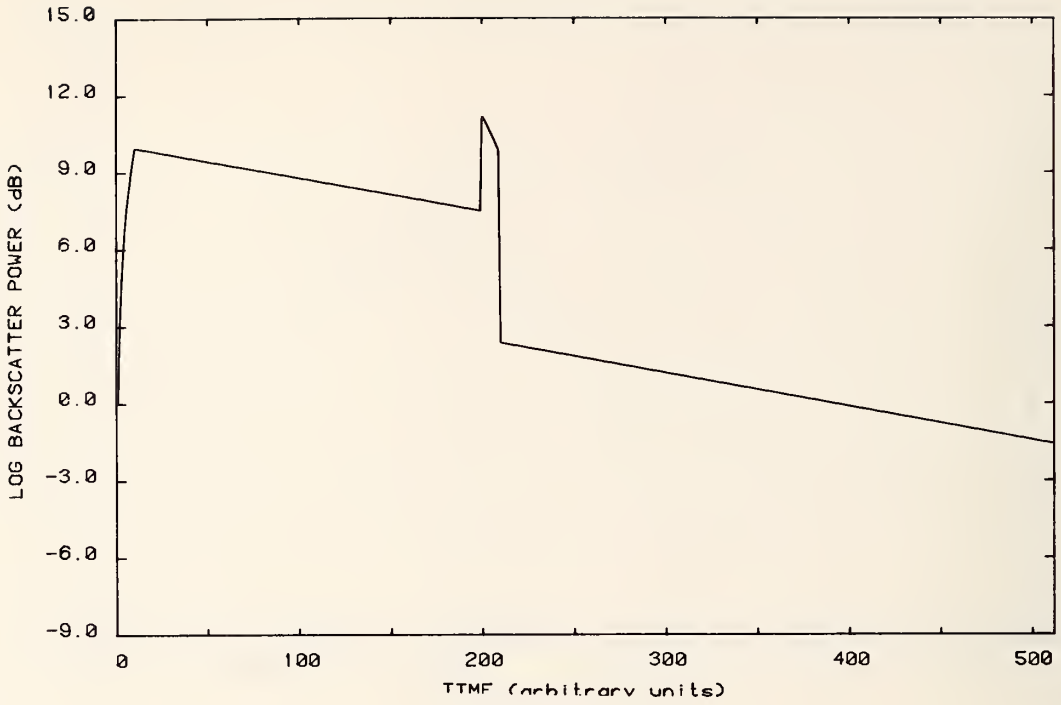

Figure 3-41. Composite imperfection; rectangular probe pulse of width 10 time units. Logarithmic display.

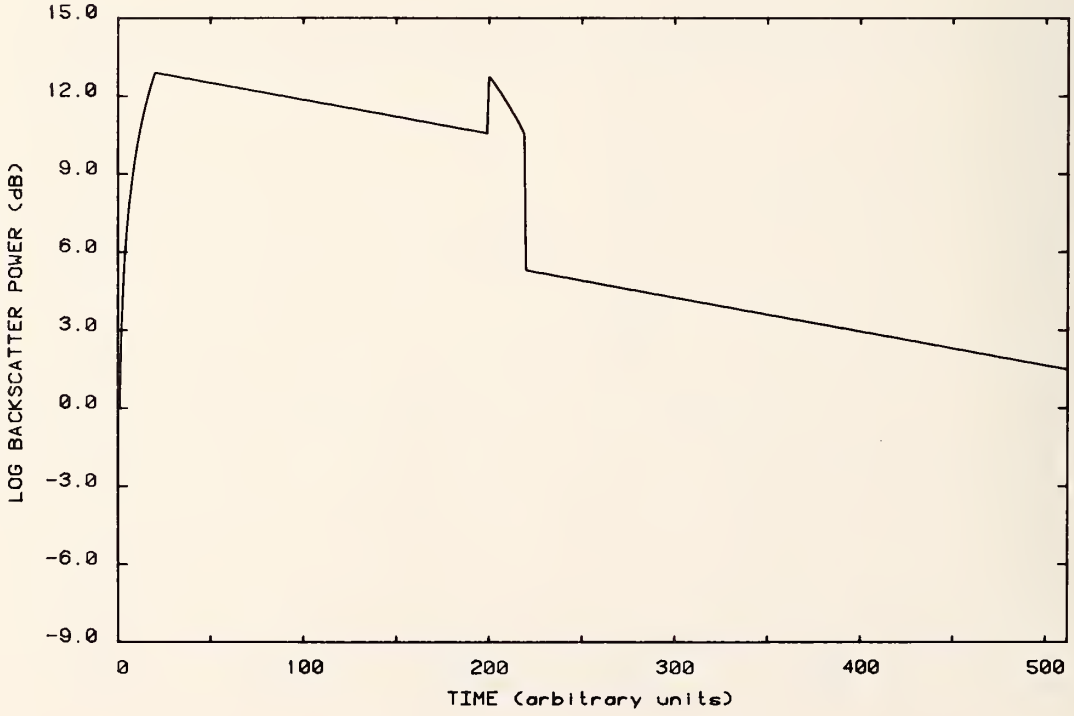

Figure 3-42. Composite imperfection; rectangular probe pulse of width 20 time units. Logarithmic display.

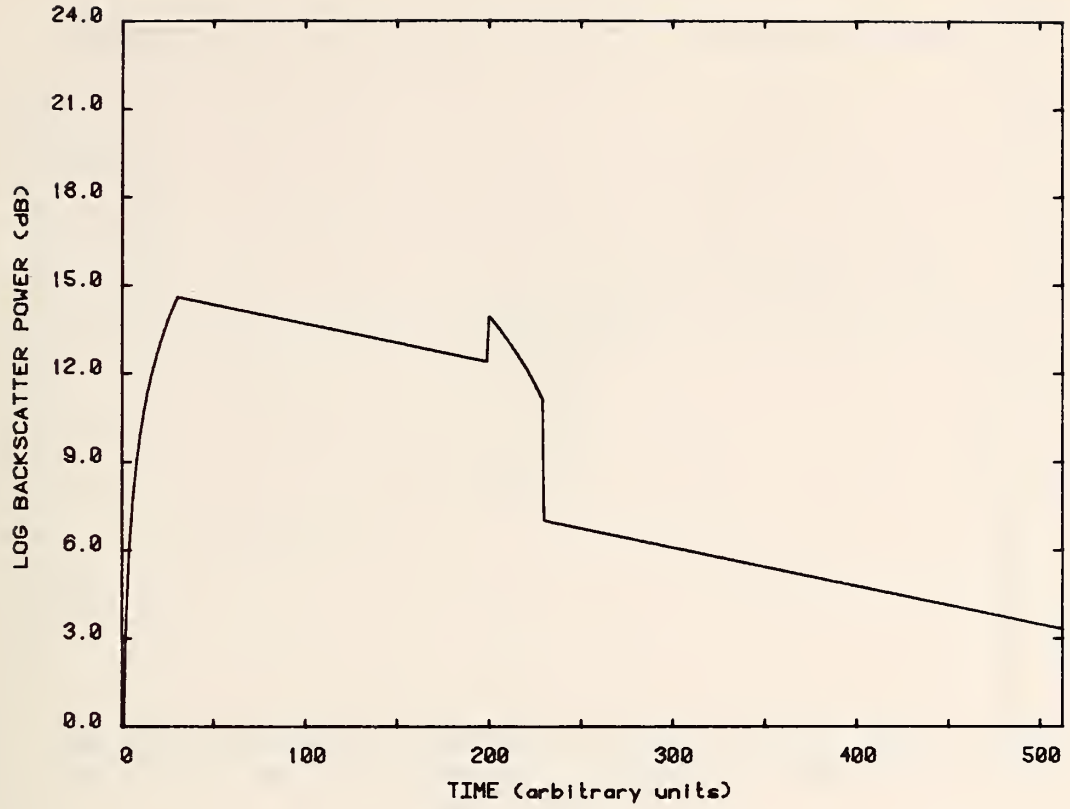

Figure 3-43. Composite imperfection; rectangular probe pulse of width 30 time units. Logarithmic display.

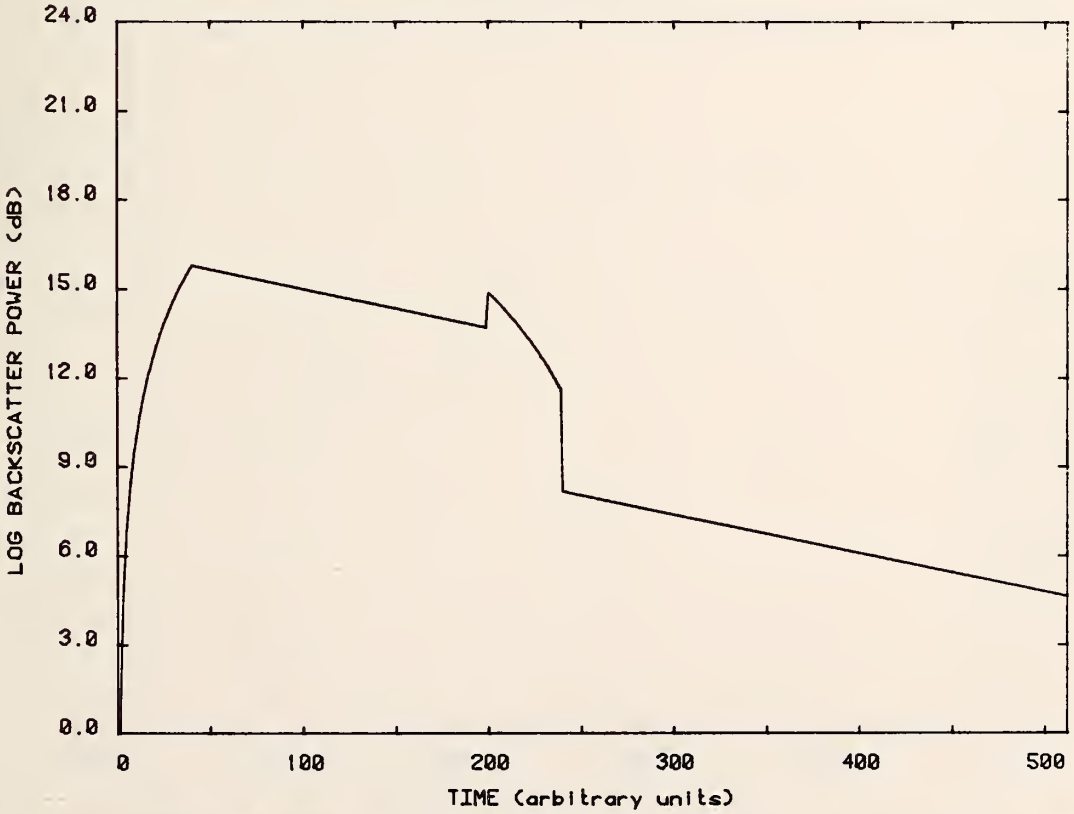

Figure 3-44. Composite imperfection; rectangular probe pulse of width 40 time units. Logarithmic display.

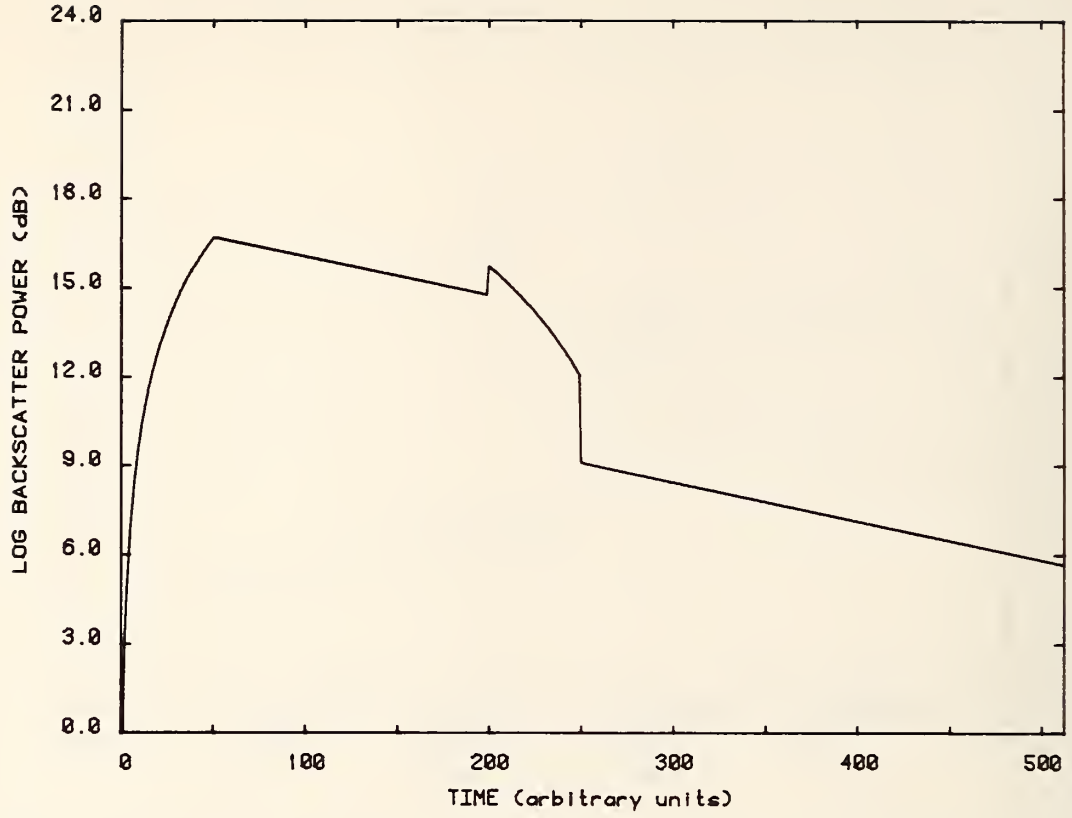

Figure 3-45. Composite imperfection; rectangular probe pulse of width 50 time units. Logarithmic display.

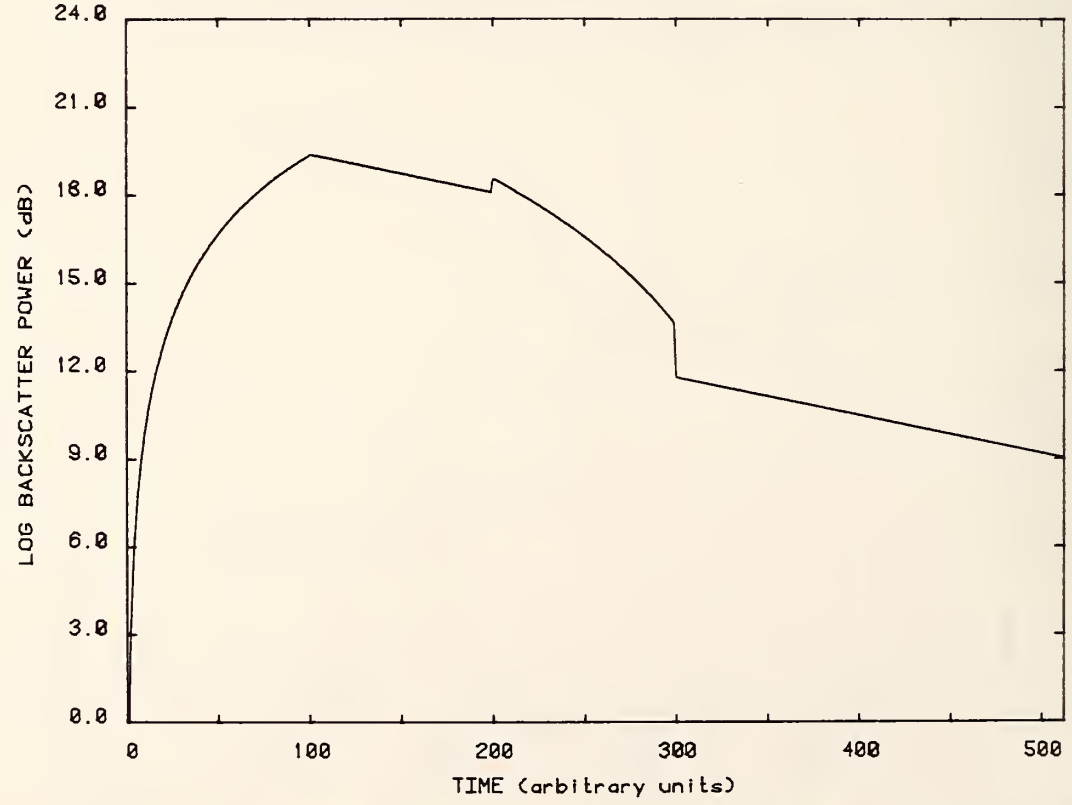

Figure 3-46. Composite imperfection; rectangular probe pulse of width 100 time units. Logarithmic display.

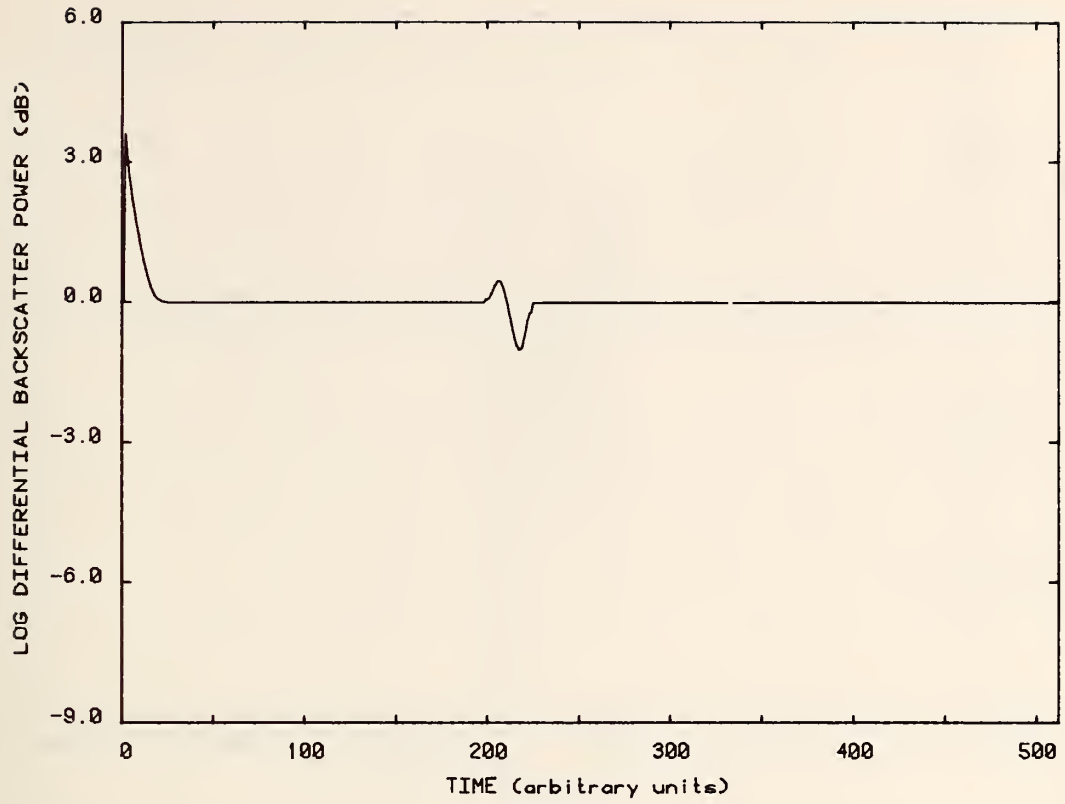

Figure 3-47. Composite imperfection; Gaussian probe pulse; equivalent rectangular width 10 time units; delay one time unit. Differential display.

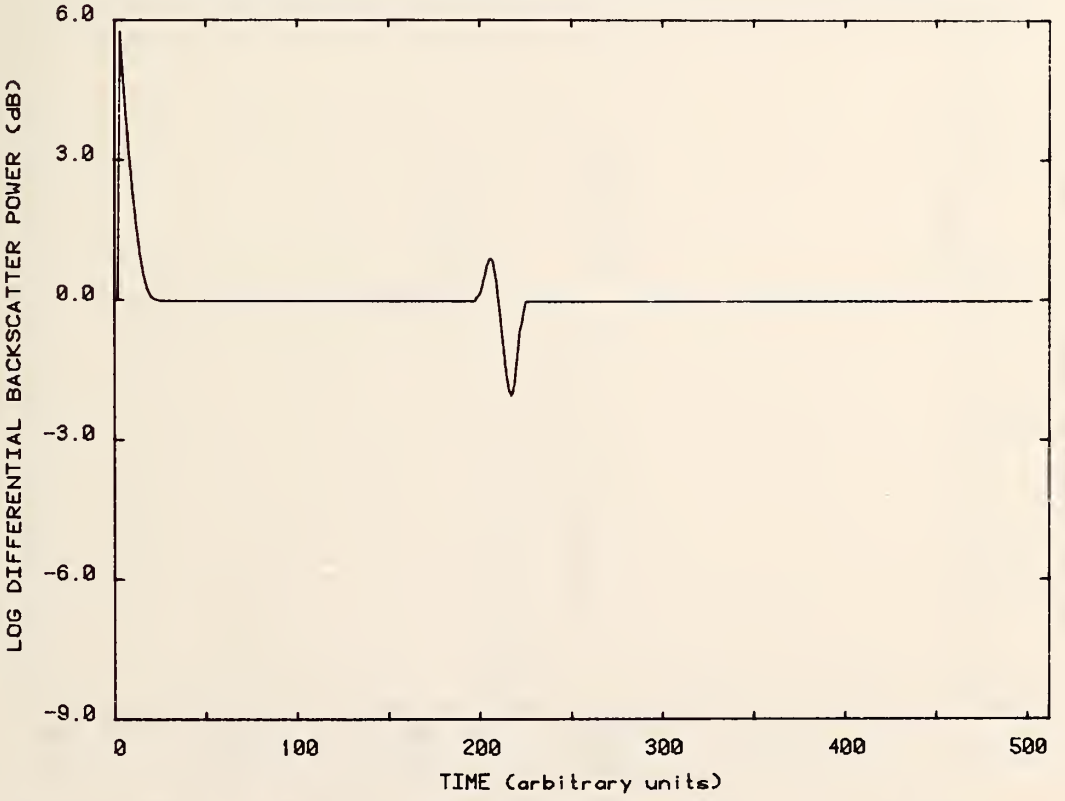

Figure 3-48. Composite imperfection; Gaussian probe pulse; equivalent rectangular width 10 time units; delay 2 time units. Differential display.

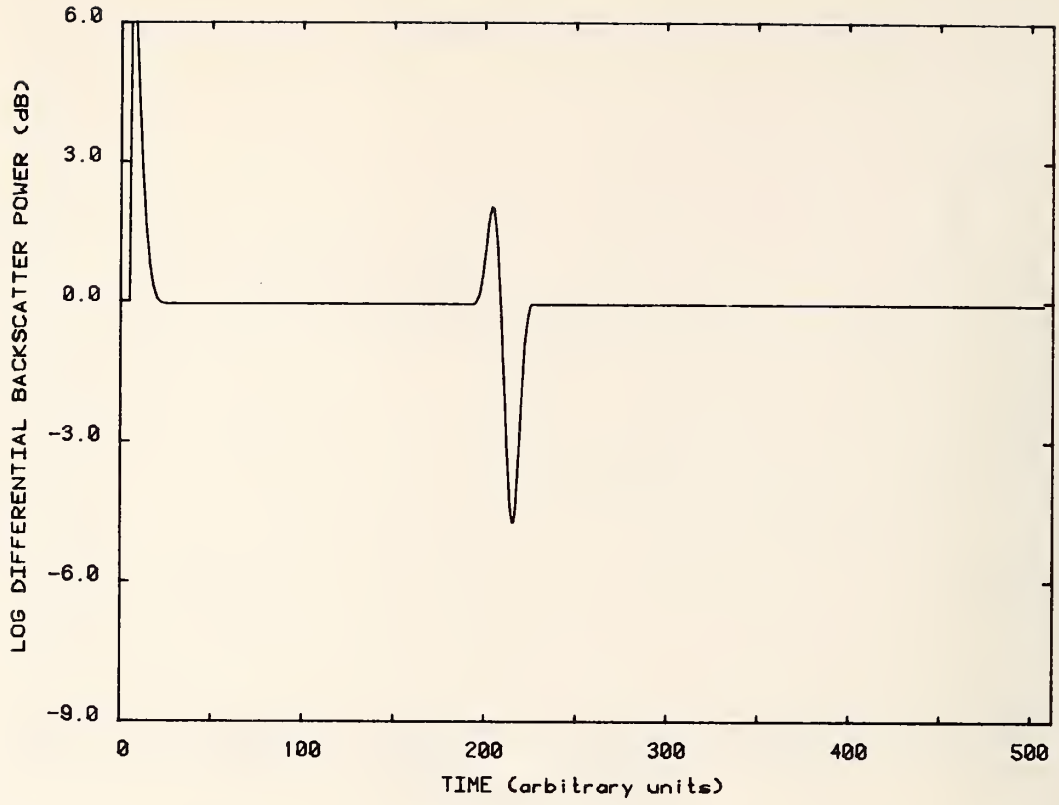

Figure 3-49. Composite imperfection; Gaussian probe pulse; equivalent rectangular width 10 time units; delay 5 time units. Differential display.

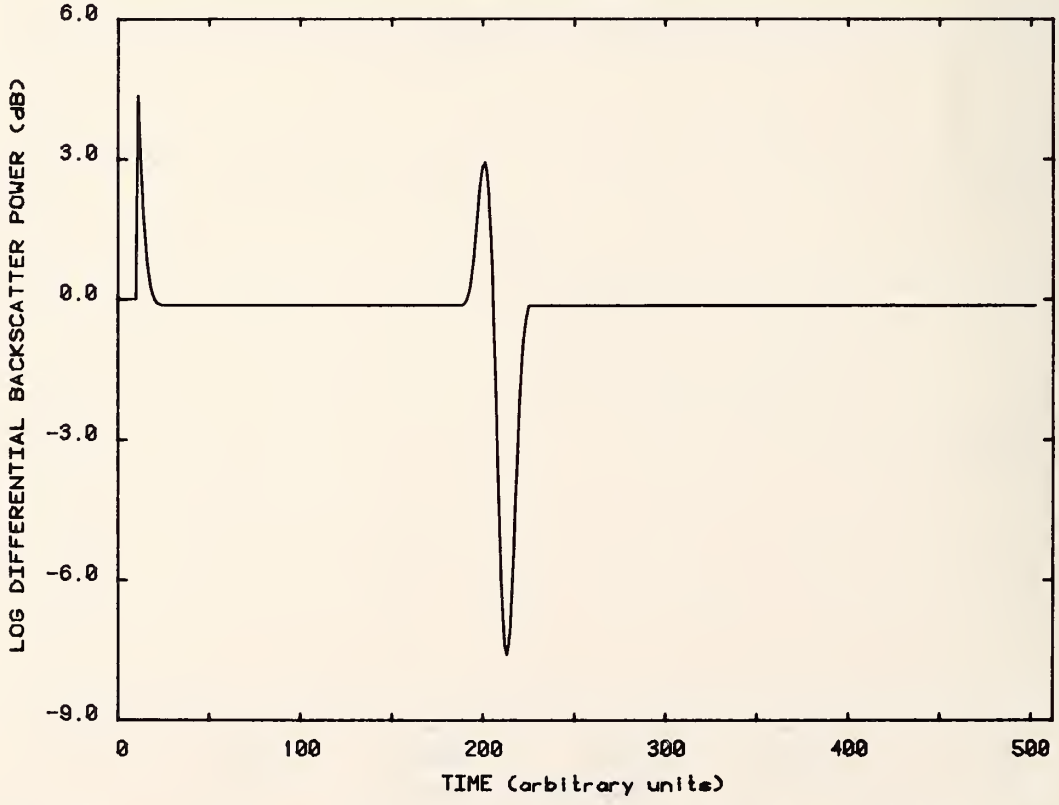

Figure 3-50. Composite imperfection, Gaussian probe pulse; equivalent rectangular width 10 time units; delay 10 time units. Differential display.

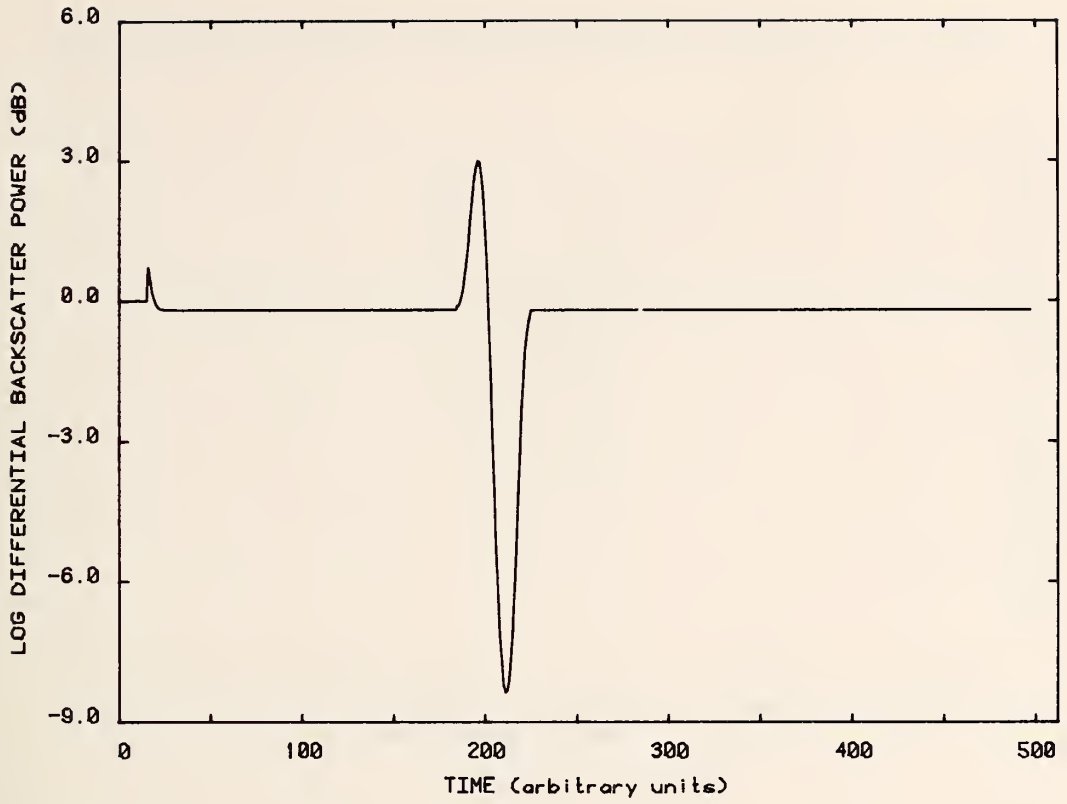

Figure 3-51. Composite imperfection, Gaussian probe pulse, equivalent rectangular width 10 time units; delay 15 time units. Differential display.

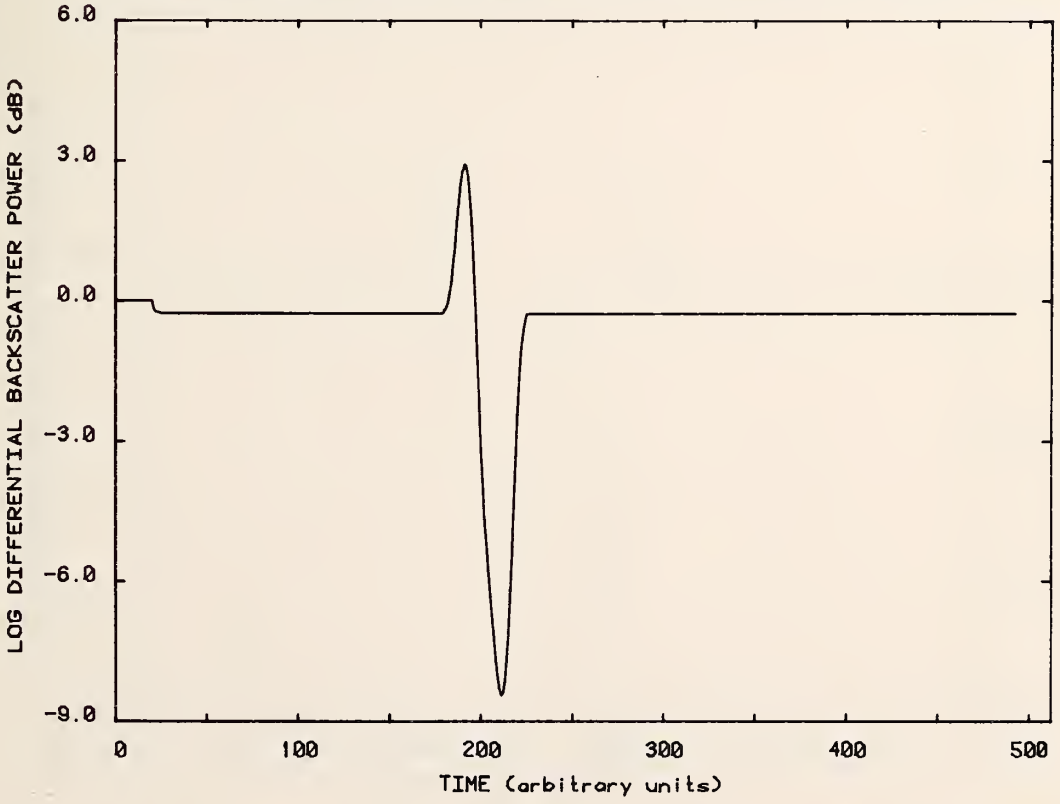

Figure 3-52. Composite imperfection; Gaussian probe pulse; equivalent rectangular width 10 time units; delay 20 time units. Differential display.

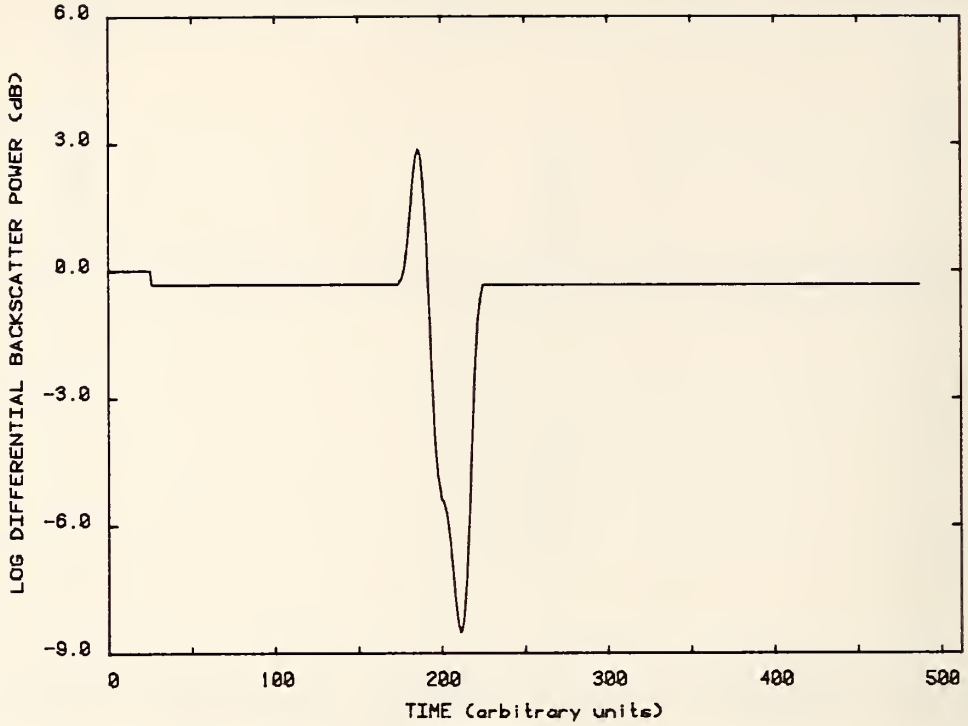

Figure 3-53. Composite imperfection; Gaussian probe pulse; equivalent rectangular width 10 time units; delay 25 time units. Differential display.

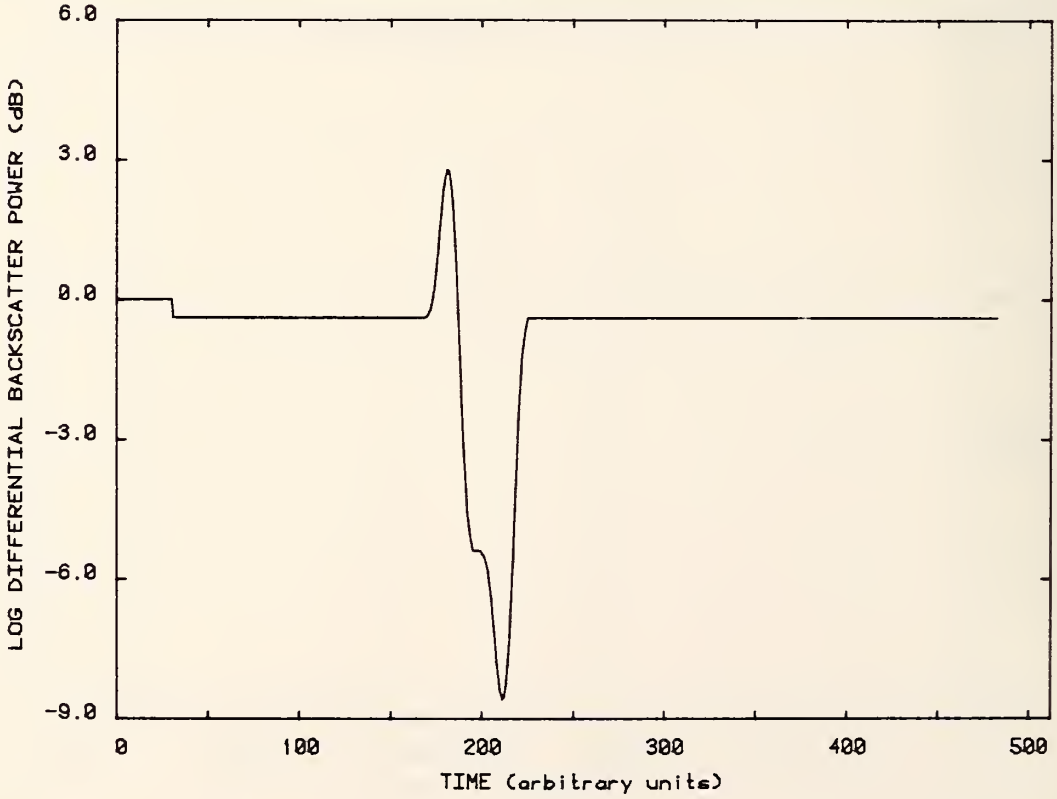

Figure 3-54. Composite imperfection; Gaussian probe pulse; equivalent rectangular width 10 time units; delay 30 time units. Differential display.

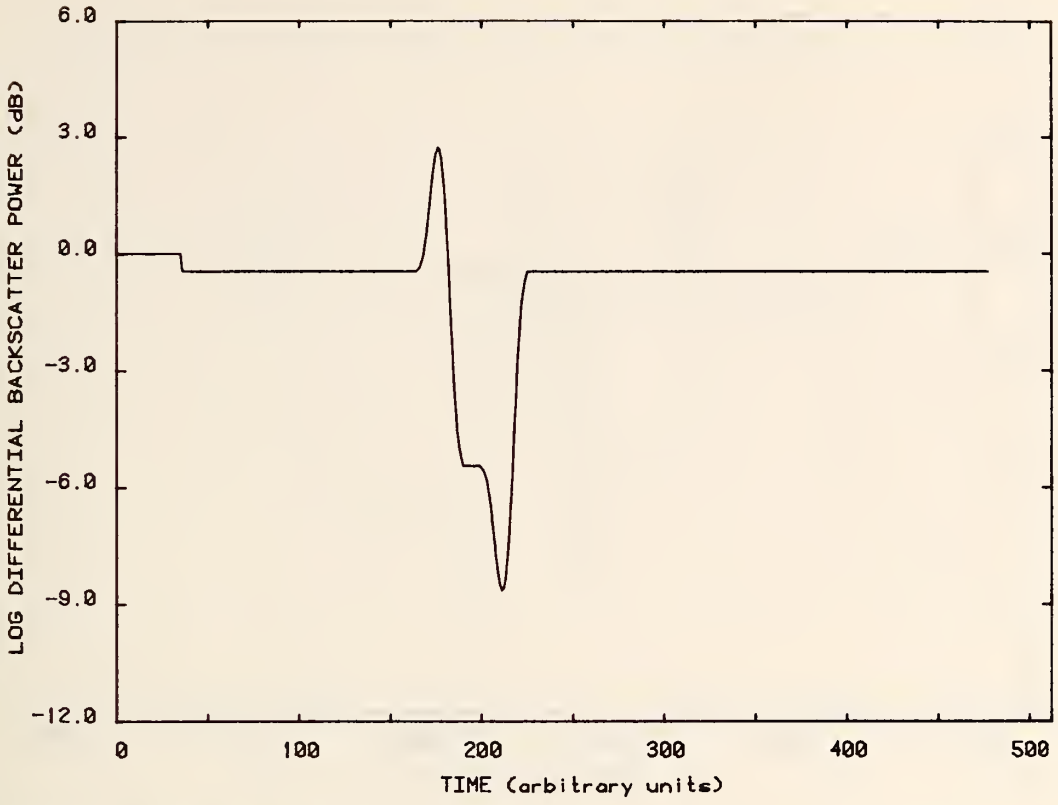

Figure 3-55. Composite imperfection; Gaussian probe pulse; equivalent rectangular width 10 time units; delay 35 time units. Differential display.

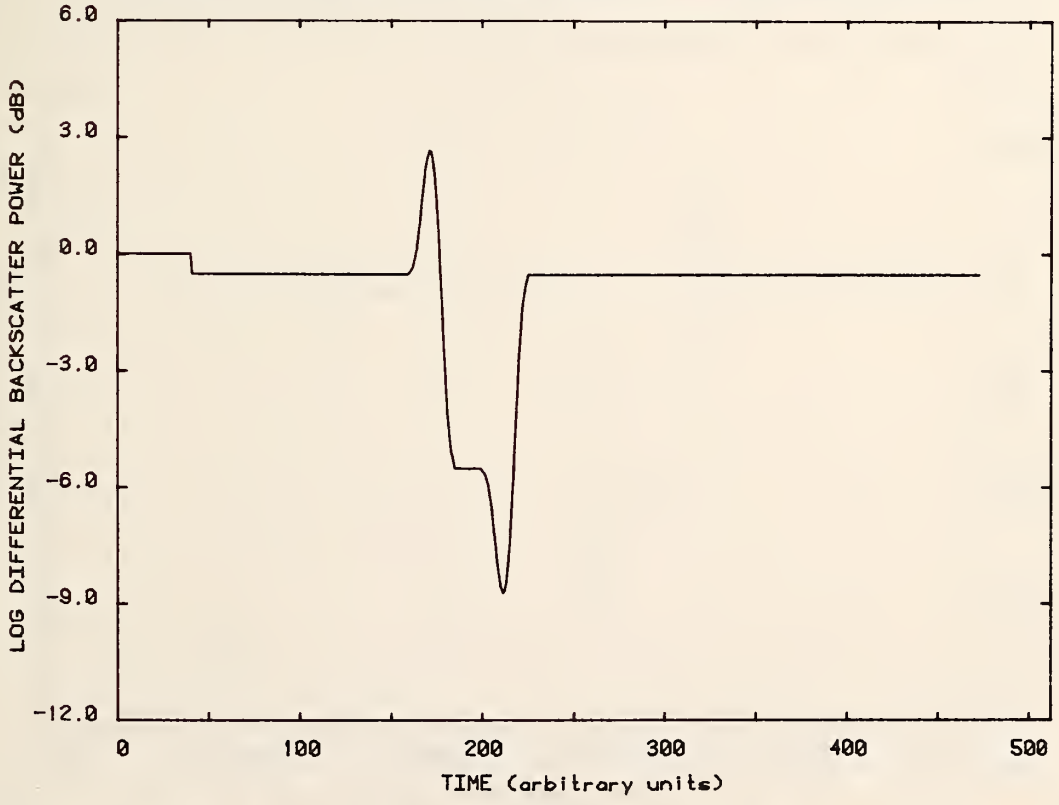

Figure 3-56. Composite imperfection; Gaussian probe pulse; equivalent rectangular width 10 time units; delay 40 time units. Differential display.

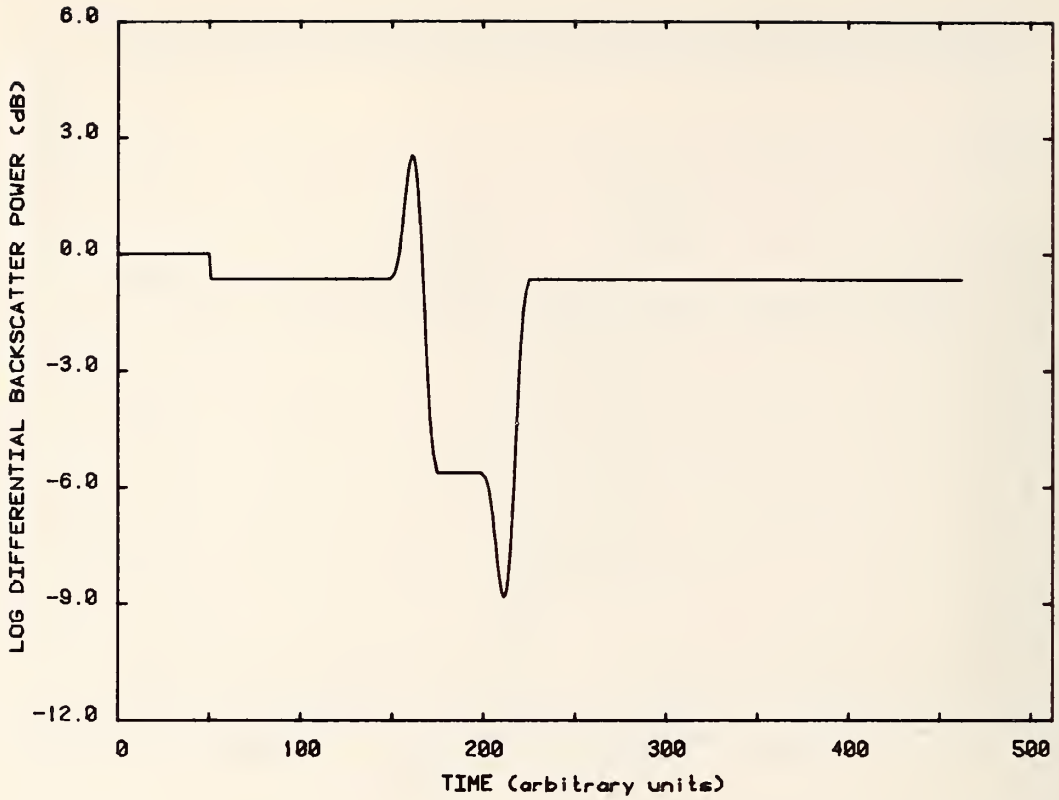

Figure 3-57. Composite imperfection; Gaussian probe pulse; equivalent rectangular width 10 time units; delay 50 time units. Differential display.

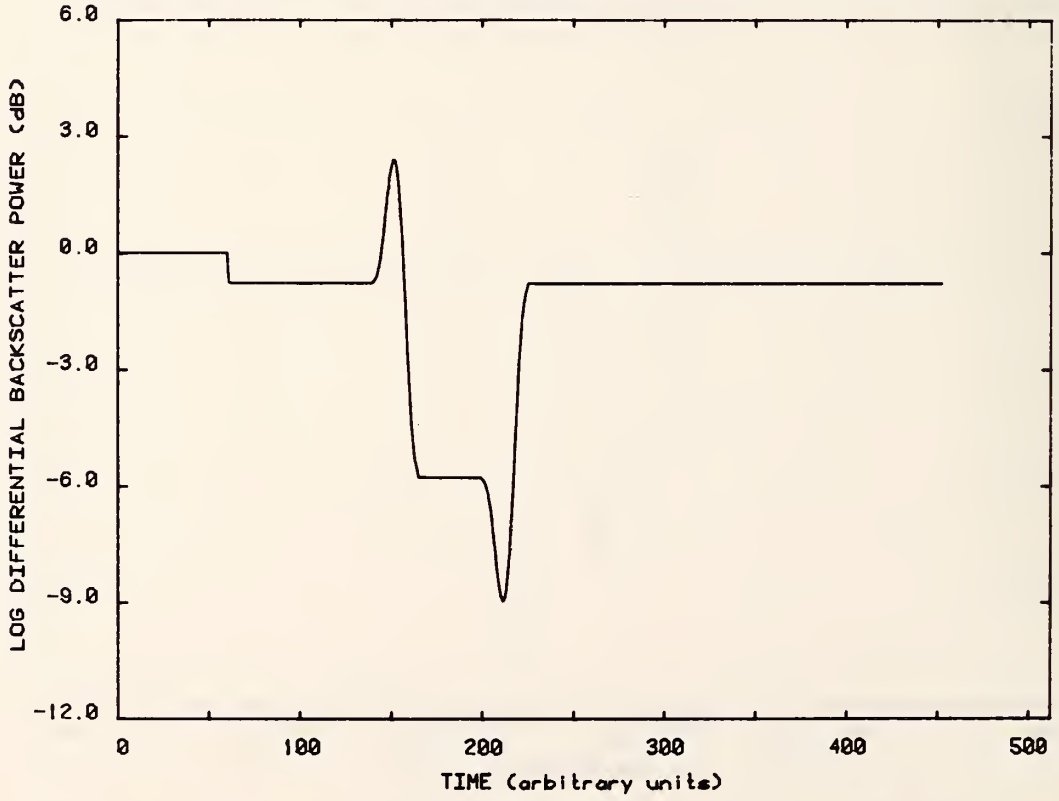

Figure 3-58. Composite imperfection; Gaussian probe pulse; equivalent rectangular width 10 time units; delay 60 time units. Differential display.

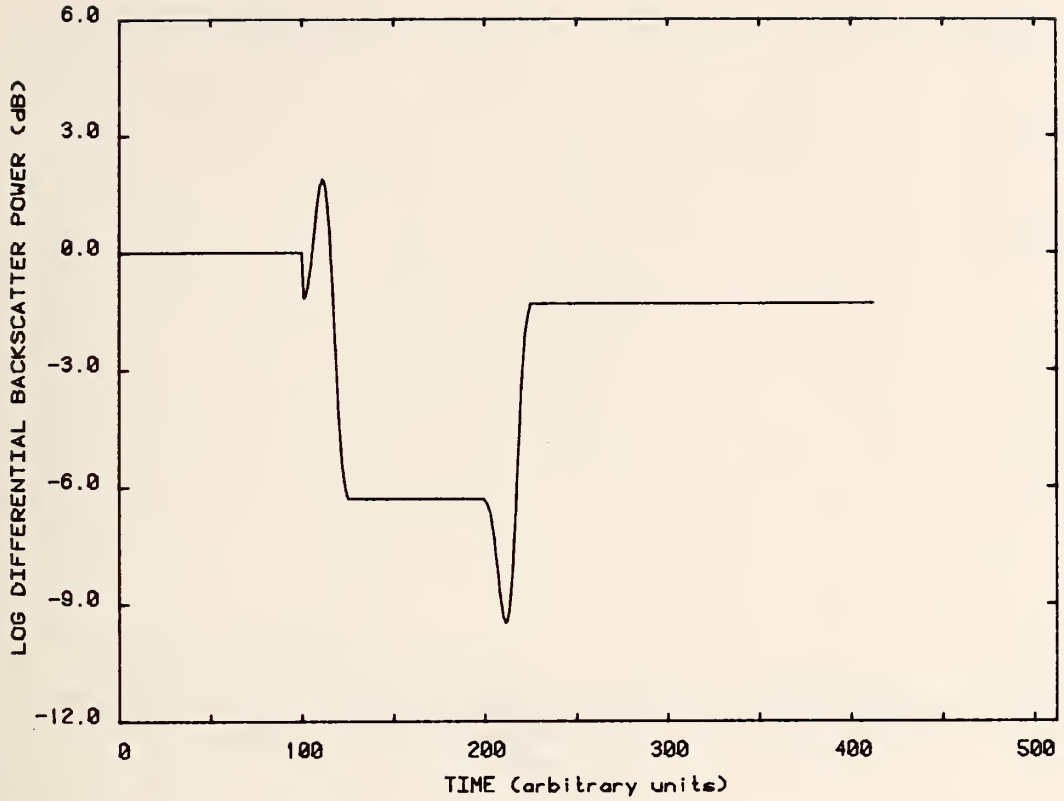

Figure 3-59. Composite imperfection; Gaussian probe pulse; equivalent rectangular width 10 time units; delay 100 time units. Differential display.

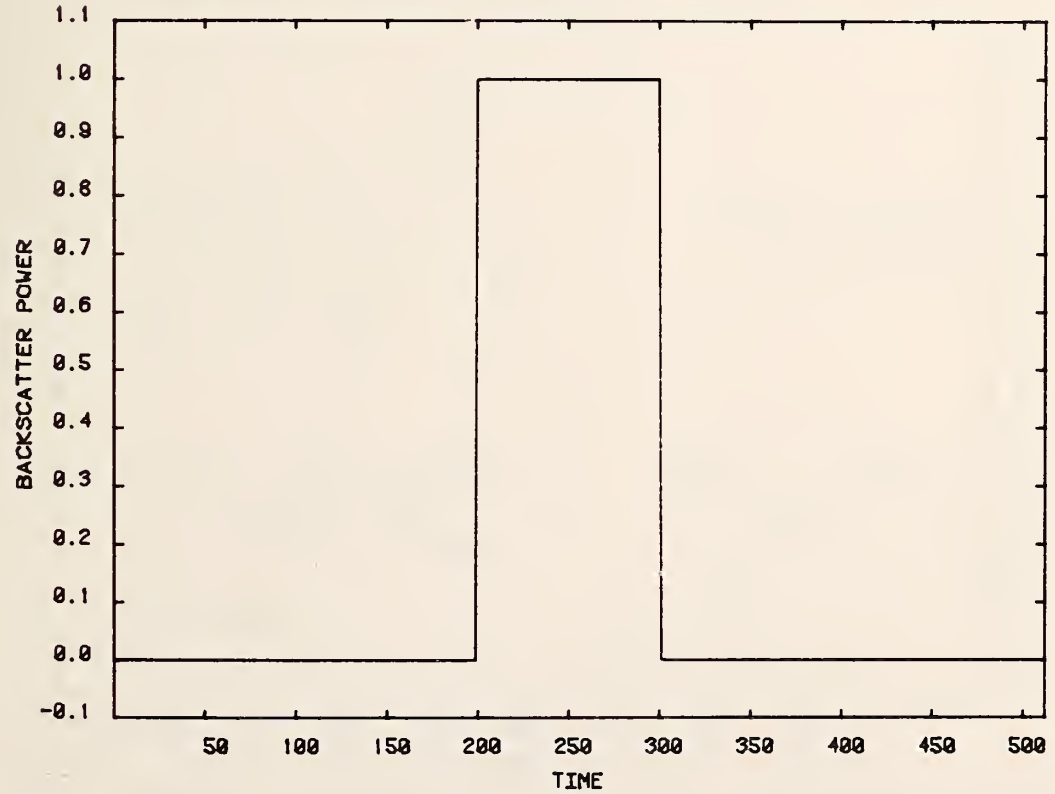

Figure 3-60. The impulse response for an extended scattering imperfection. Linear display.

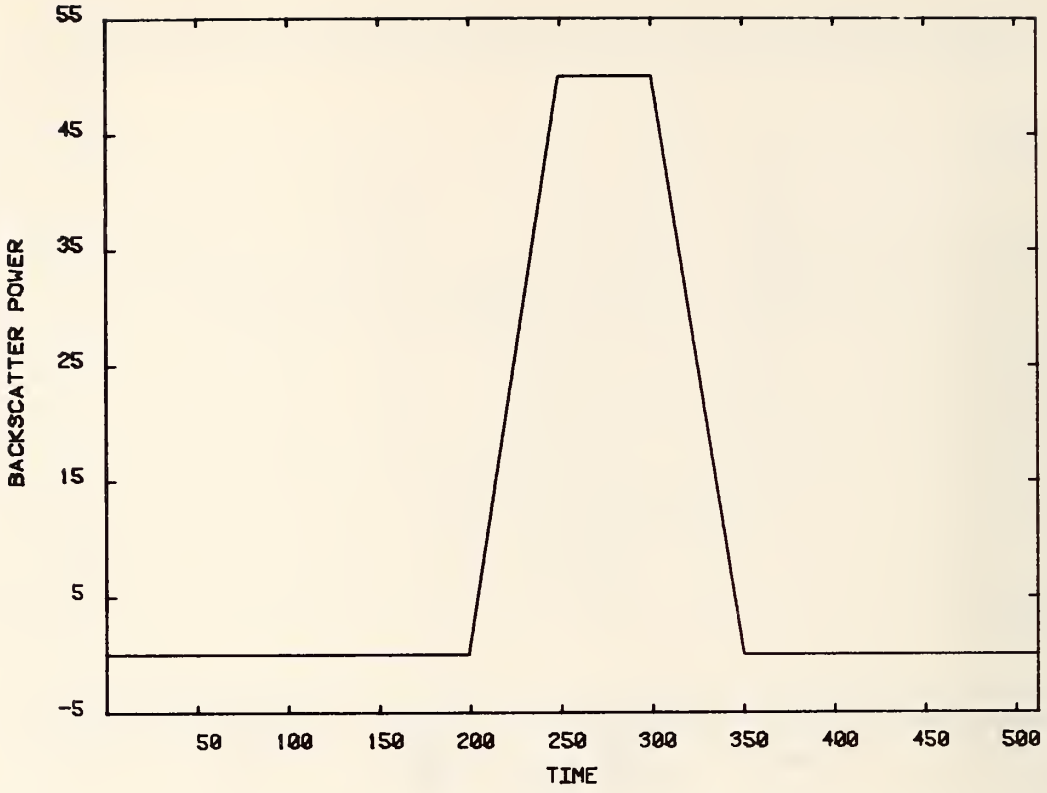

Figure 3-61. Extended scatter-like imperfection; rectangular probe pulse of width 50 time units. Linear display.

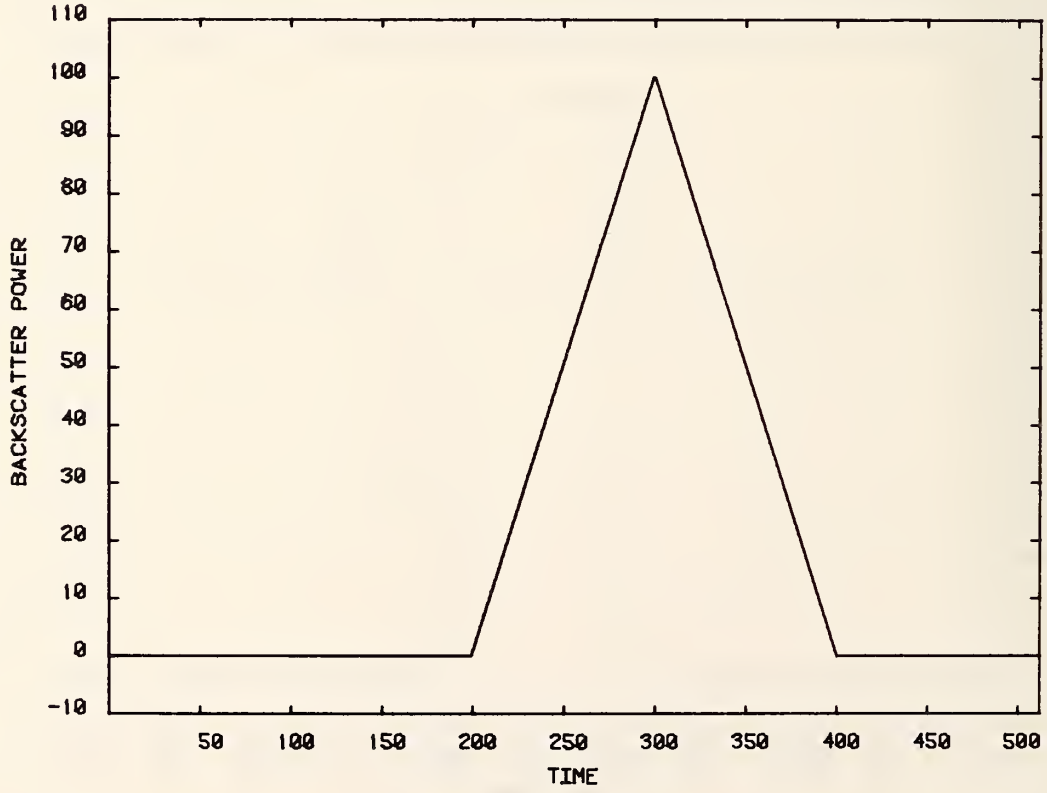

Figure 3-62. Extended scatter-like imperfection; rectangular probe pulse of width 100 time units. Linear display.

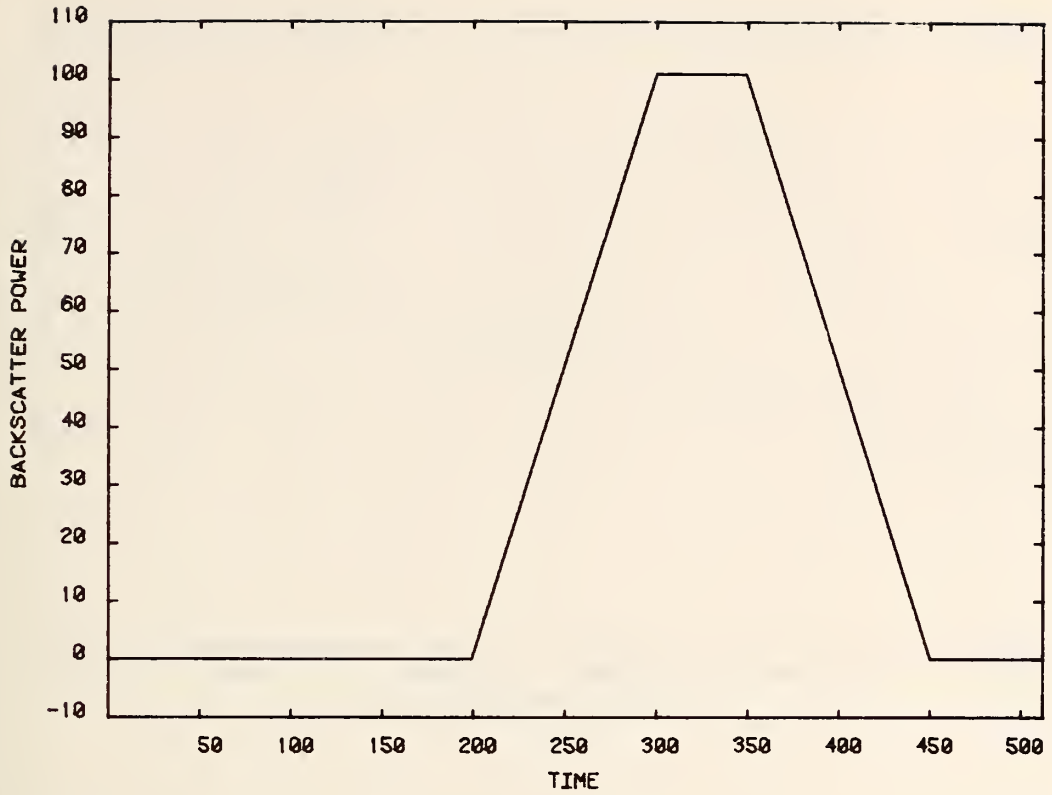

Figure 3-63. Extended scatter-like imperfection; rectangular probe pulse of width 150 time units. Linear display.

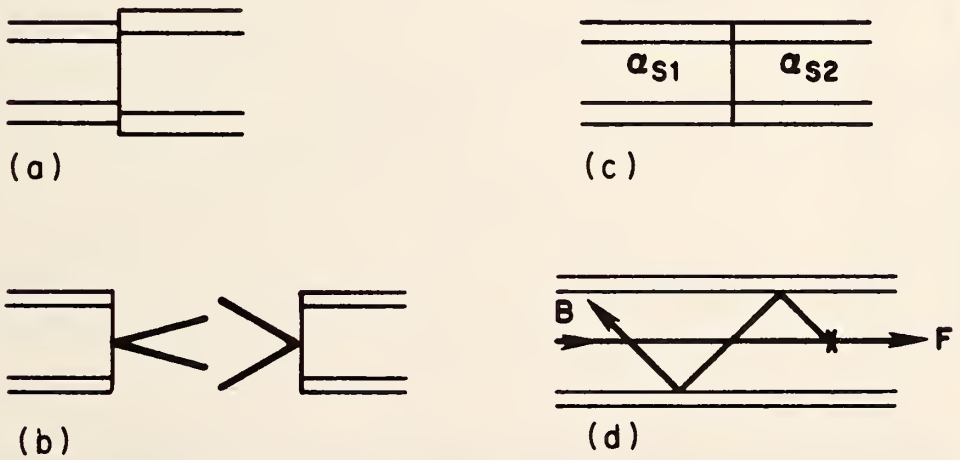

Figure 3-64. Examples of conditions in optical fibers which exhibit nonuniform and/or nonreciprocal transmission properties: (a) Splice between fibers of different diameter, (b) splice between fibers of different numerical aperture, (c) splice between fibers having different scattering loss, and (d) fiber with a different mode volume excited in the backward direction.

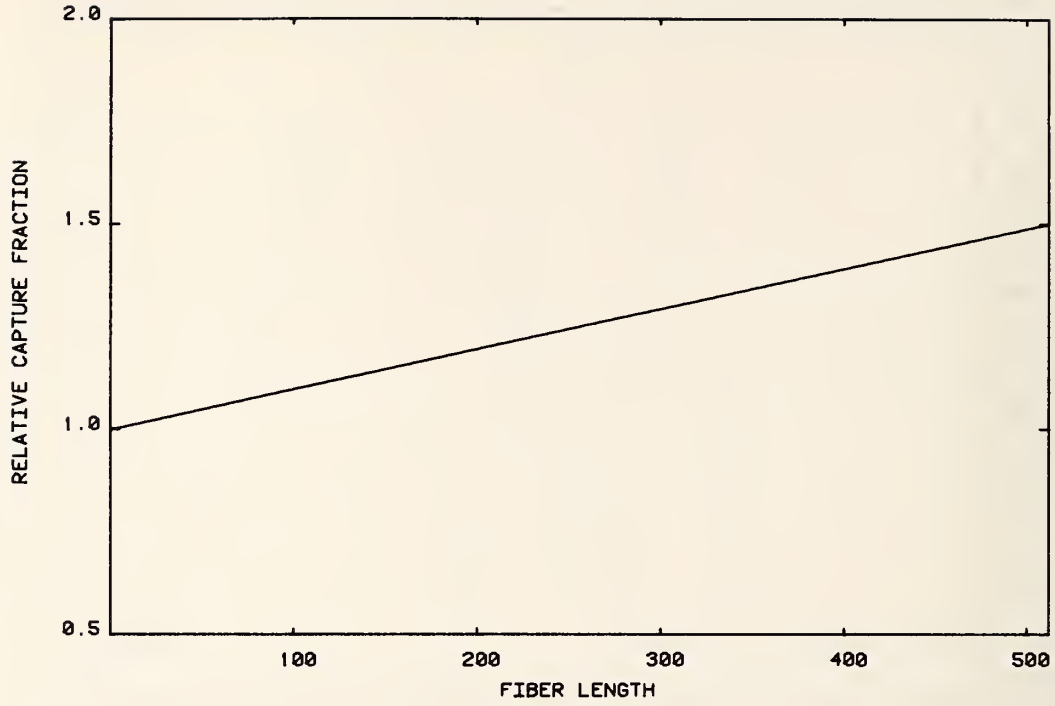

Figure 3-65. Variation of capture fraction with length in the forward direction.

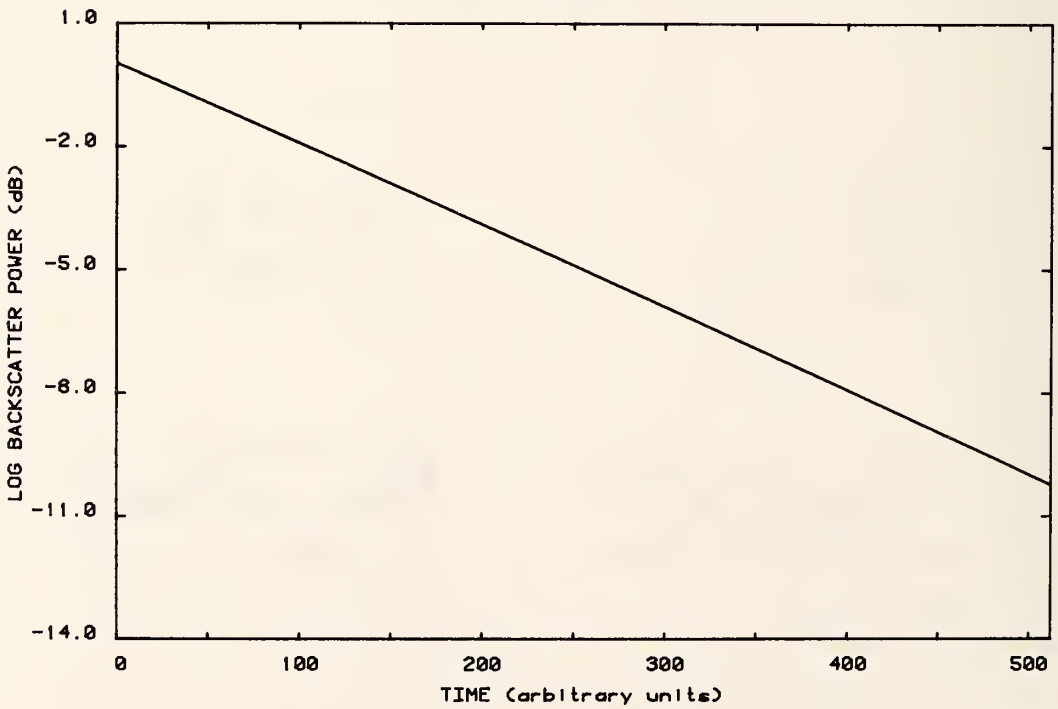

Figure 3-66. Impulse response signature of fiber with perturbation shown in figure 3-65. Logarithmic display.

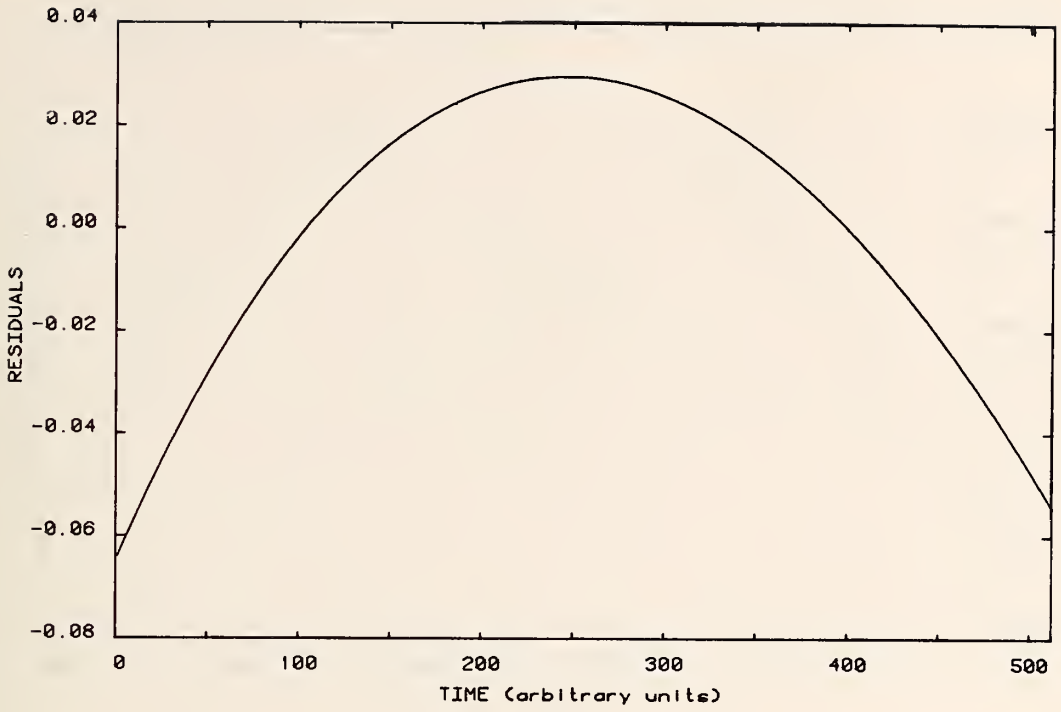

Figure 3-67. Residuals for signature in figure 3-66.

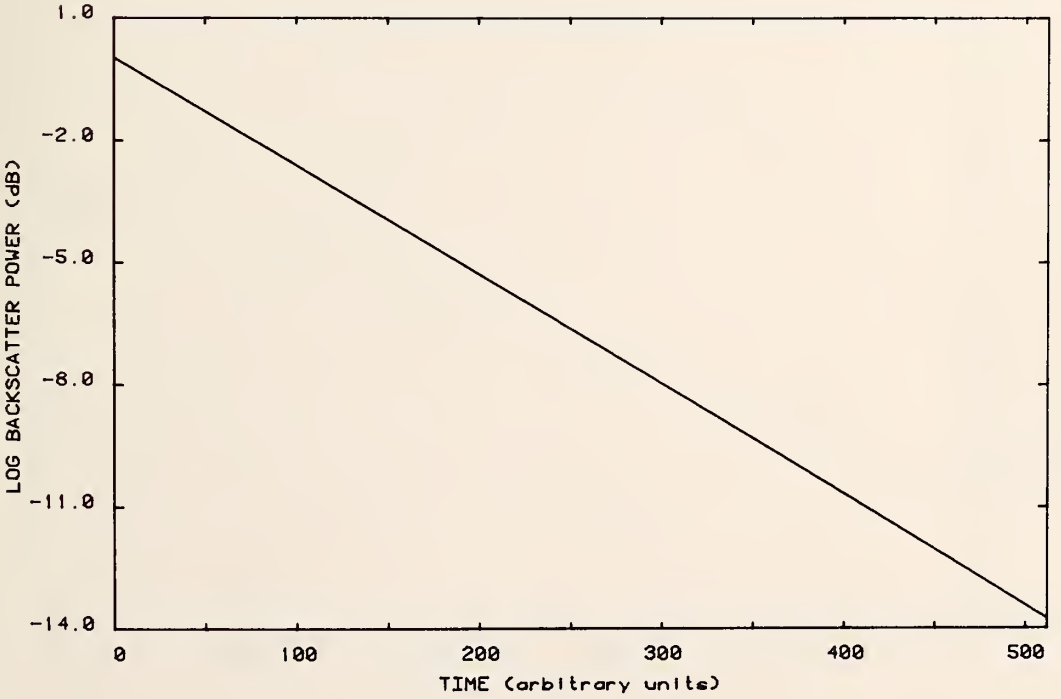

Figure 3-68. Impulse response signature for fiber shown in figure 3-66 when fiber is reversed end-for-end.

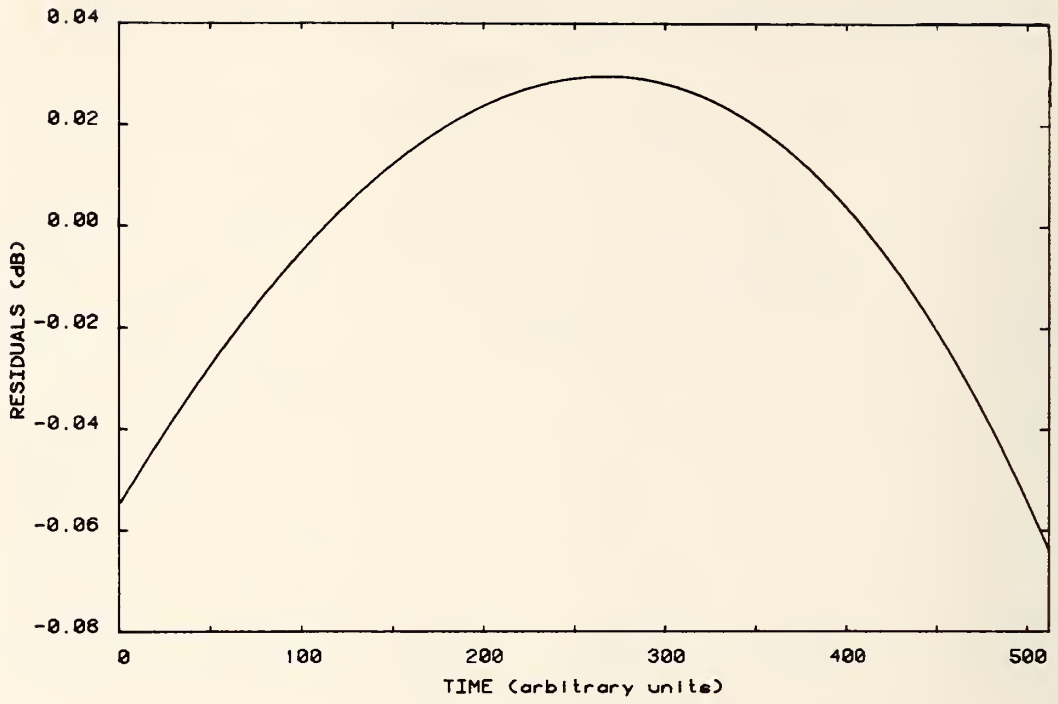

Figure 3-69. Residuals for signature of fiber shown inn figure 3-68.

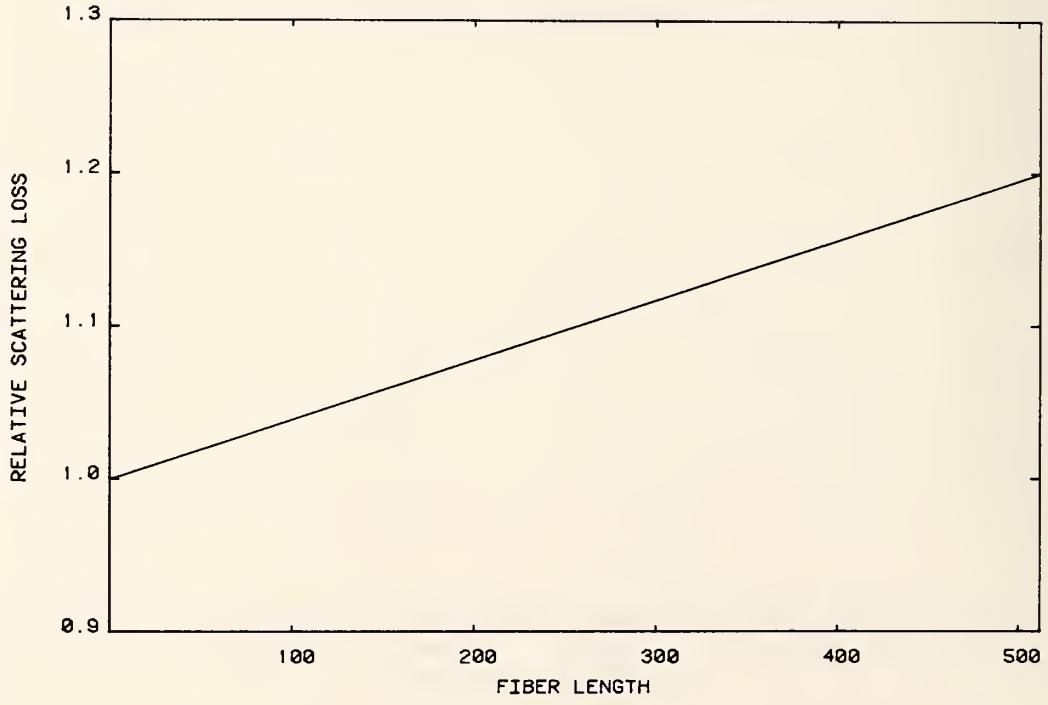

Figure 3-70. Variation of scattering loss with length in the forward direction.

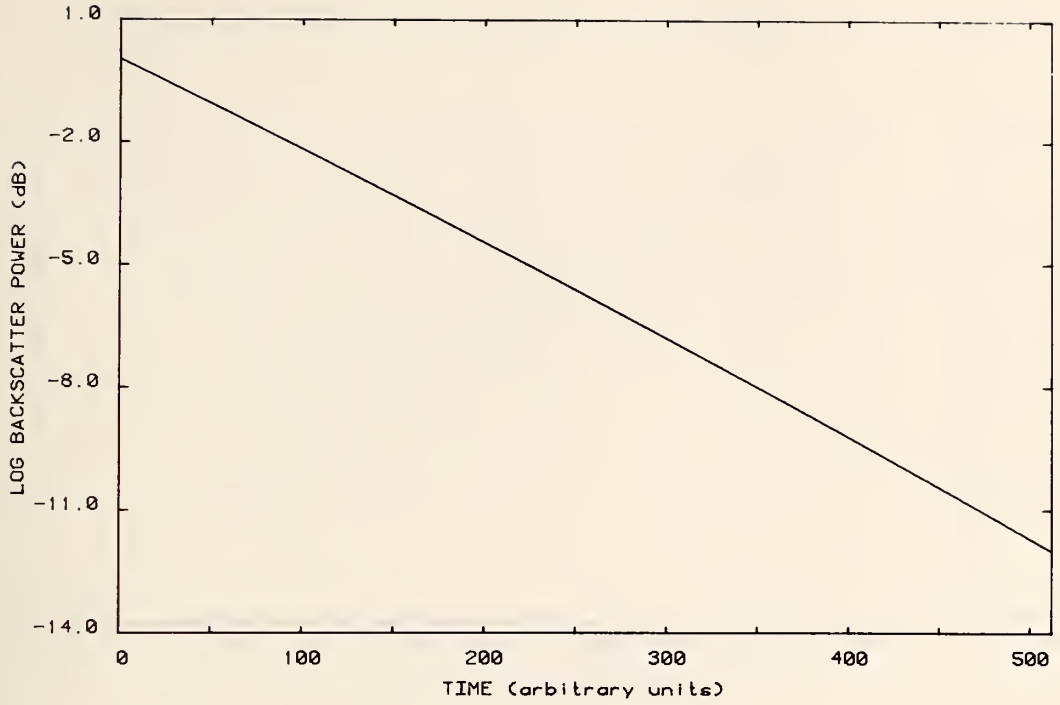

Figure 3-71. Impulse response signature for fiber with perturbation shown in figure 3-70. Logarithmic display.

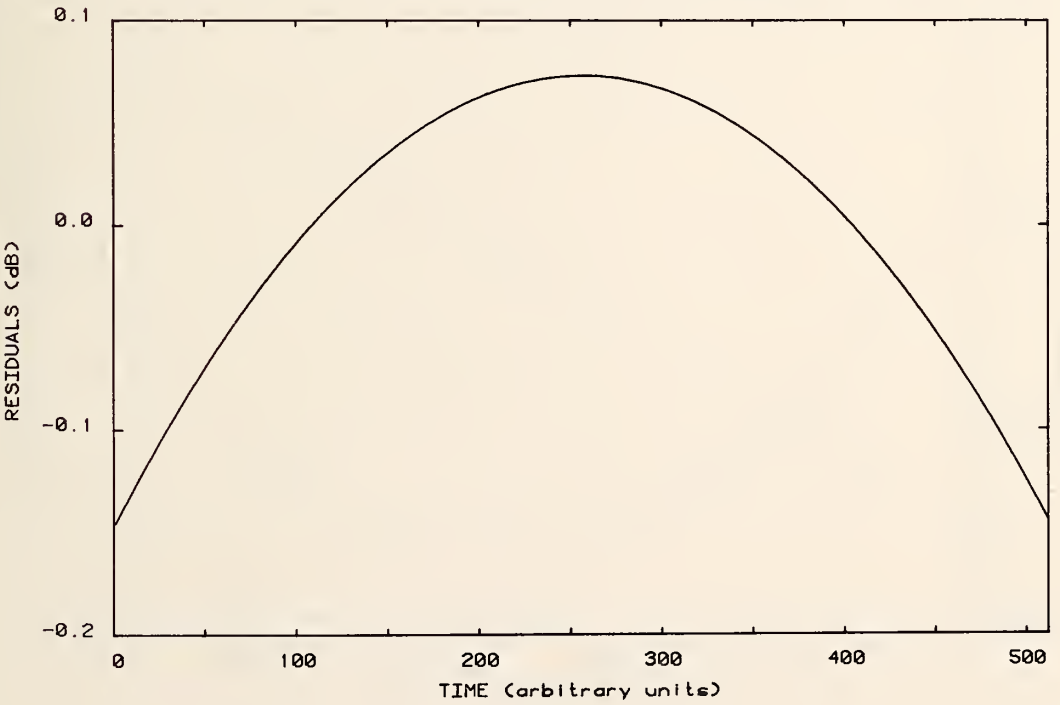

Figure 3-72. Residuals for signature of fiber shown in figure 3-71.

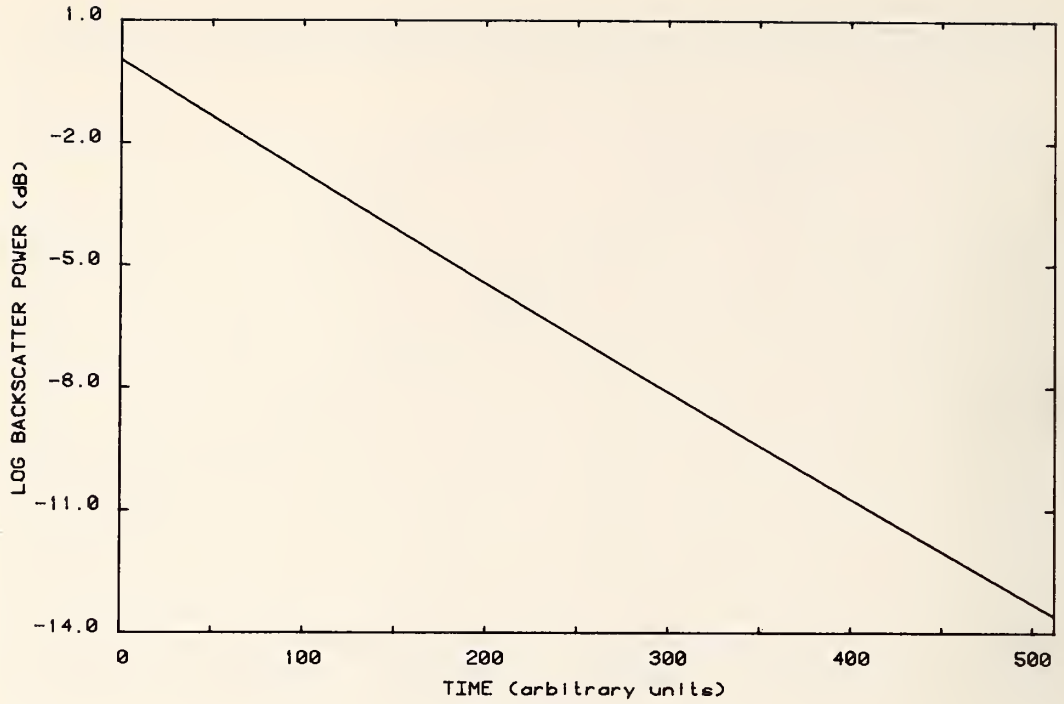

Figure 3-73. Impulse response signature for fiber shown in figure 3-71 when fiber is reversed end-for-end.

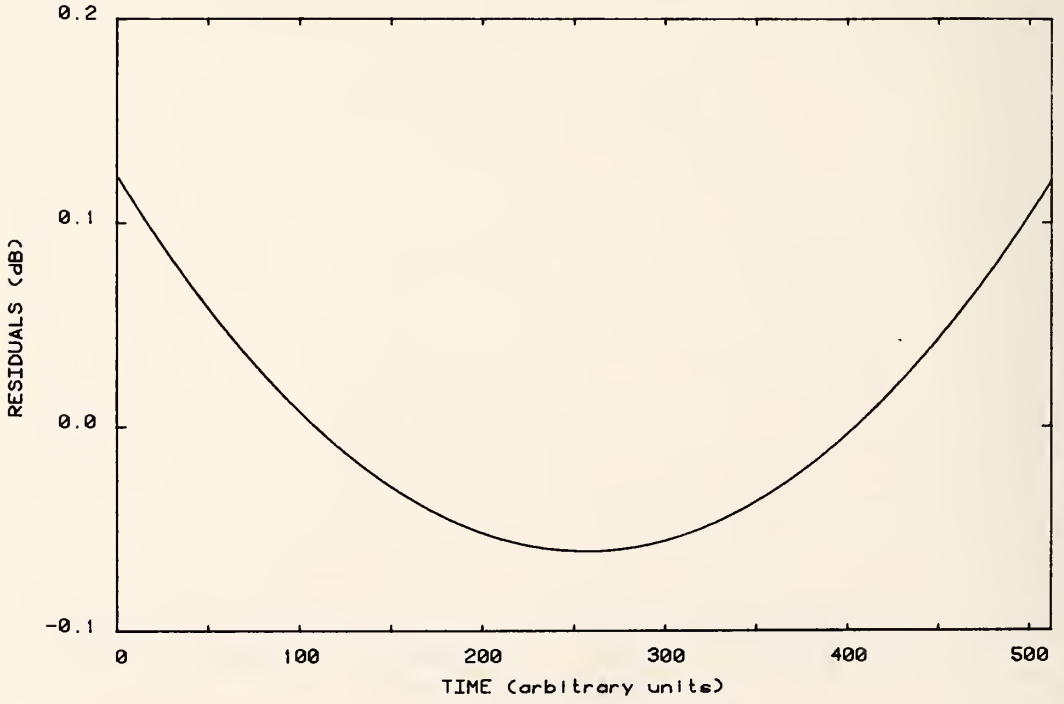

Figure 3-74. Residuals for signature of fiber shown in figure 3-73.

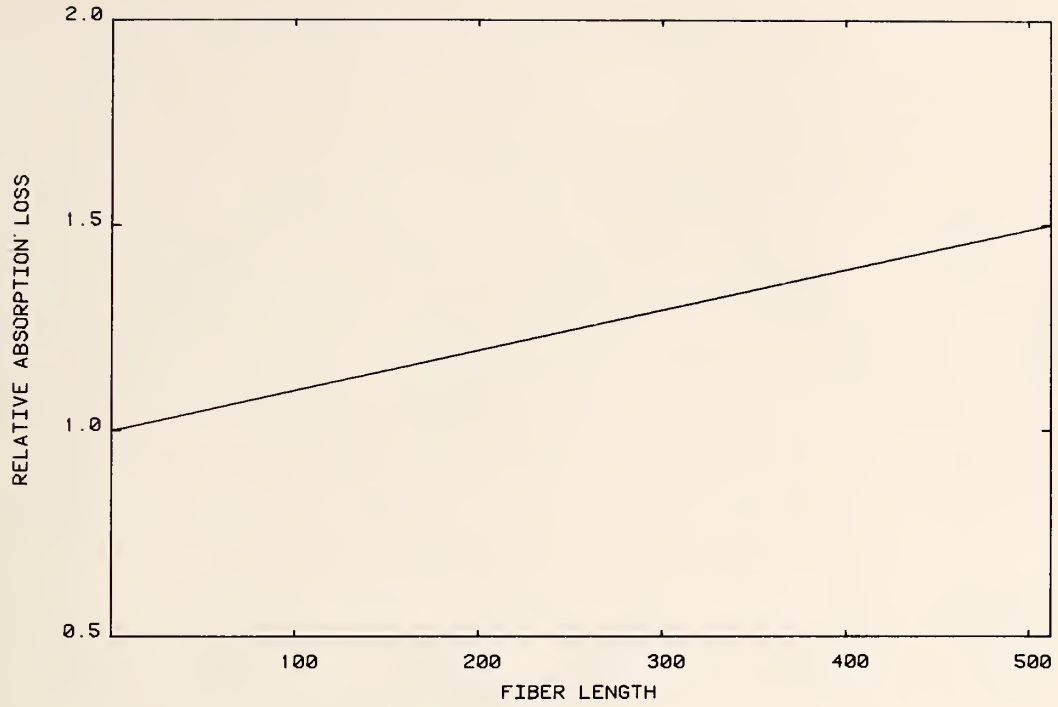

Figure 3-75. Variation of absorption loss with length in the forward direction.

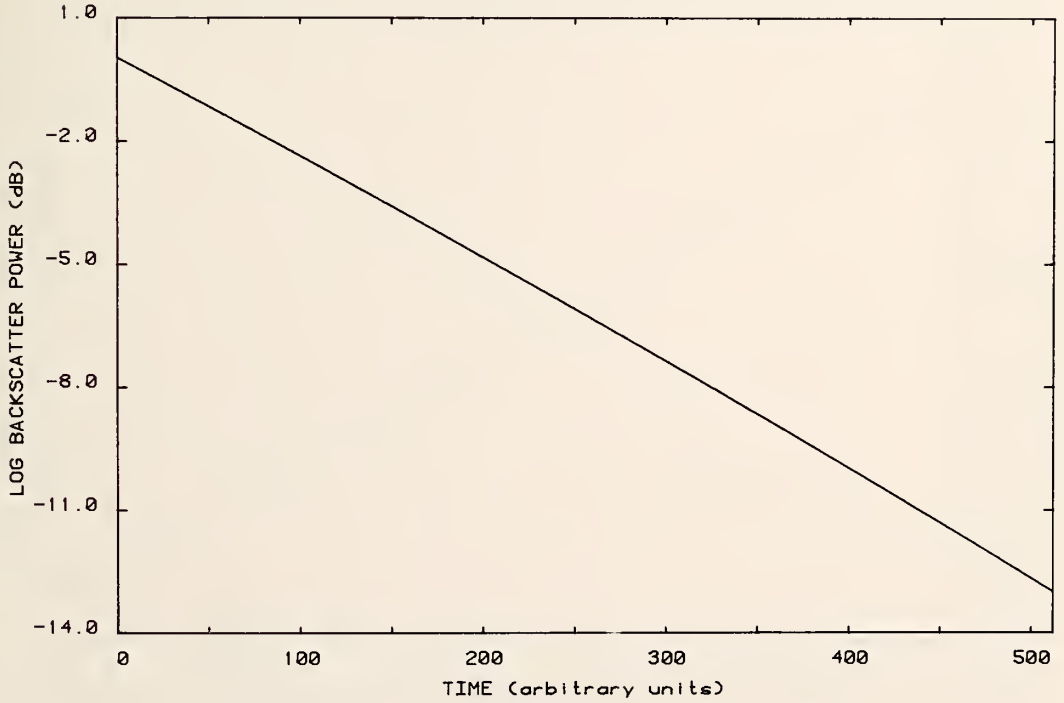

Figure 3-76. Impulse response signature for fiber with perturbation shown in figure 3-75. Logarithmic display.

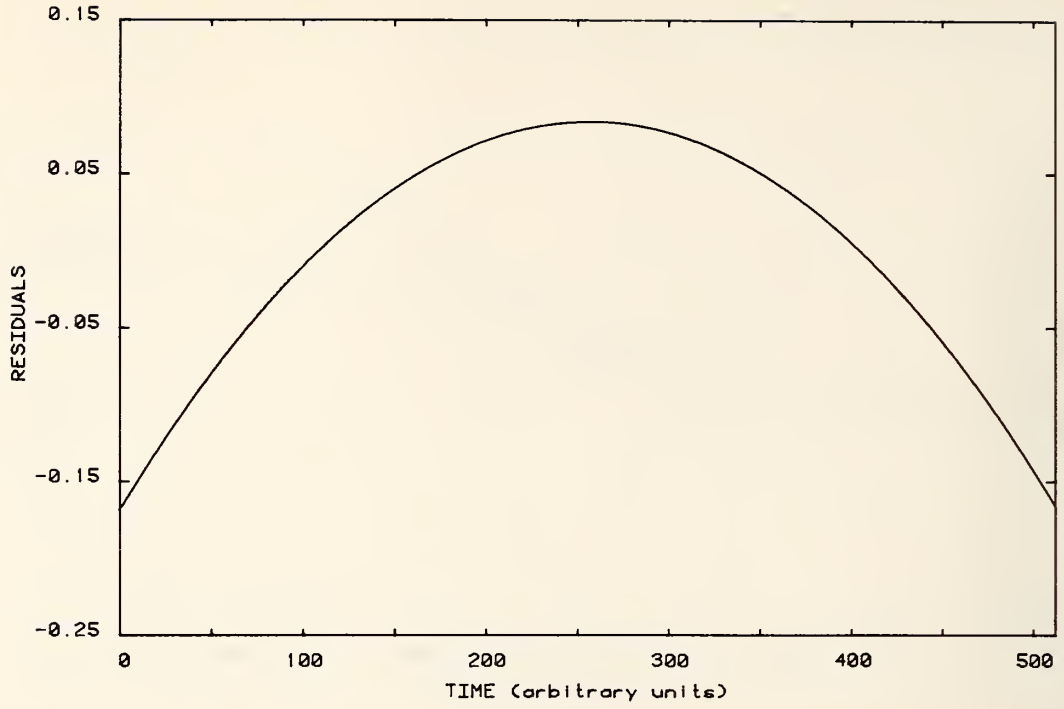

Figure 3-77. Residuals for signature of fiber shown in figure 3-76.

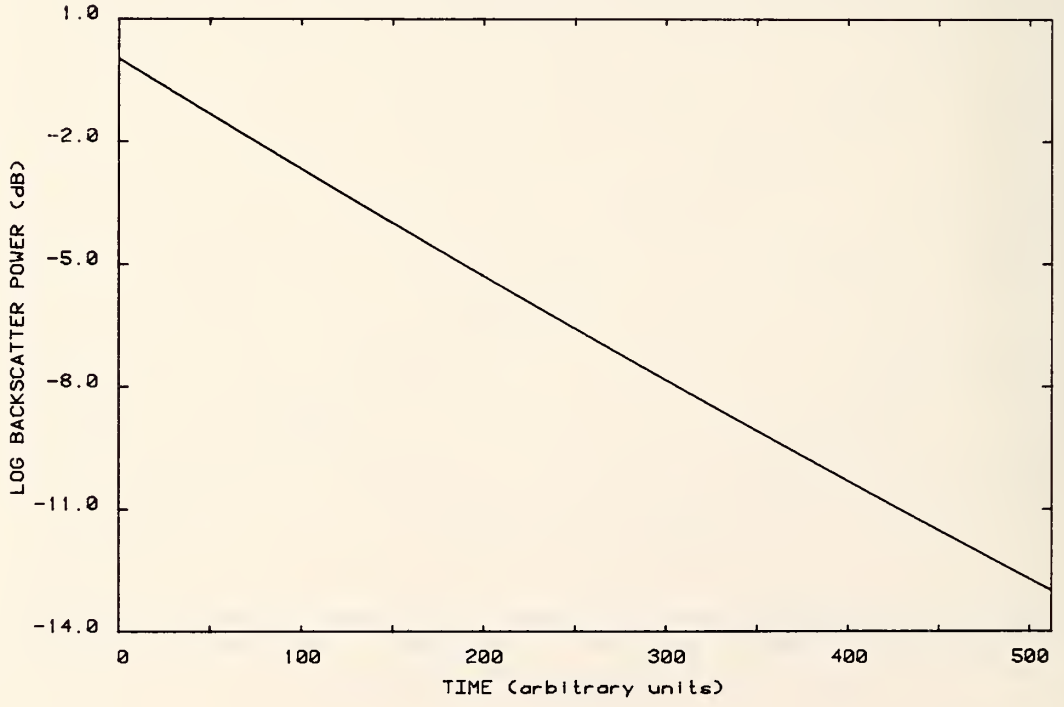

Figure 3-78. Impulse response signature for fiber shown in figure 3-75 when fiber is reversed end-for-end.

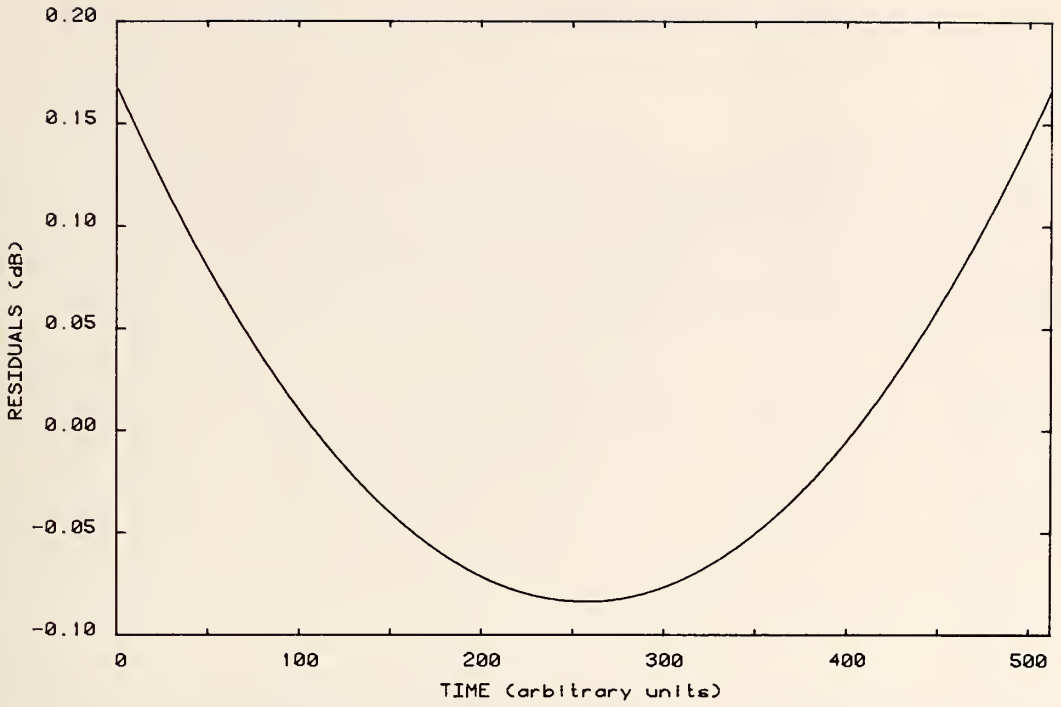

Figure 3-79. Residuals for signature of fiber shown in figure 3-78.

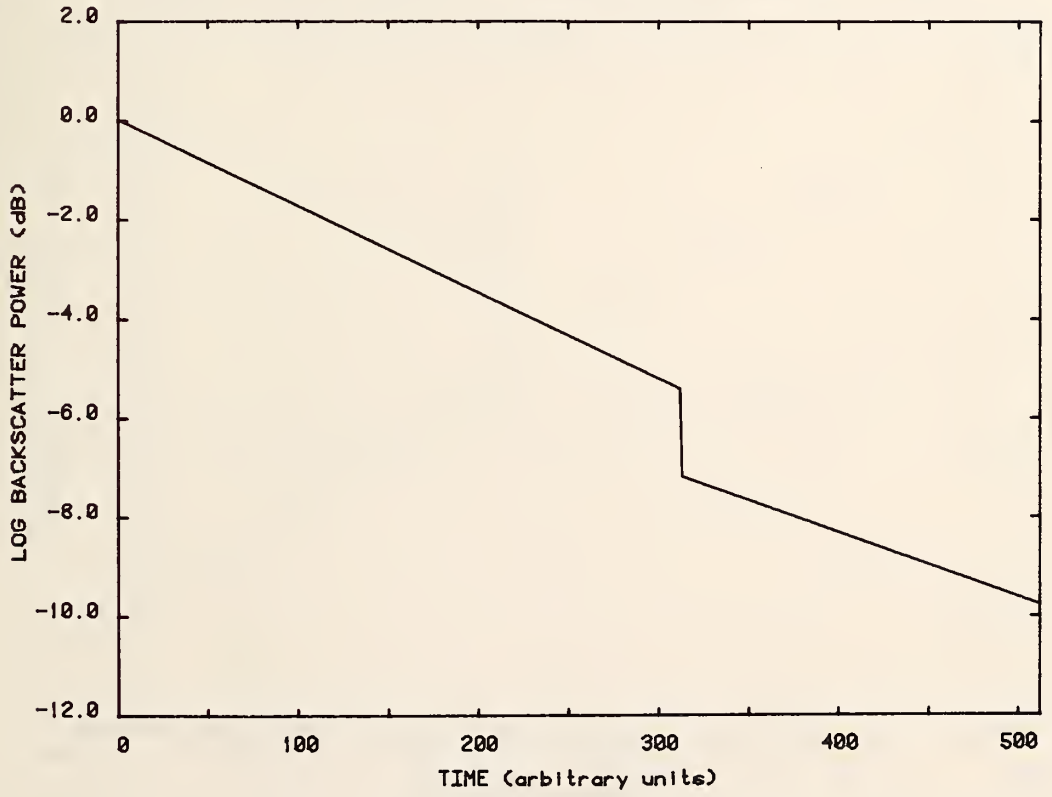

Figure 3-80. Impulse response signature of a splice in the forward direction. Logarithmic display.

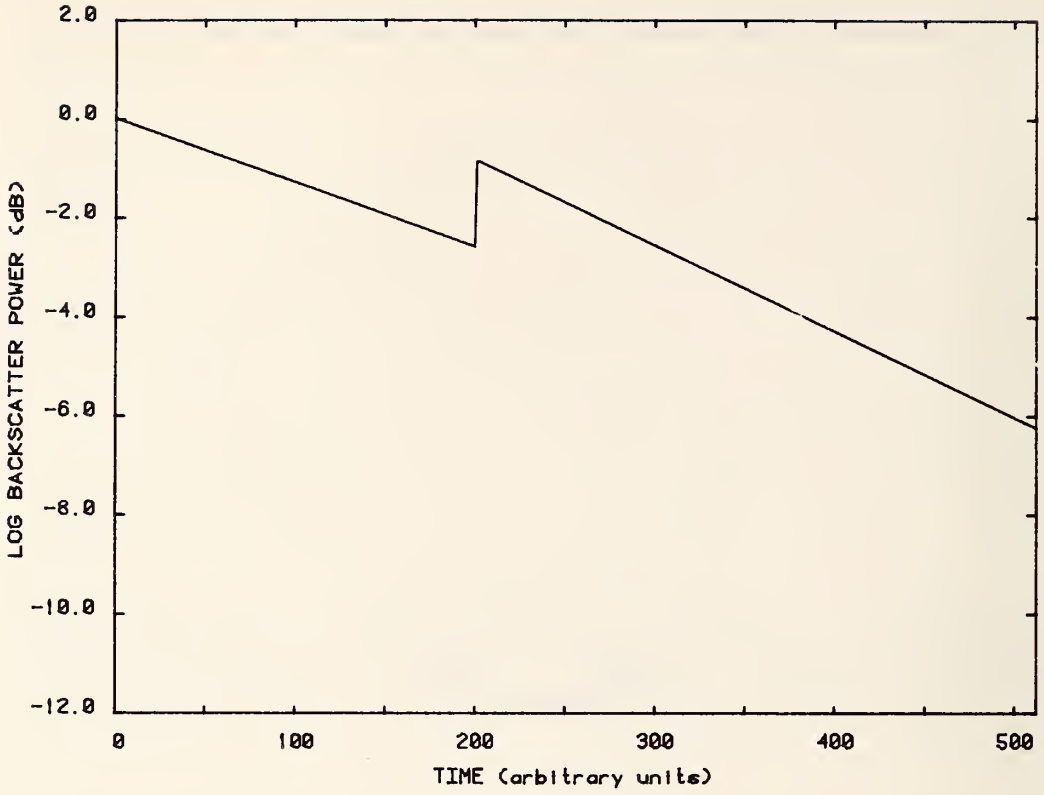

Figure 3-81. Impulse response signature of the spliced fiber in figure 3-80 when the fiber is reversed end-for-end.

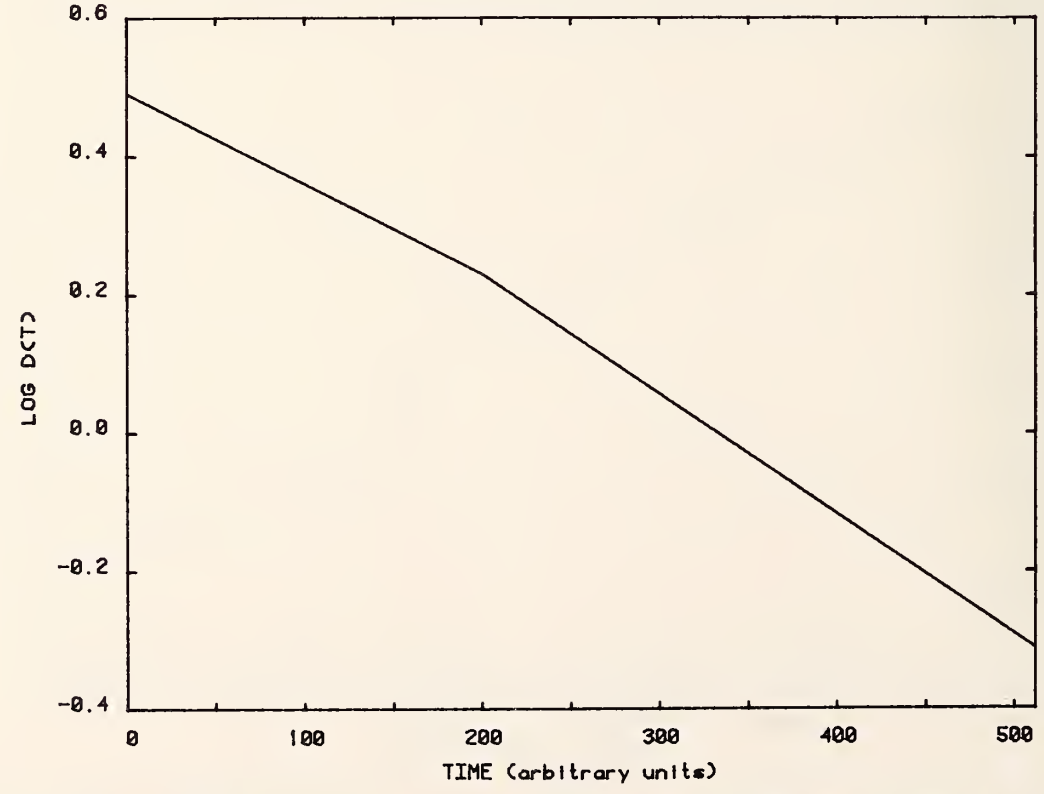

Figure 3-82. Logarithm of the power loss of fiber shown in figures 3-80 and 3-81.

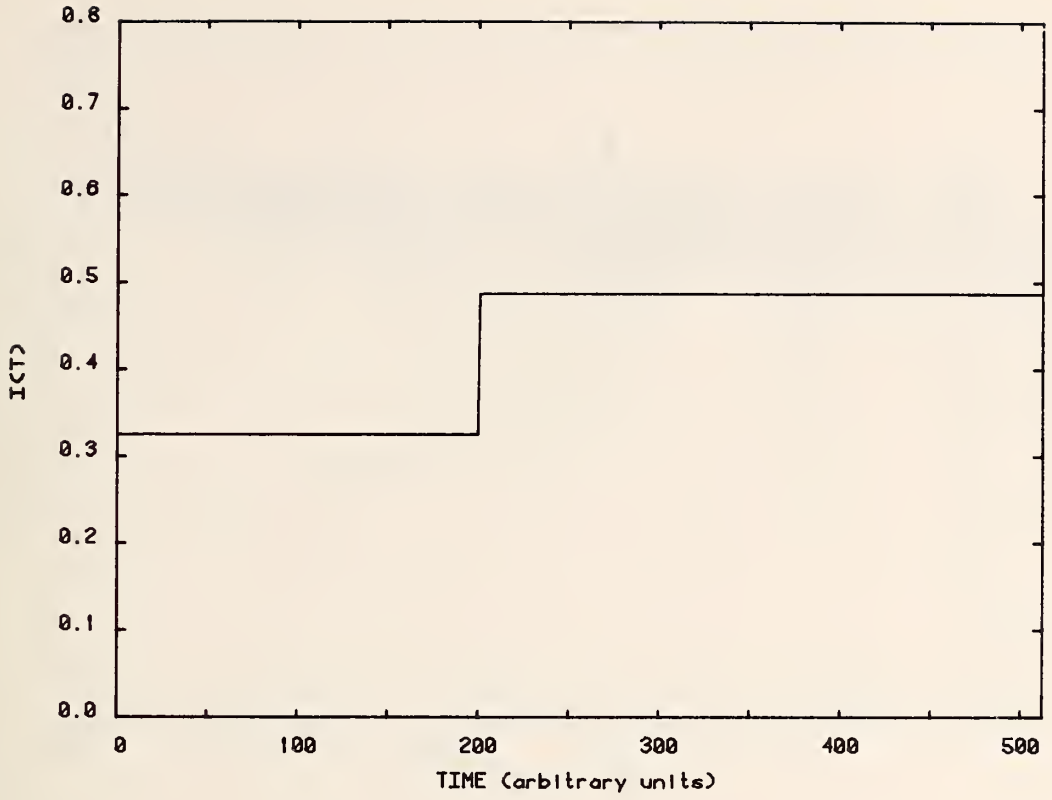

Figure 3-83. Variation of the scattering parameter with length for fiber shown in figures 3-80 and 3-81.

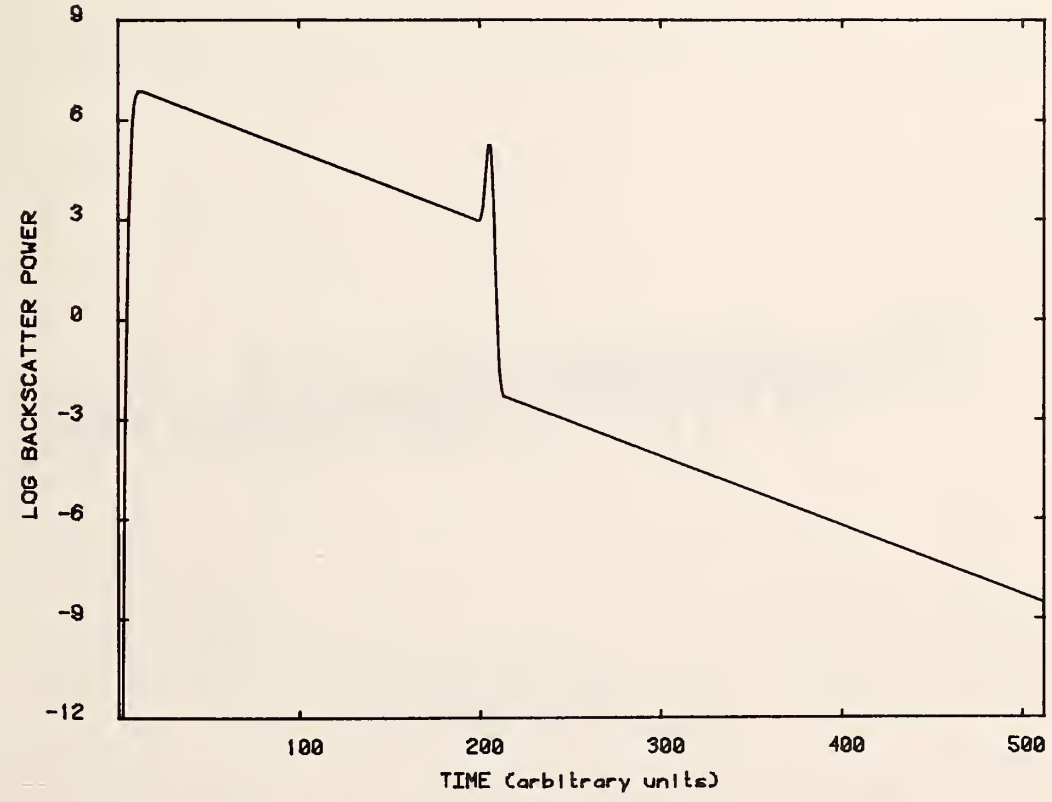

Figure 3-84. Signature of a fiber with composite defect; measurement at 800 nm. Logarithmic display.

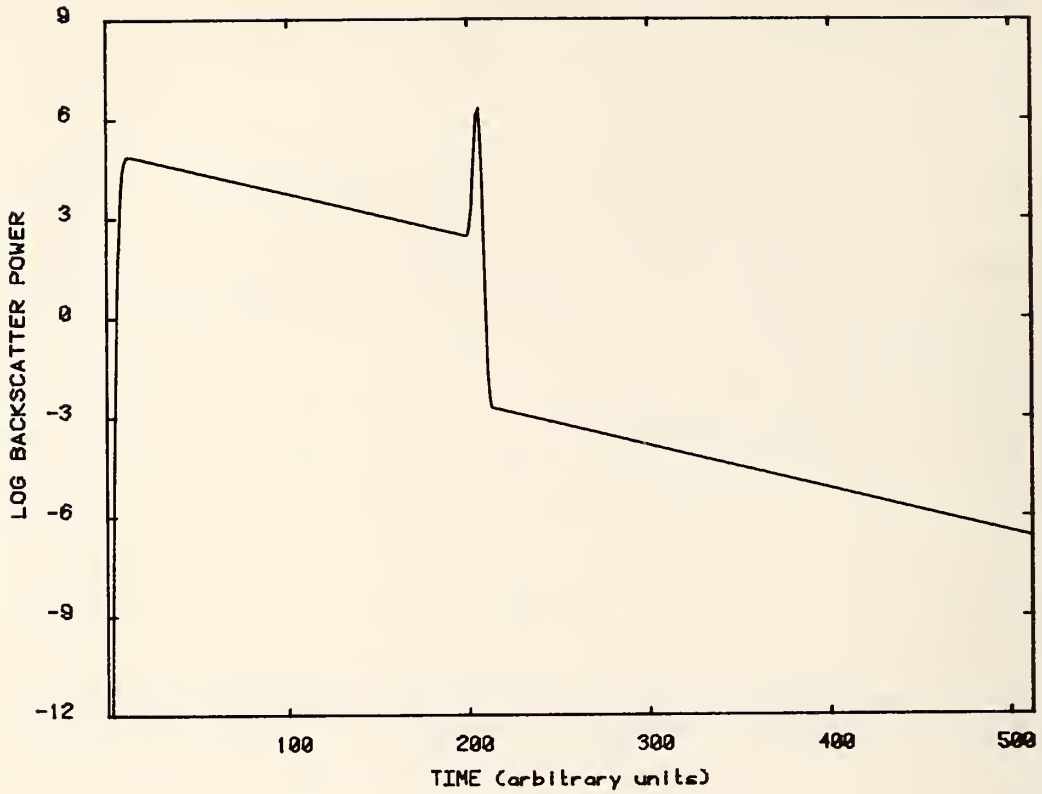

Figure 3-85. Signature of fiber in figure 3-93; measurement at 900 nm.

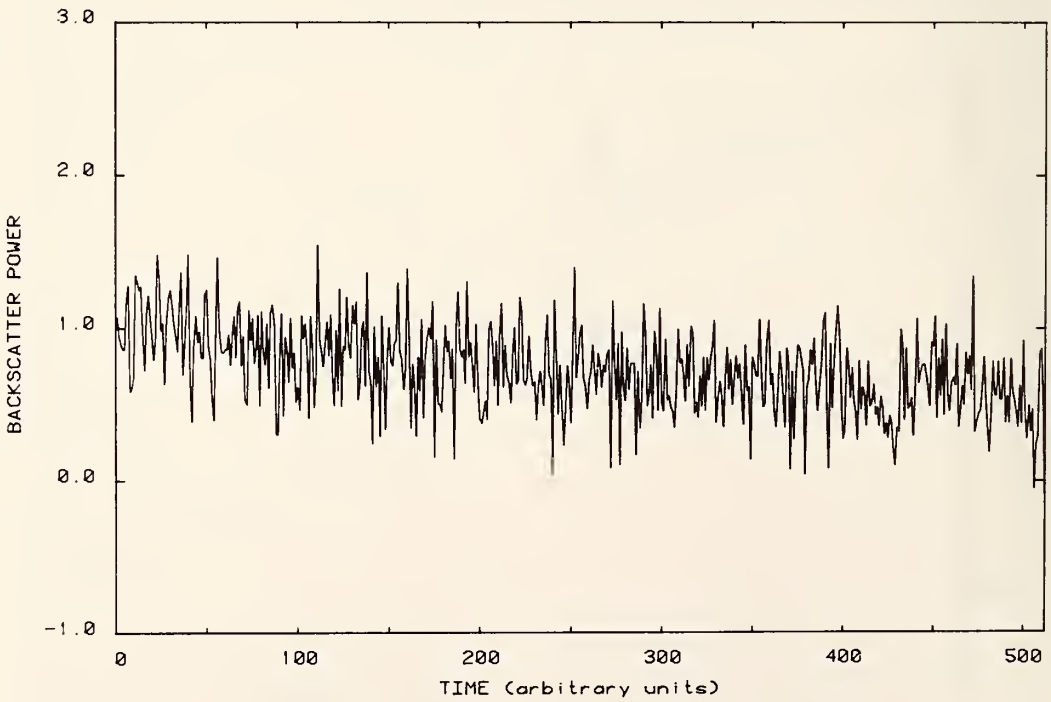

Figure 3-86. Signature with noise; SNR = 10 dB. Linear display.

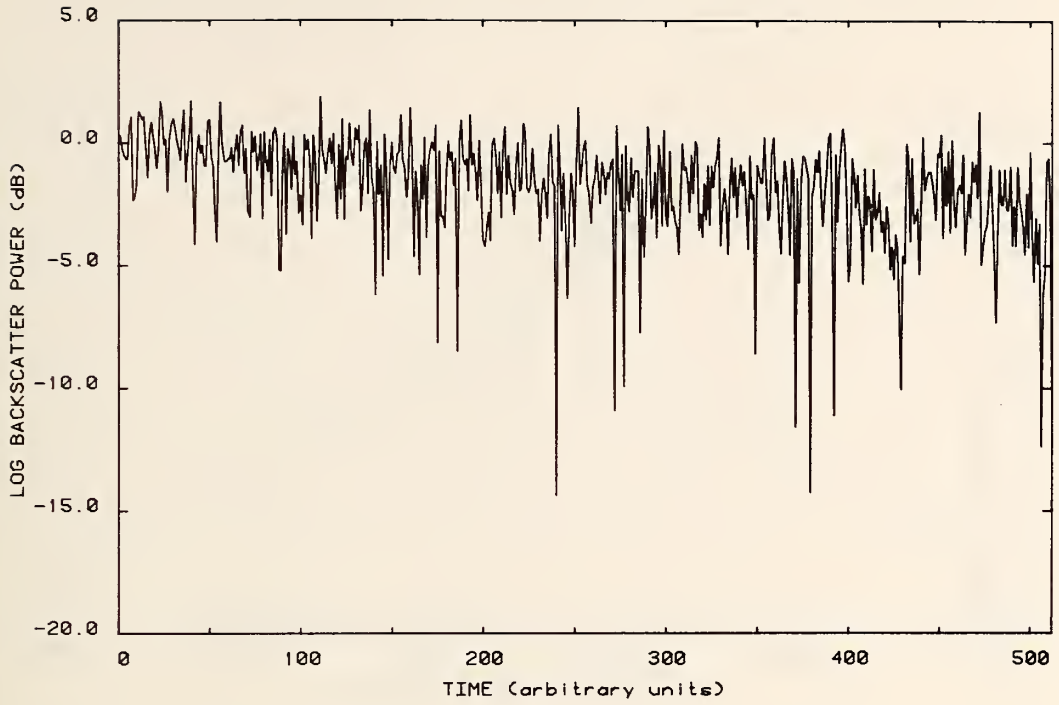

Figure 3-87. Signature of fiber in figure 3-95. Logarithmic display.

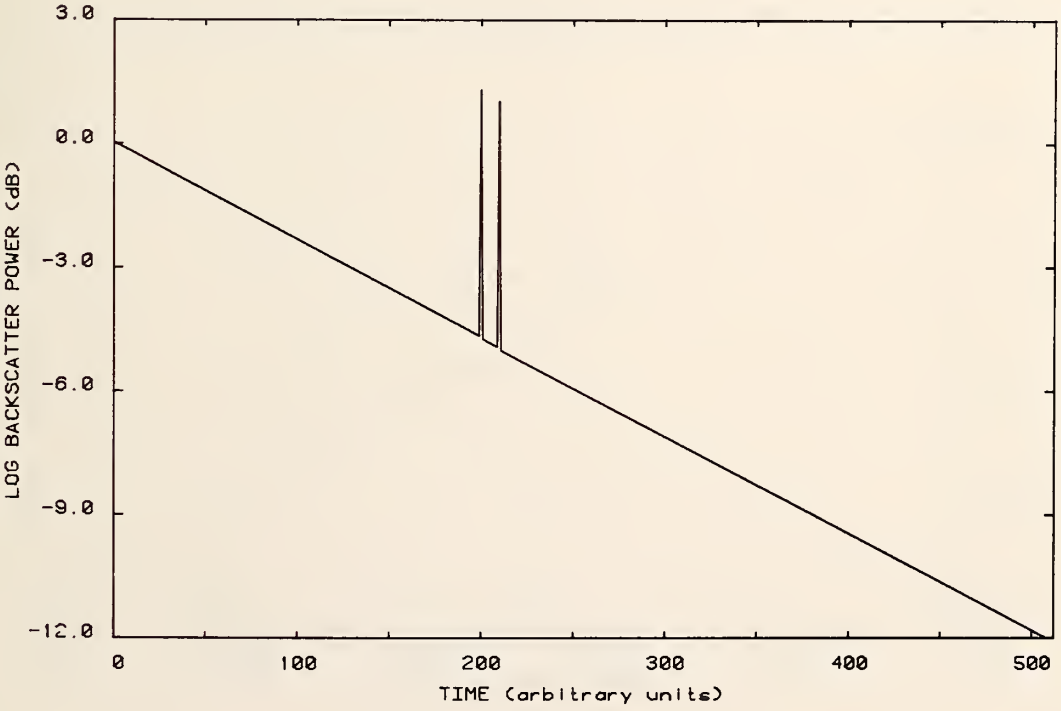

Figure 3-88. The impulse response for two scatter-like imperfections. Logarithmic display.

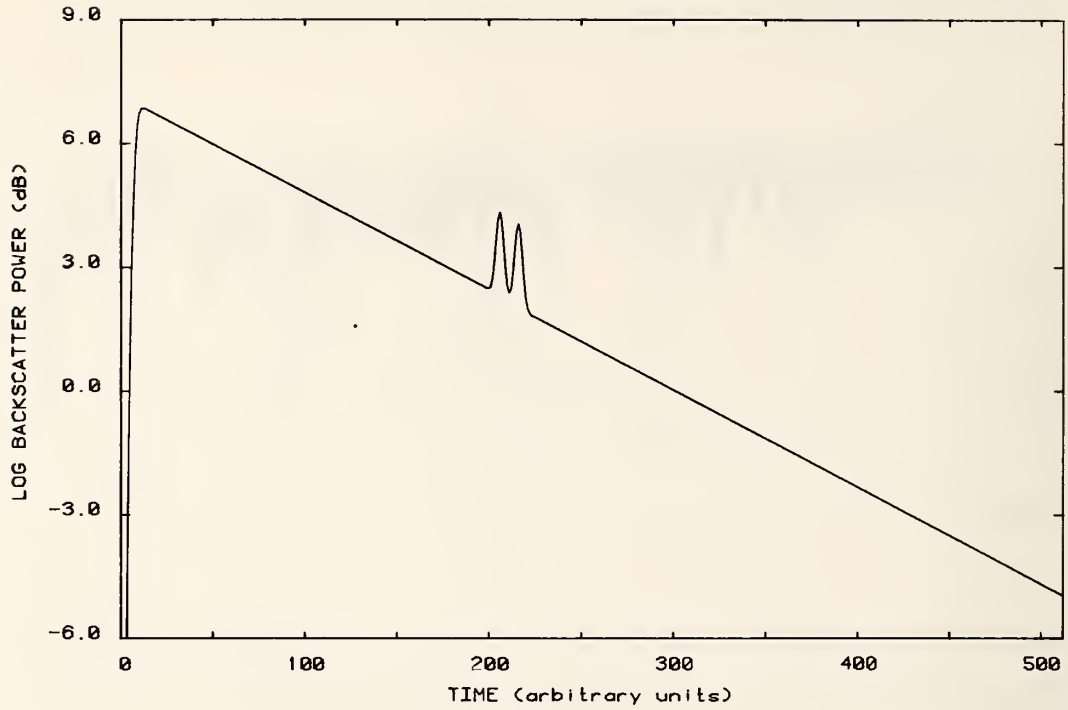

Figure 3-89. Scatter-like imperfections; Gaussian probe pulse; equivalent rectangular width 5 time units. Logarithmic display.

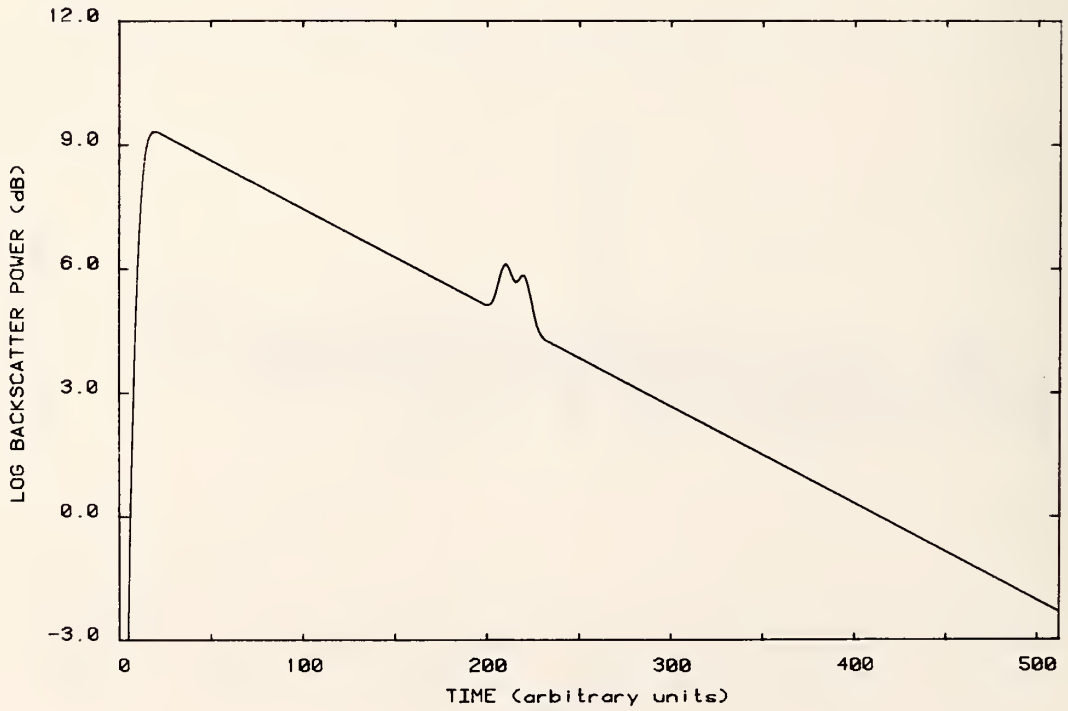

Figure 3-90. Scatter-like imperfections; Gaussian probe pulse; equivalent rectangular width 9 time units. Logarithmic display.

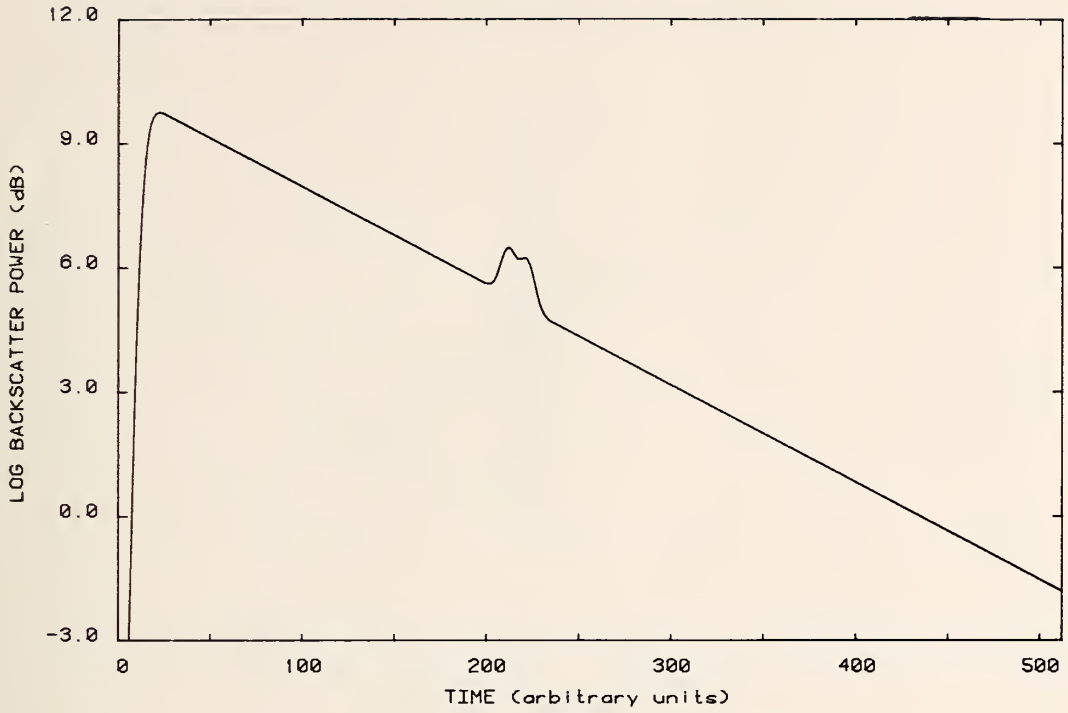

Figure 3-91. Scatter-like imperfections; Gaussian probe pulse; equivalent rectangular width 10 time units. Logarithmic display.

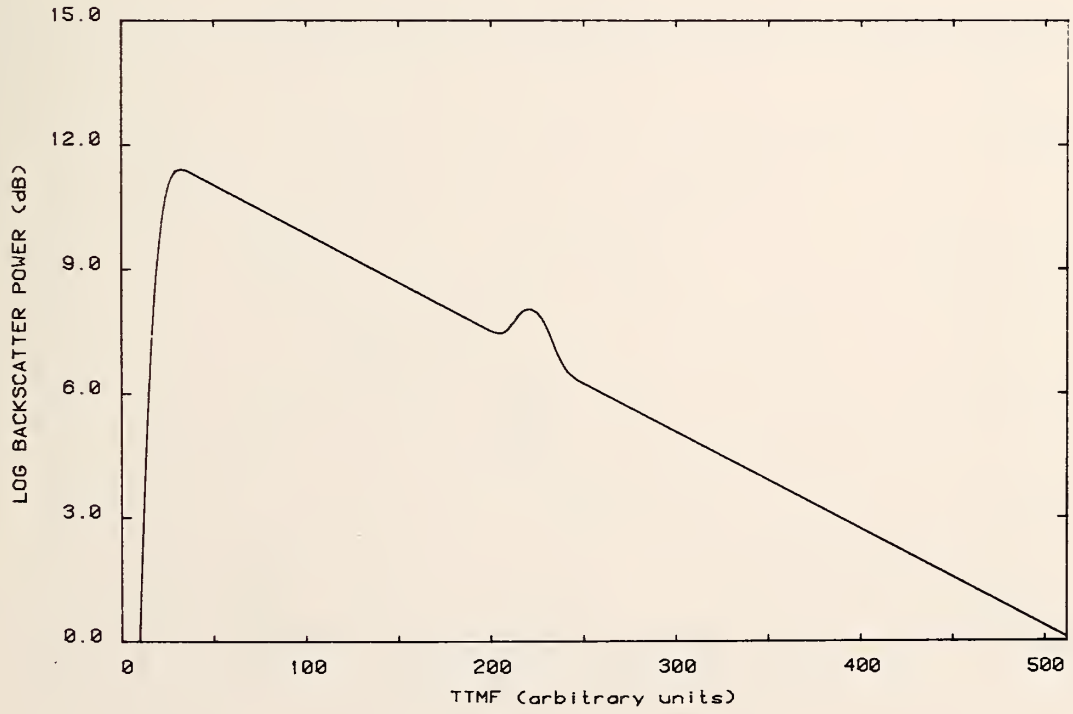

Figure 3-92. Scatter-like imperfections; Gaussian probe pulse; equivalent rectangular width 15 time units. Logarithmic display.

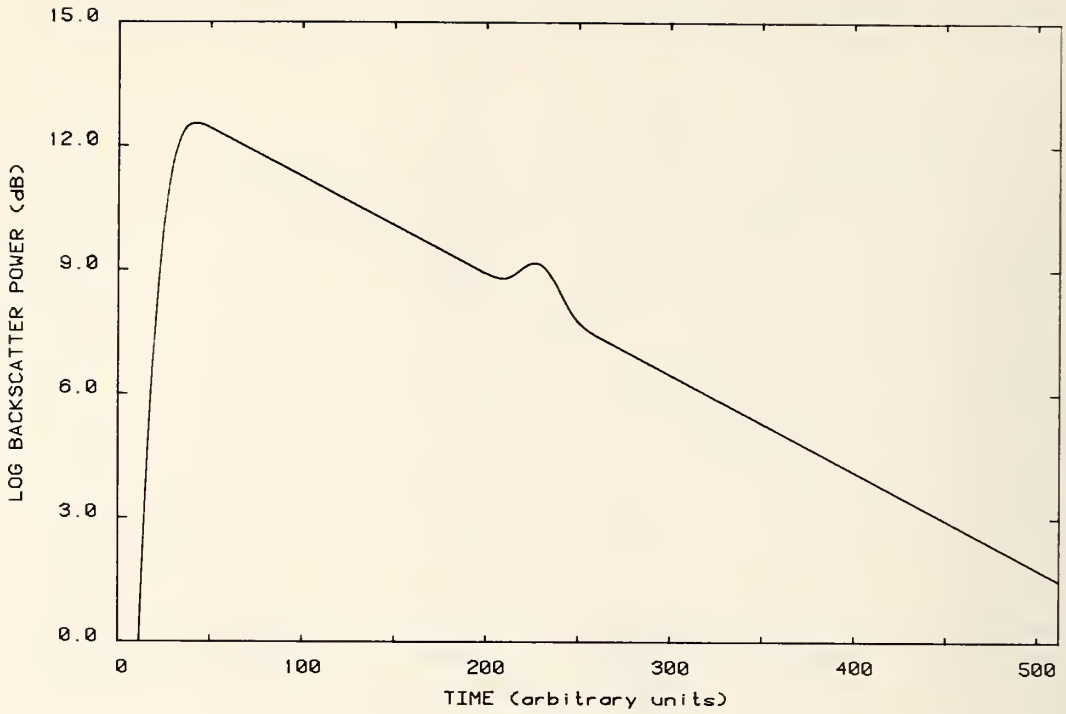

Figure 3-93. Scatter-like imperfections; Gaussian probe pulse; equivalent rectangular width 20 time units. Logarithmic display.

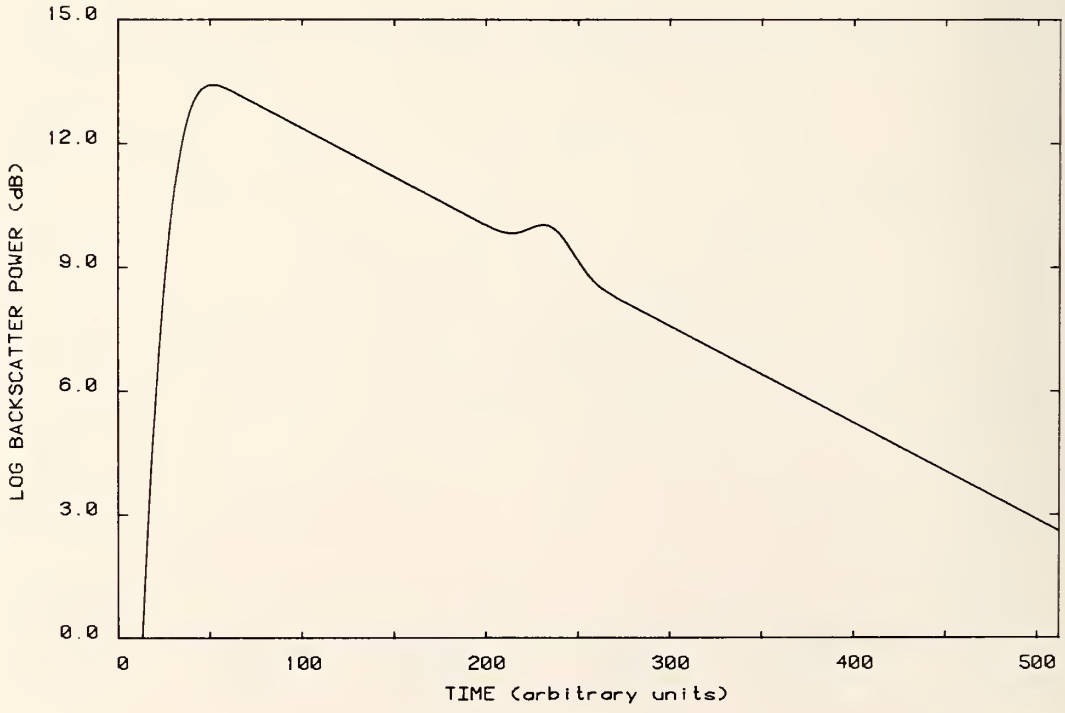

Figure 3-94. Scatter-like imperfections; Gaussian probe pulse; equivalent rectangular width 25 time units. Logarithmic display.

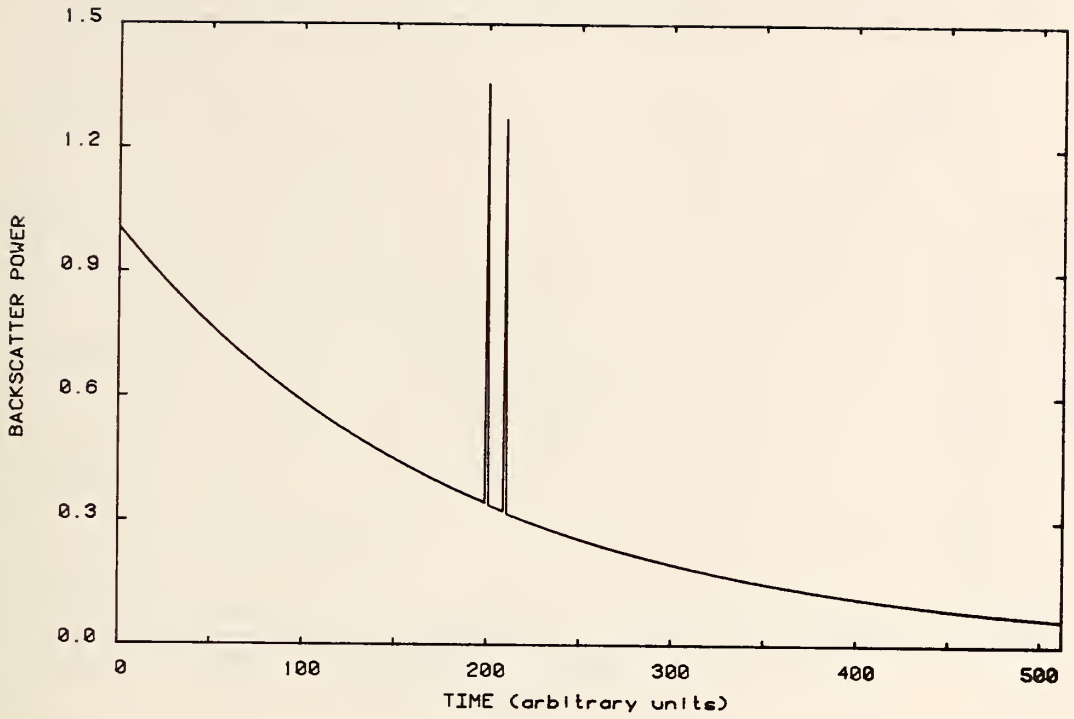

Figure 3-95. The impulse response for two scatter-like imperfections. Linear display.

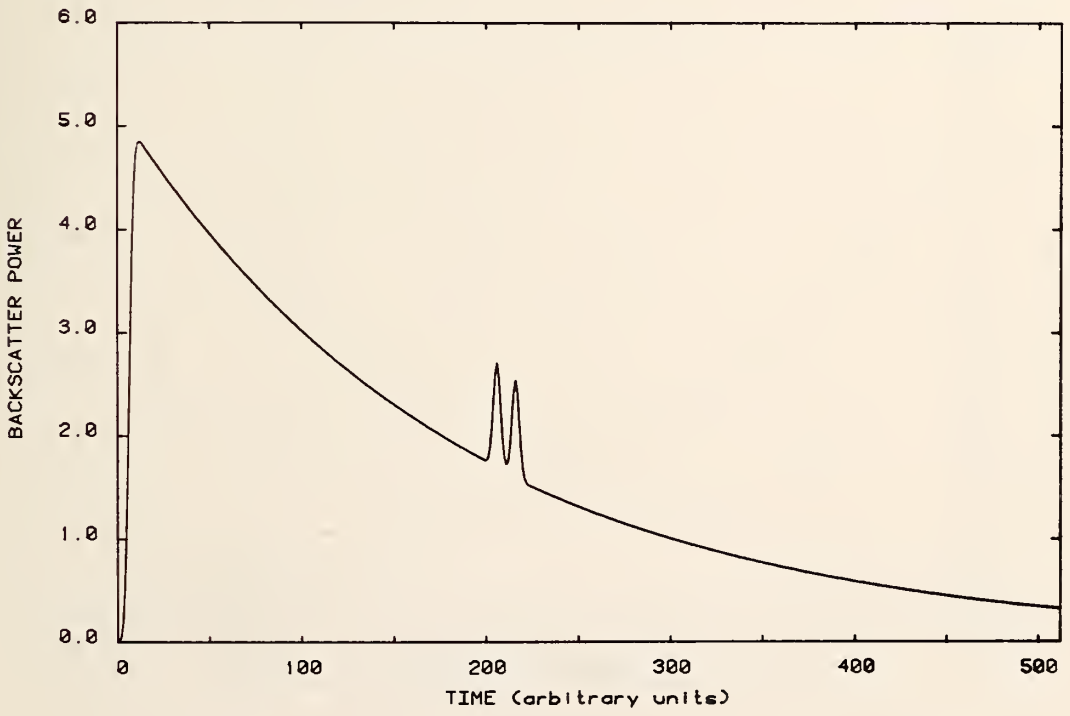

Figure 3-96. Scatter-like imperfections; Gaussian probe pulse; equivalent rectangular width 5 time units. Linear display.

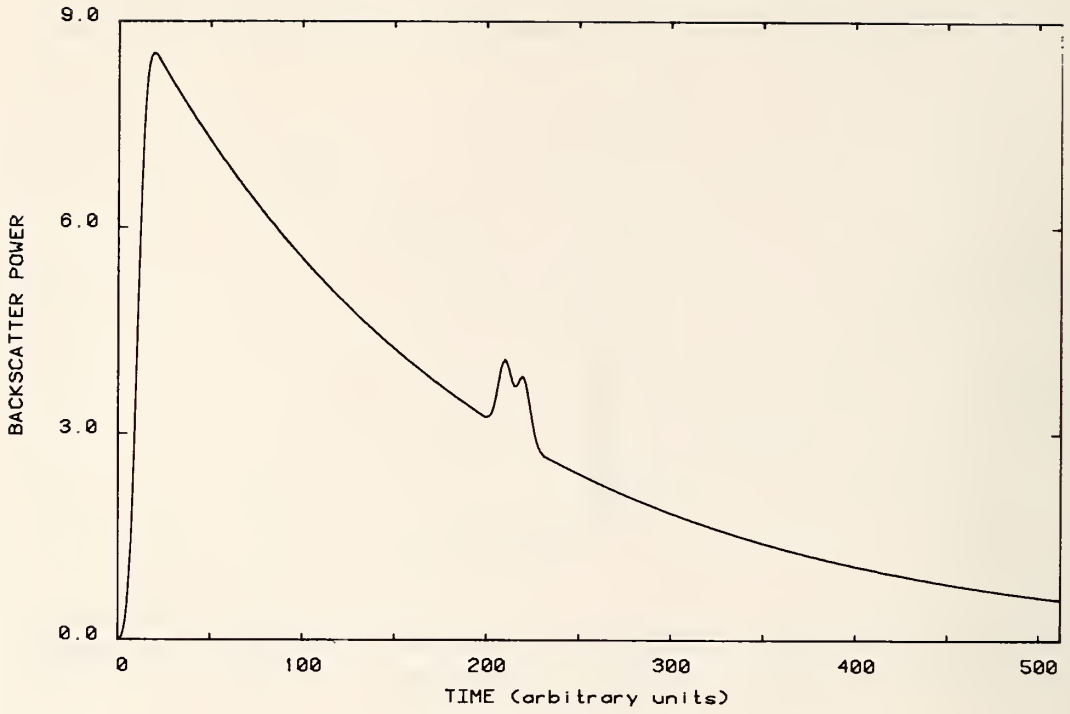

Figure 3-97. Scatter-like imperfections; Gaussian probe pulse; equivalent rectangular width 9 time units. Linear display.

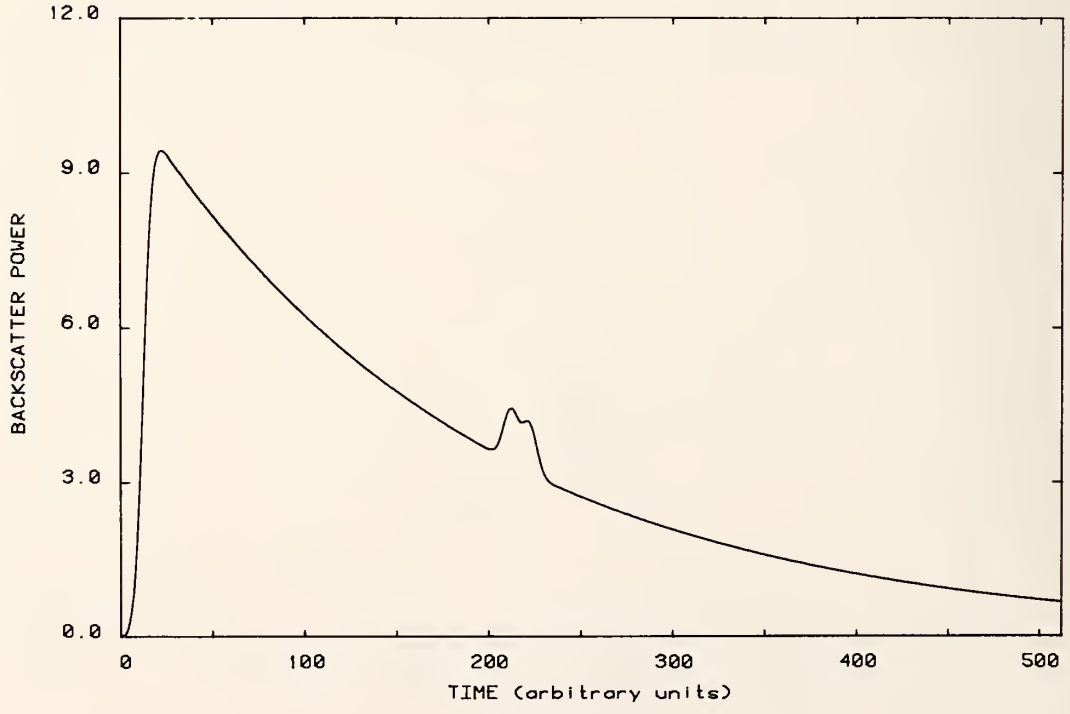

Figure 3-98. Scatter-like imperfections; Gaussian probe pulse; equivalent rectangular width 10 time units. Linear display.

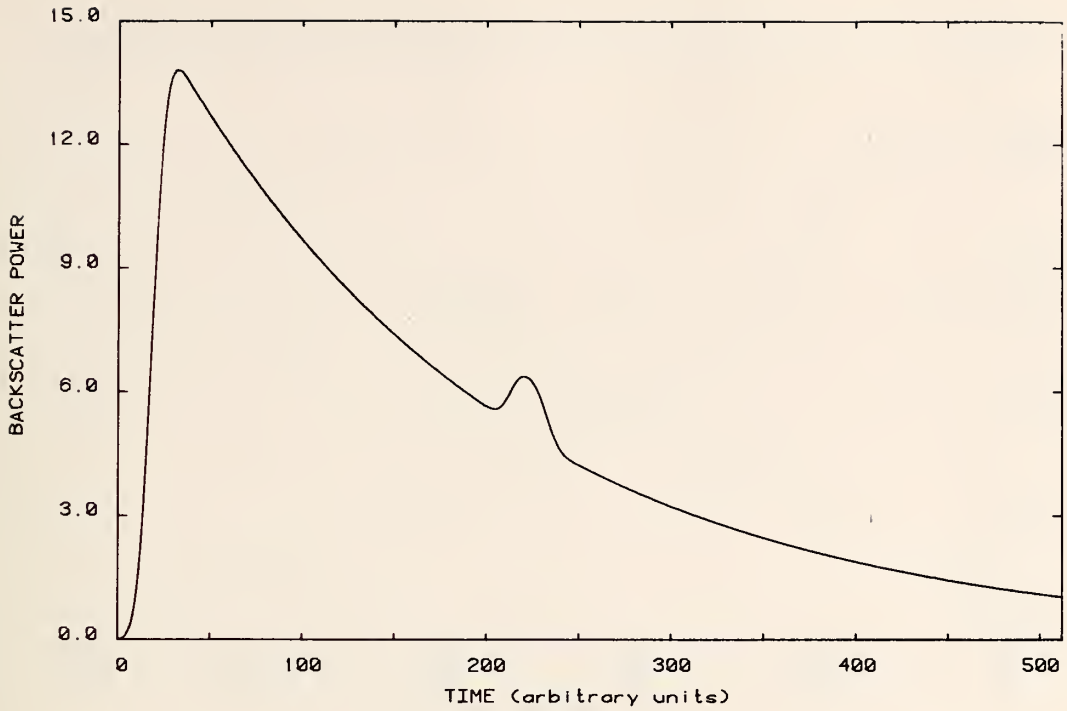

Figure 3-99. Scatter-like imperfections; Gaussian probe pulse; equivalent rectangular width 15 time units. Linear display.

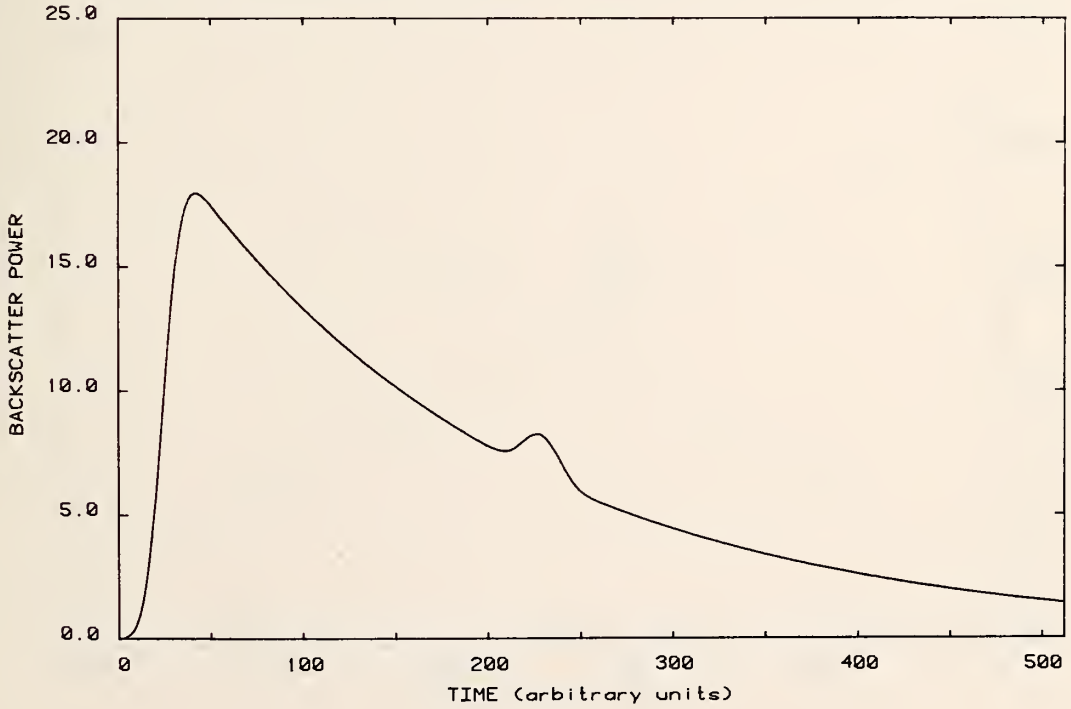

Figure 3-100. Scatter-like imperfections; Gaussian probe pulse; equivalent rectangular width 20 time units. Linear display.

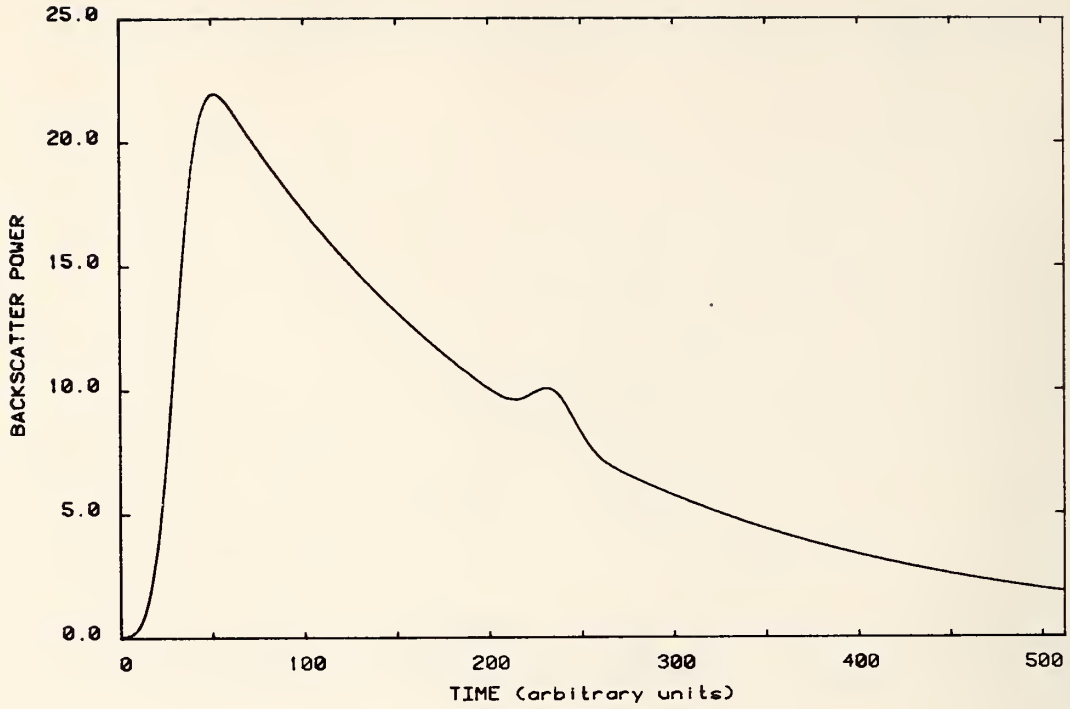

Figure 3-101. Scatter-like imperfections; Gaussian probe pulse; equivalent rectangular width 25 time units. Linear display.

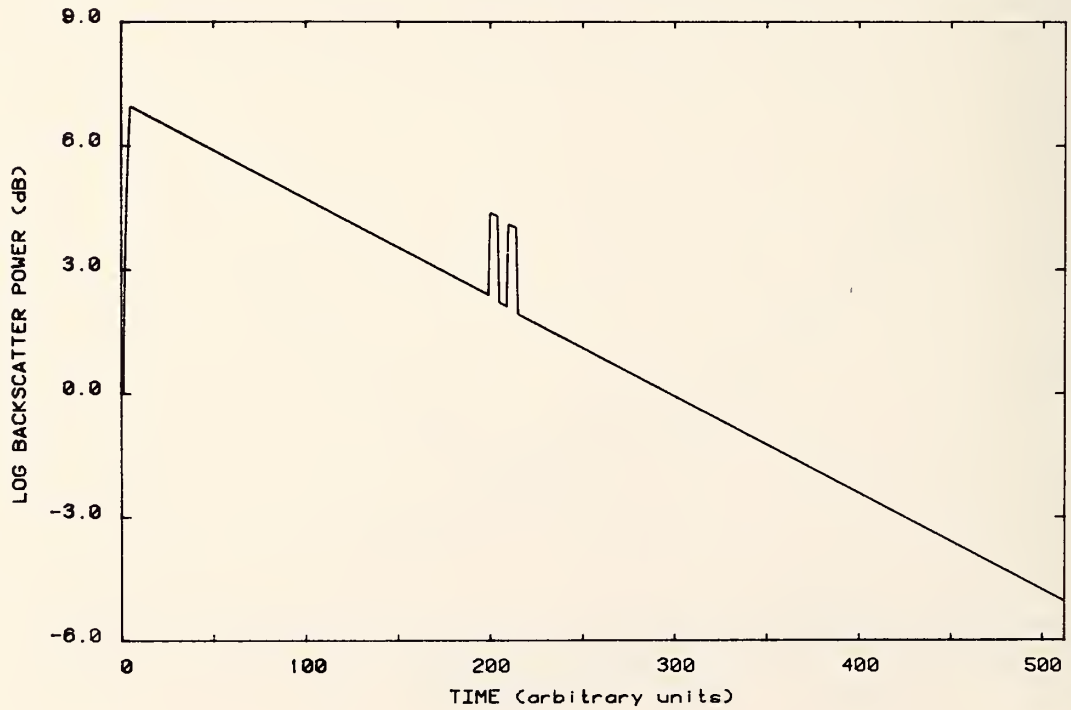

Figure 3-102. Scatter-like imperfections; rectangular probe pulse of width 5 time units. Logarithmic display.

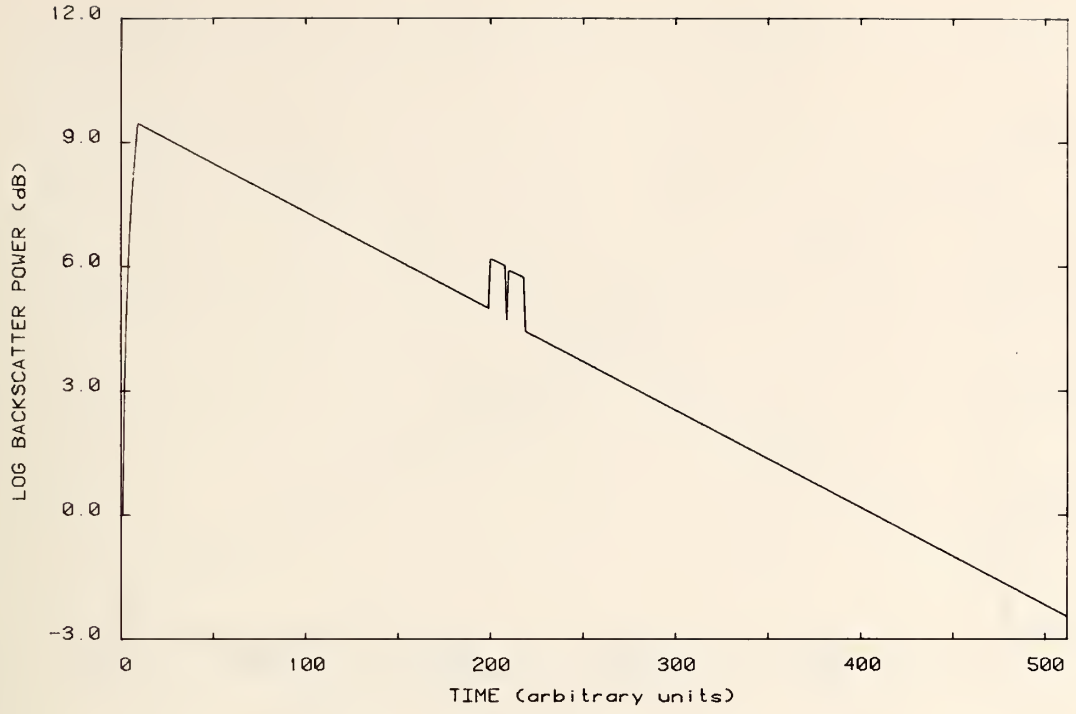

Figure 3-103. Scatter-like imperfections; rectangular probe pulse of width 9 time units. Logarithmic display.

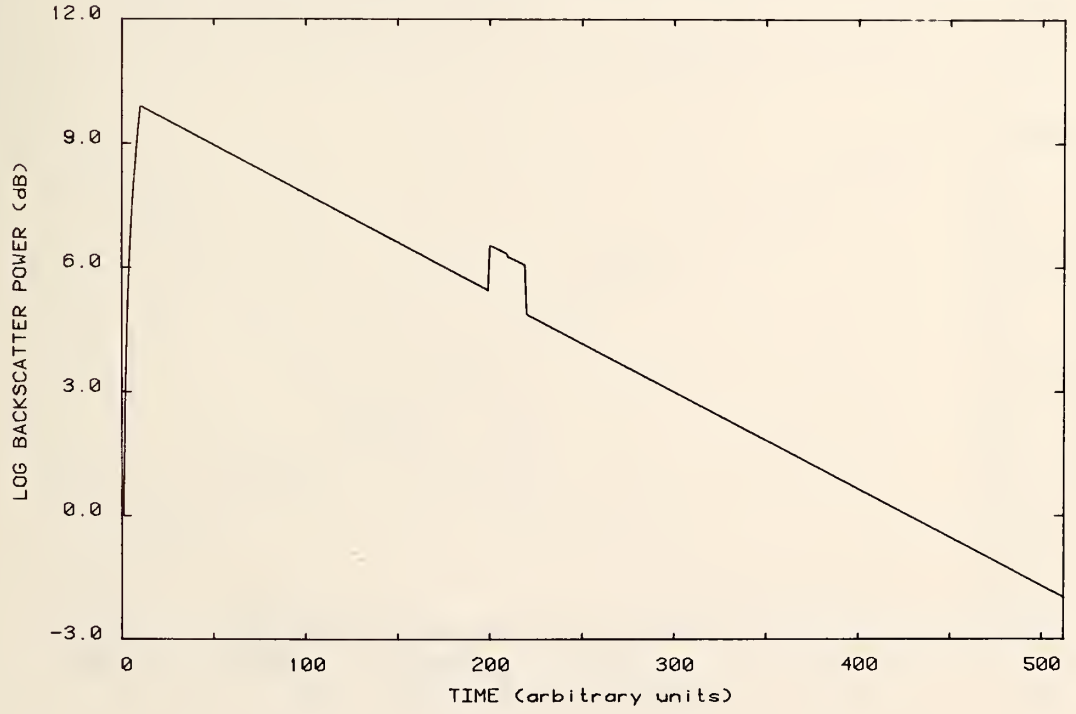

Figure 3-104. Scatter-like imperfections; rectangular probe pulse of width 10 time units. Logarithmic display.

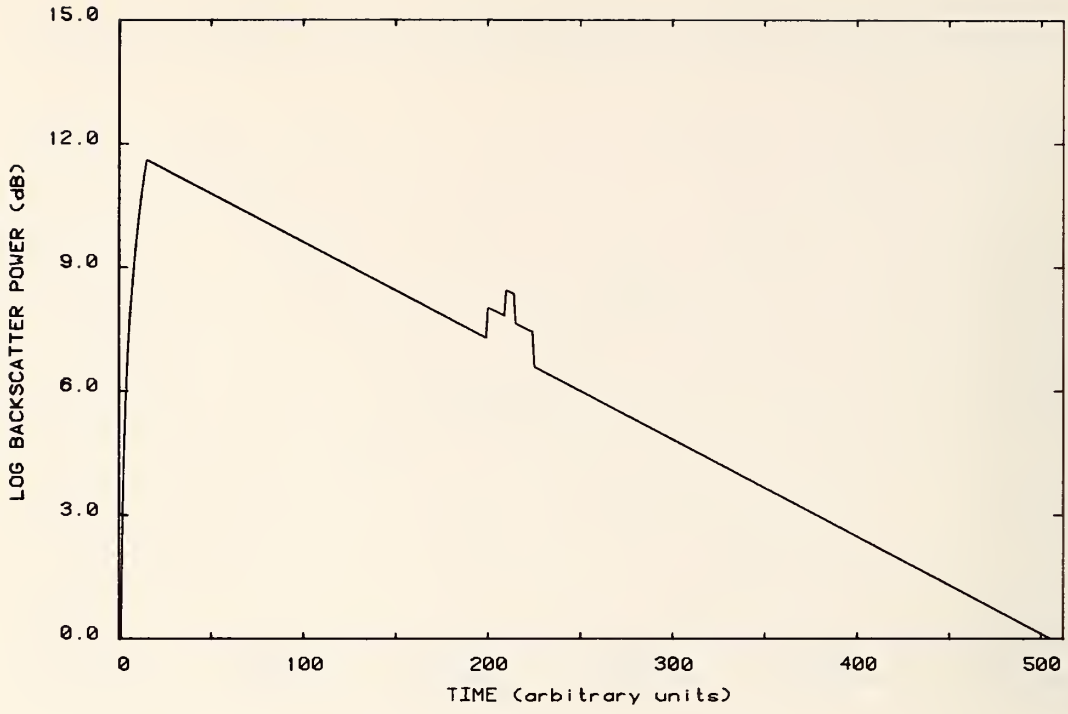

Figure 3-105. Scatter-like imperfections; rectangular probe pulse of width 15 time units. Logarithmic display.

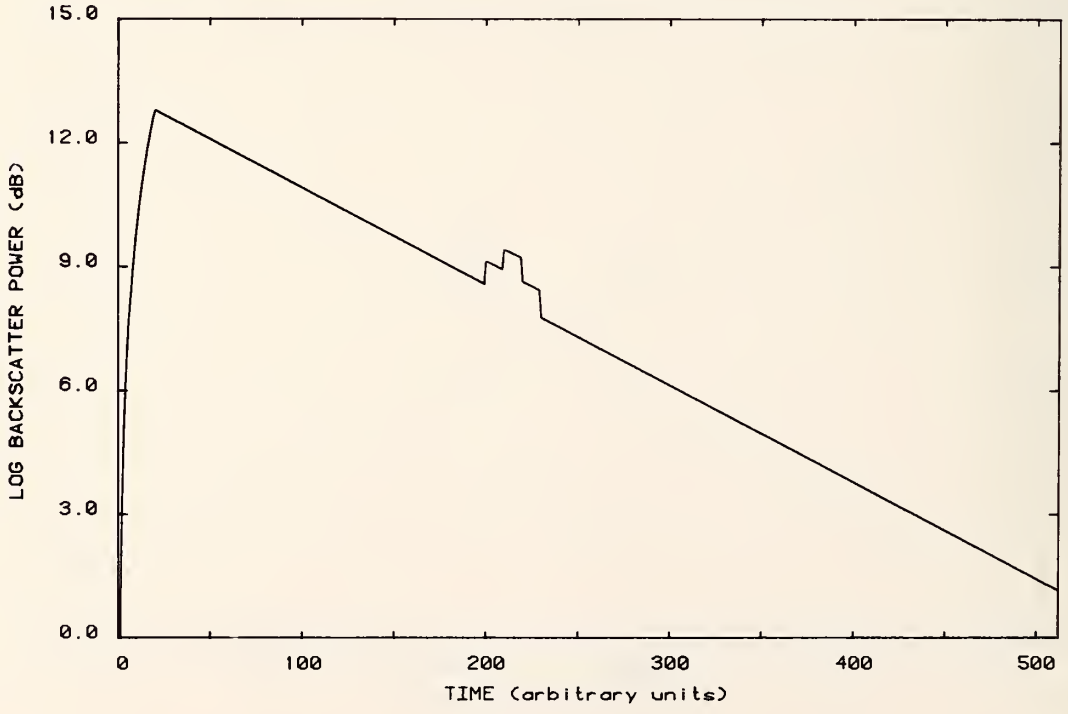

Figure 3-106. Scatter-like imperfections; rectangular probe pulse of width 20 time units. Logarithmic display.

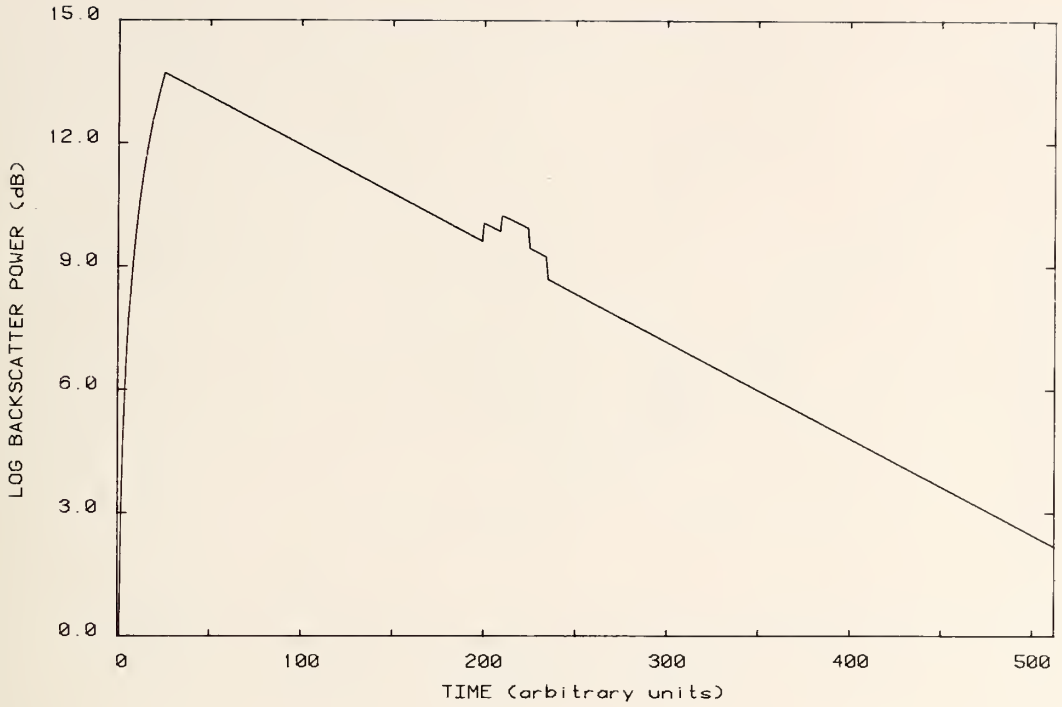

Figure 3-107. Scatter-like imperfections; rectangular probe pulse of width 25 time units. Logarithmic display.

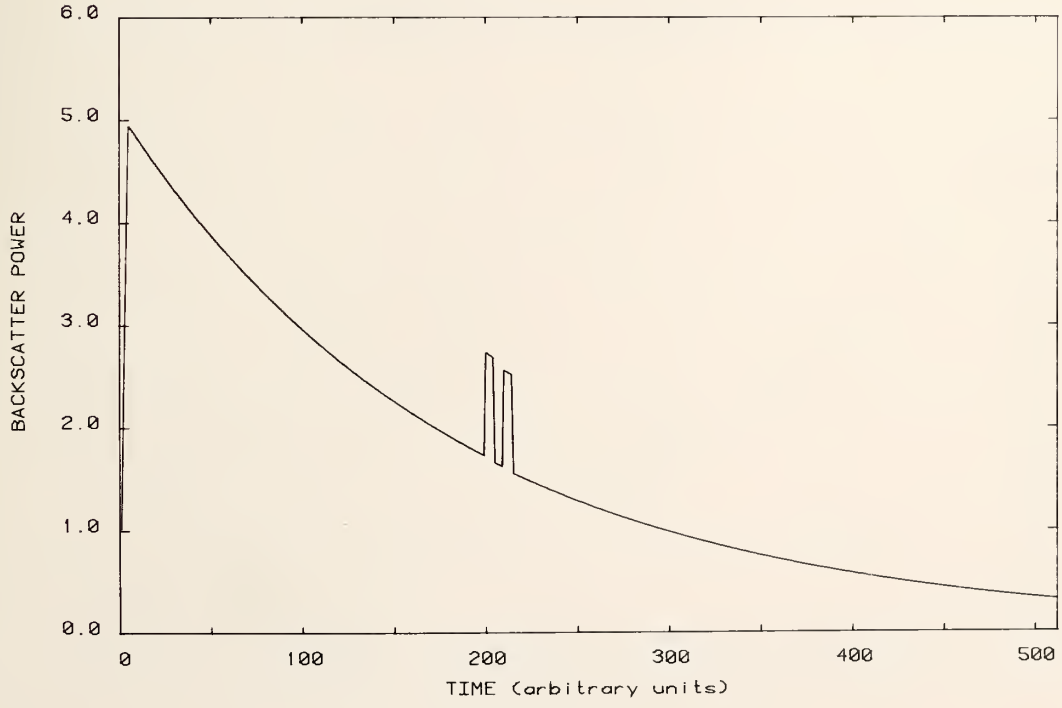

Figure 3-108. Scatter-like imperfections; rectangular probe pulse of width 5 time units. Linear display.

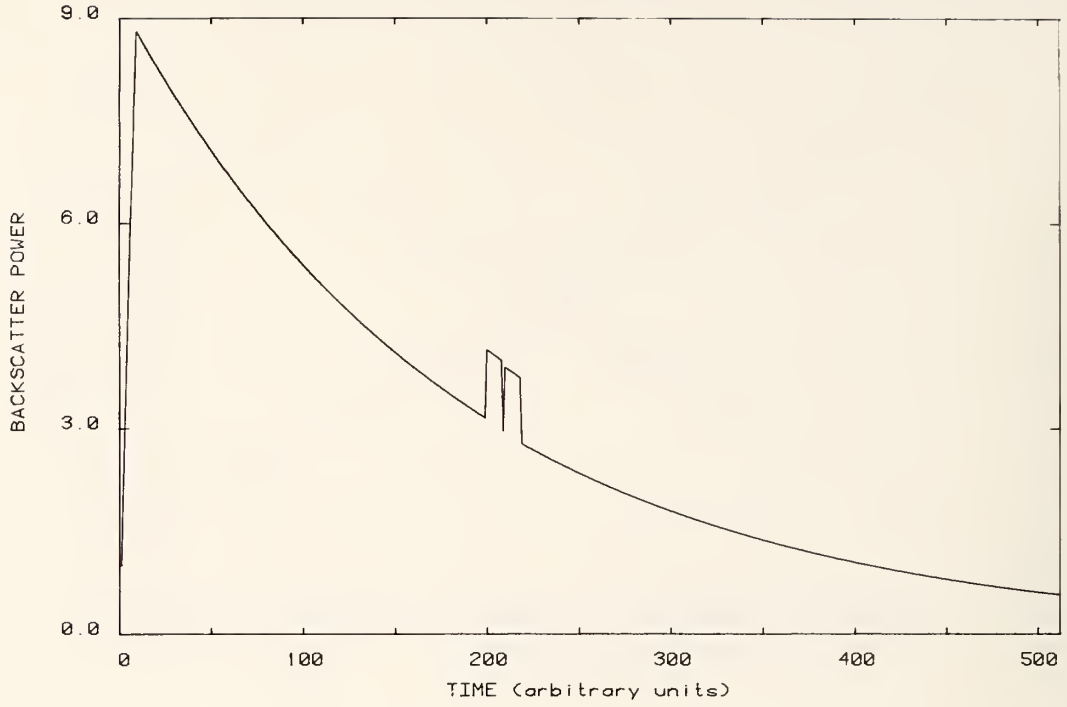

Figure 3-109. Scatter-like imperfections; rectangular probe pulse of width 9 time units. Linear display.

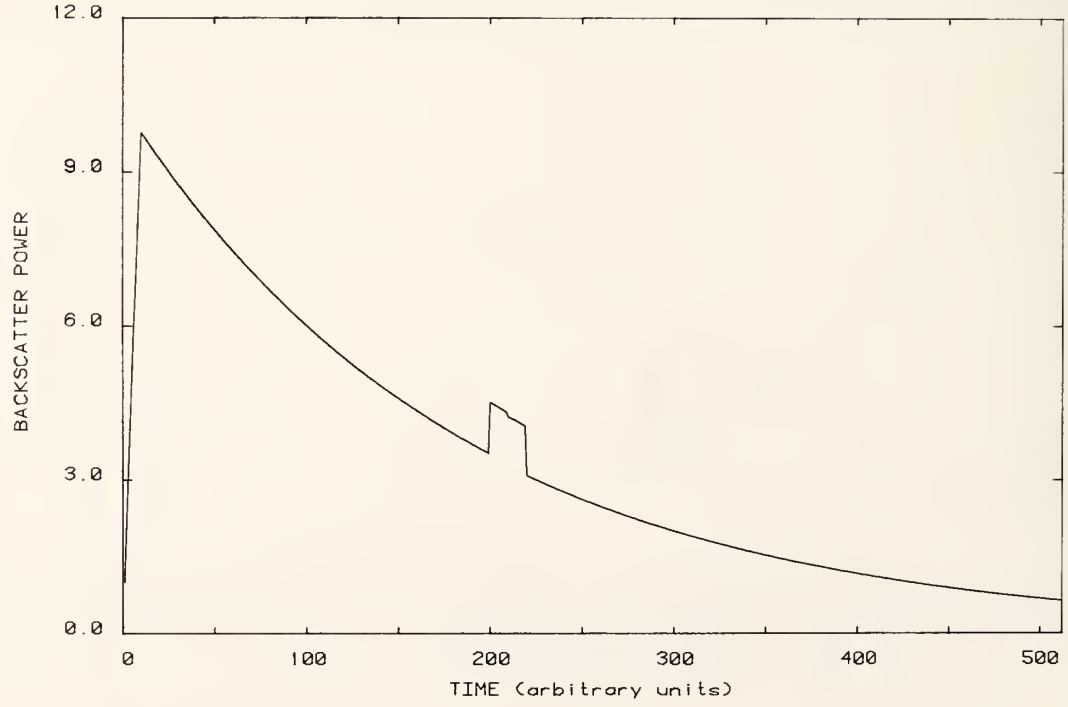

Figure 3-110. Scatter-like imperfections; rectangular probe pulse of width 10 time units. Linear display.

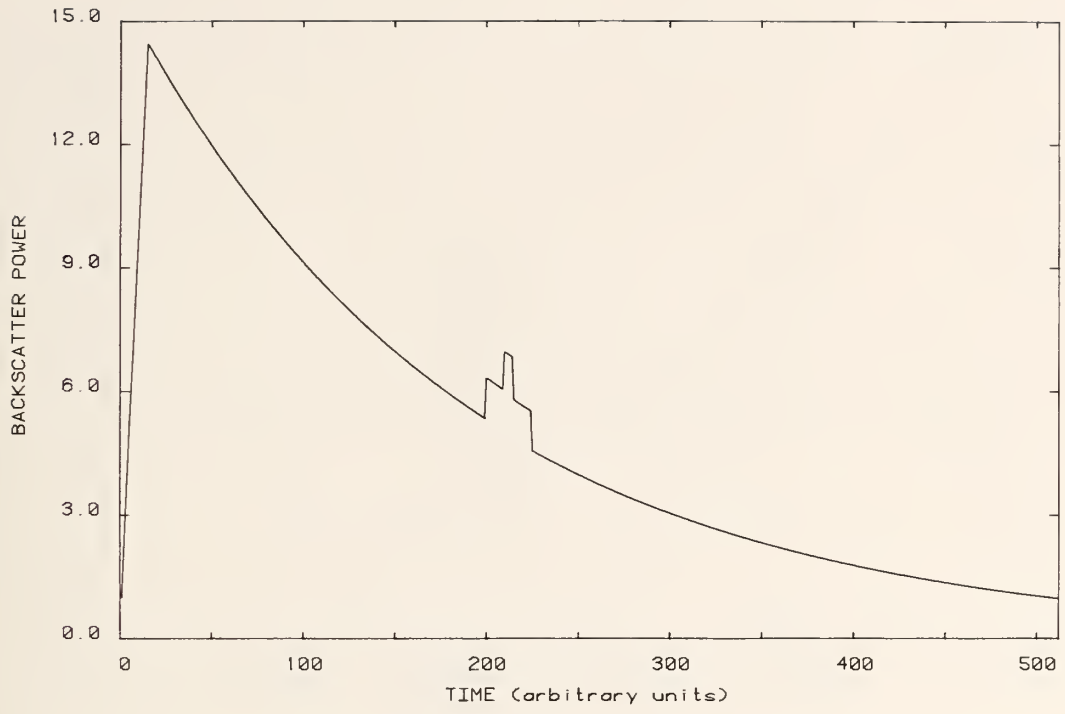

Figure 3-111. Scatter-like imperfections; rectangular probe pulse of width 15 time units. Linear display.

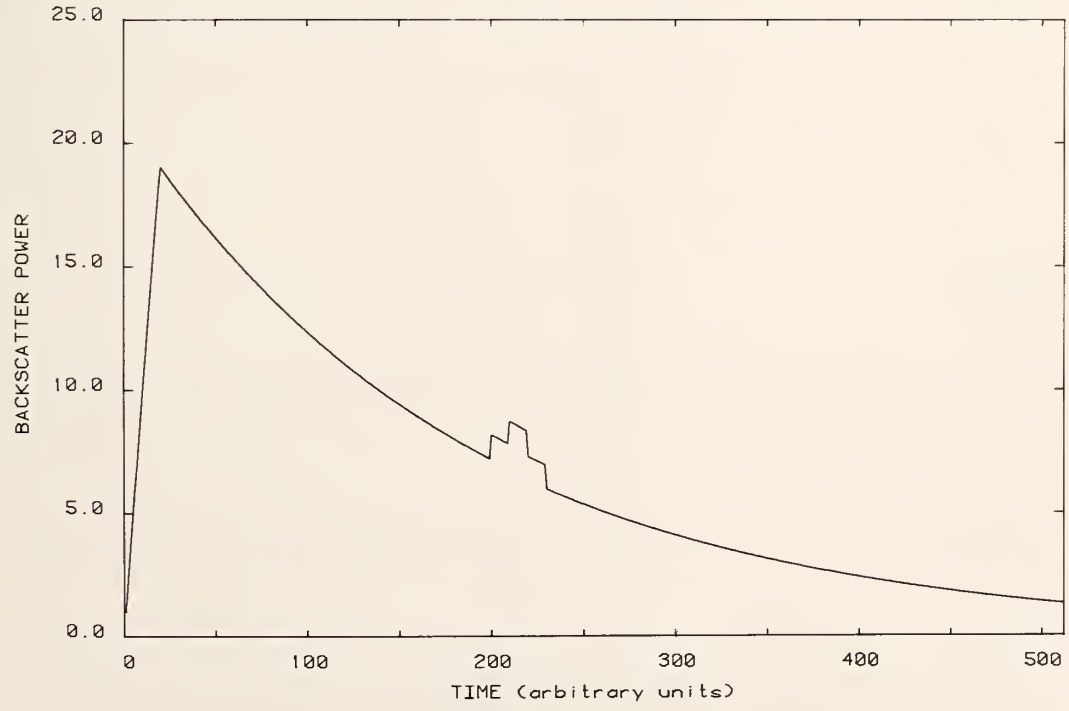

Figure 3-112. Scatter-like imperfections; rectangular probe pulse of width 20 time units. Linear display.

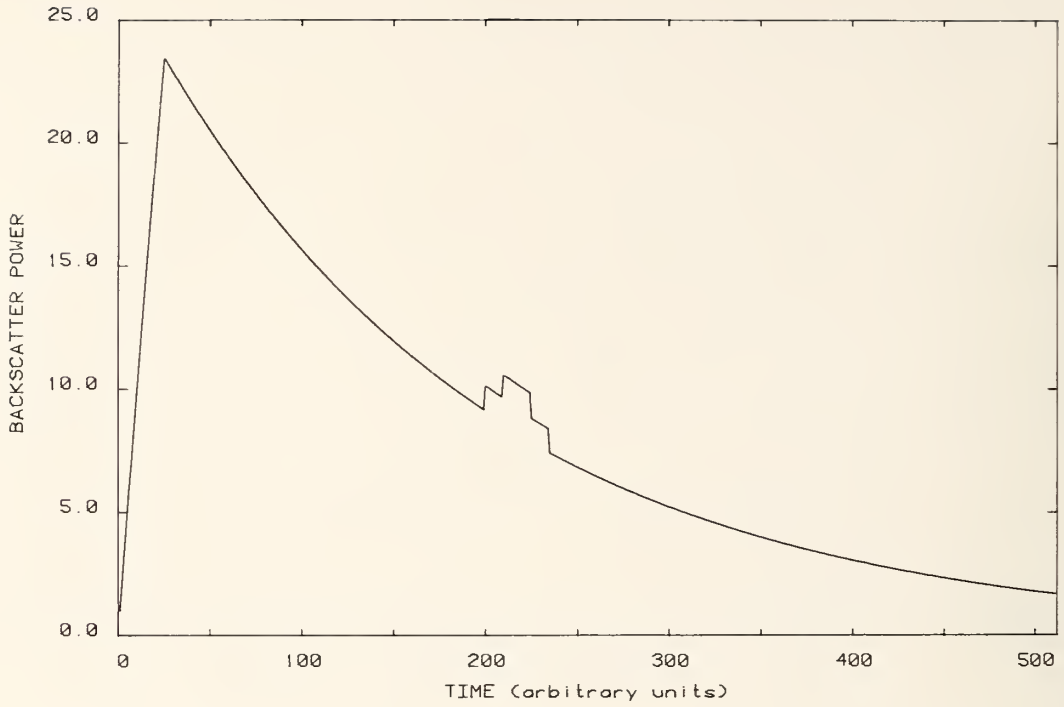

Figure 3-113. Scatter-like imperfections; rectangular probe pulse of width 25 time units. Linear display.

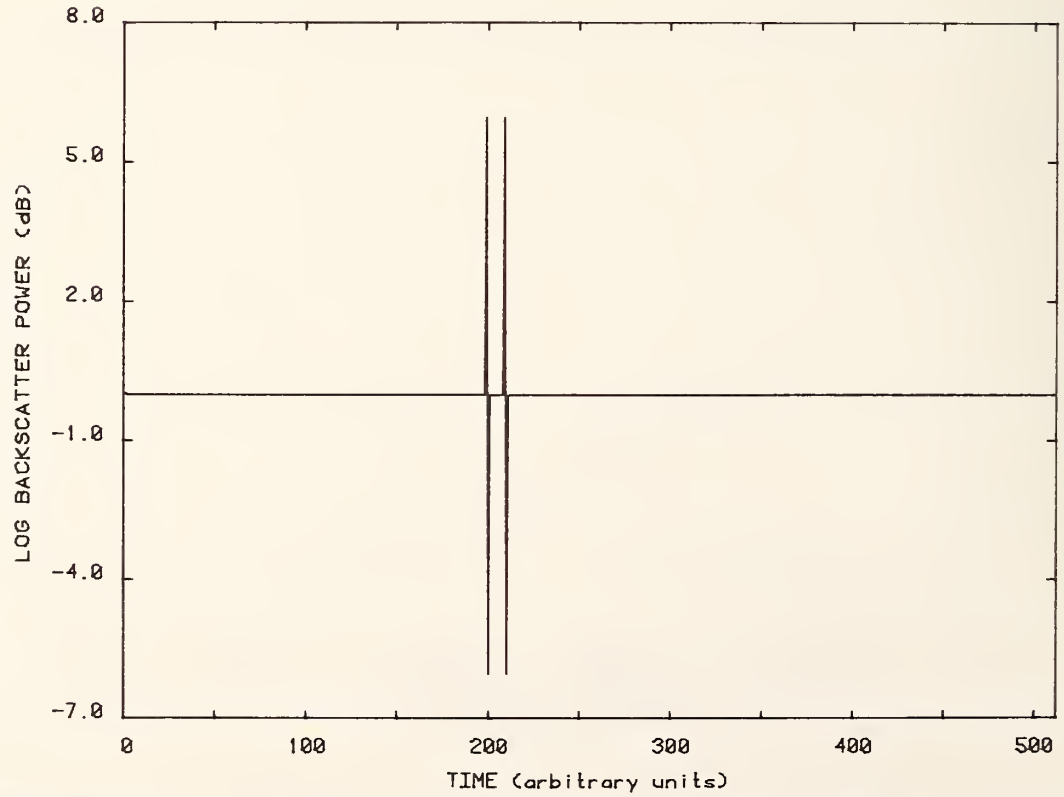

Figure 3-114. Impulse response for two scatter-like imperfections; delay one time unit. Differential display.

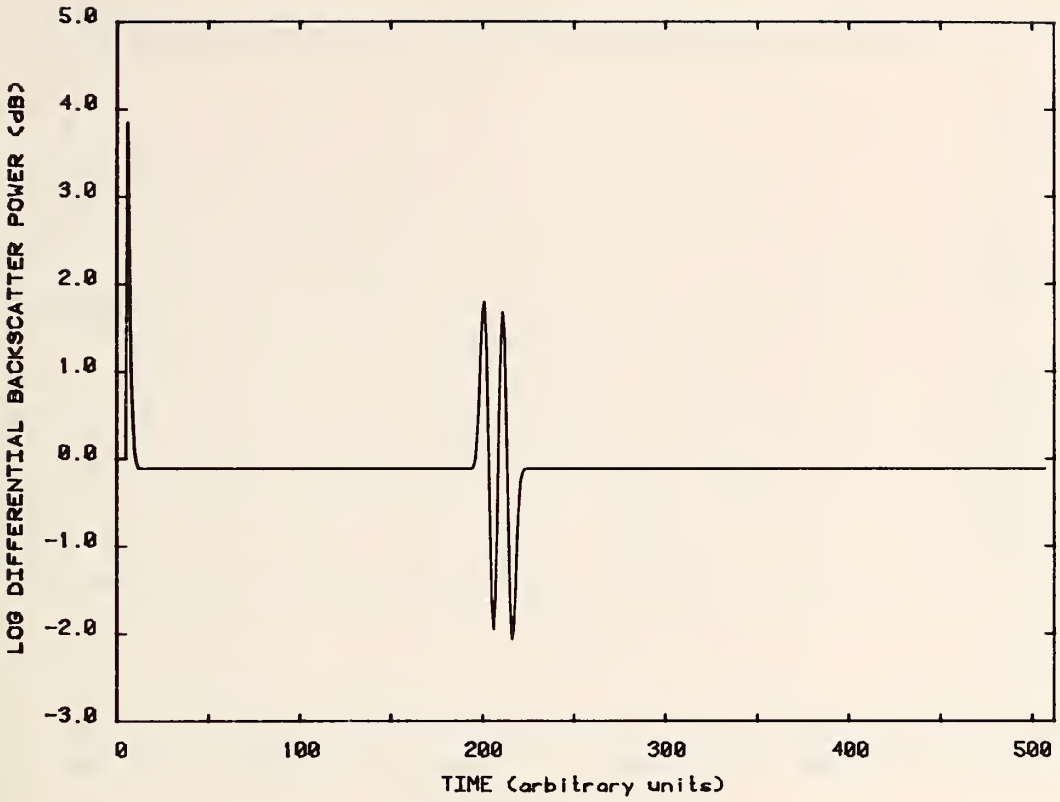

Figure 3-115. Scatter-like imperfections; Gaussian probe pulse; equivalent rectangular width 5 time units; delay 5 time units. Differential display.

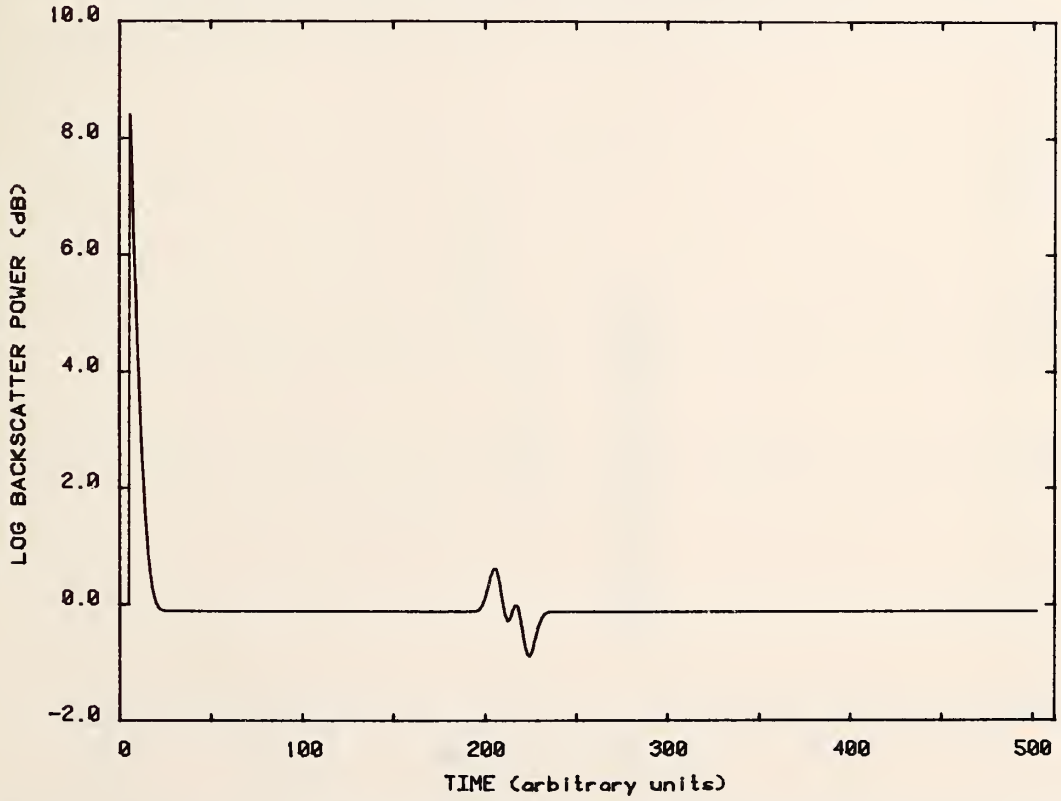

Figure 3-116. Scatter-like imperfections; Gaussian probe pulse; equivalent rectangular width; delay 5 time units. Differential display.

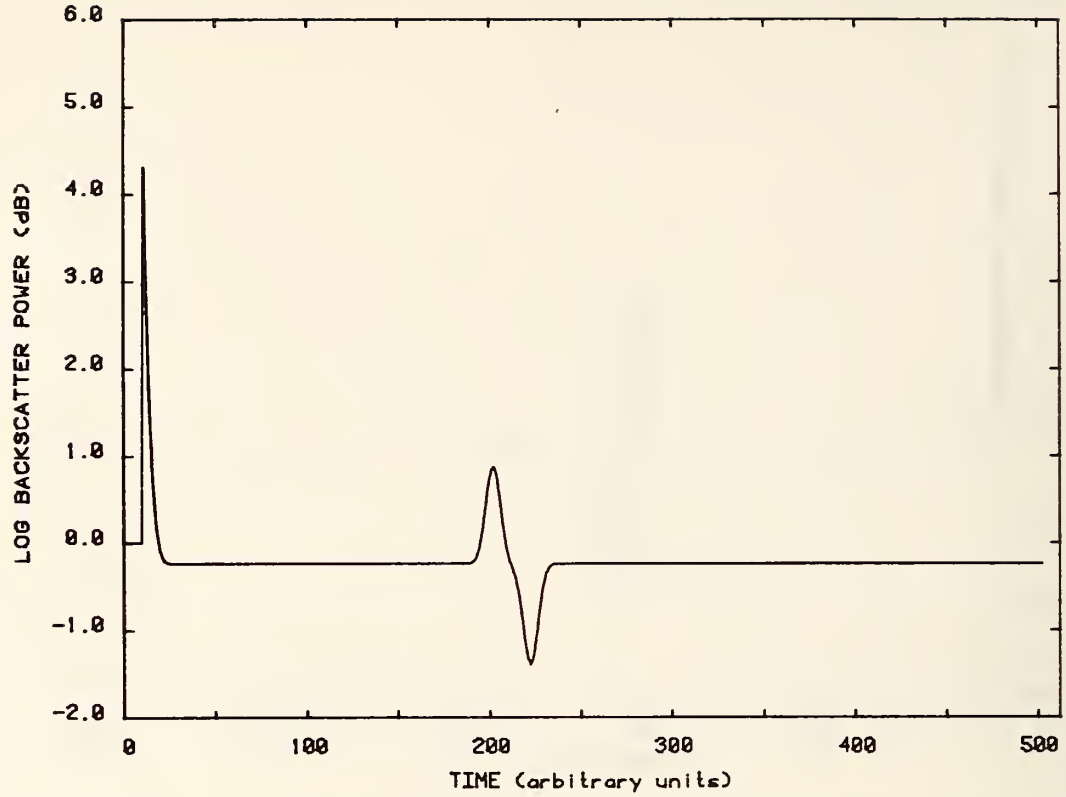

Figure 3-117. Scatter-like imperfections; Gaussian probe pulse; equivalent rectangular width 10 time units; delay 10 time units. Differential display.

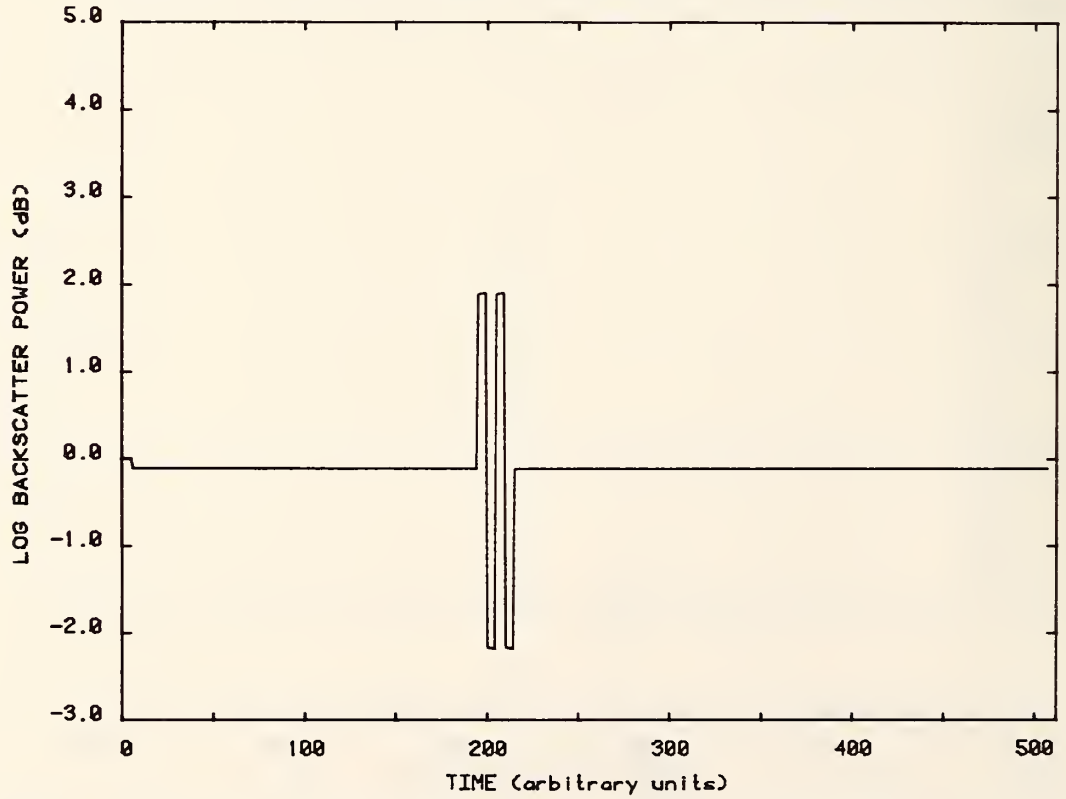

Figure 3-118. Scatter-like imperfections; rectangular probe pulse of width 5 time units; delay 5 time units. Differential display.

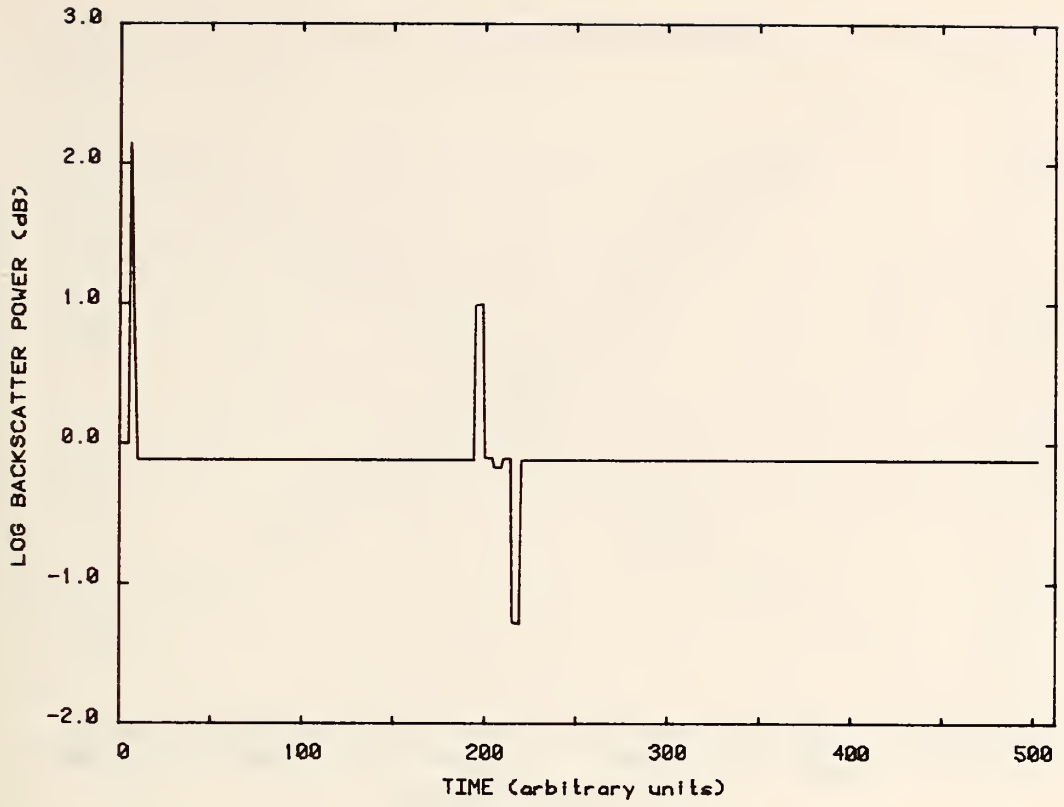

Figure 3-119. Scatter-like imperfections; rectangular probe pulse of width 10 time units; delay 5 time units. Differential display.

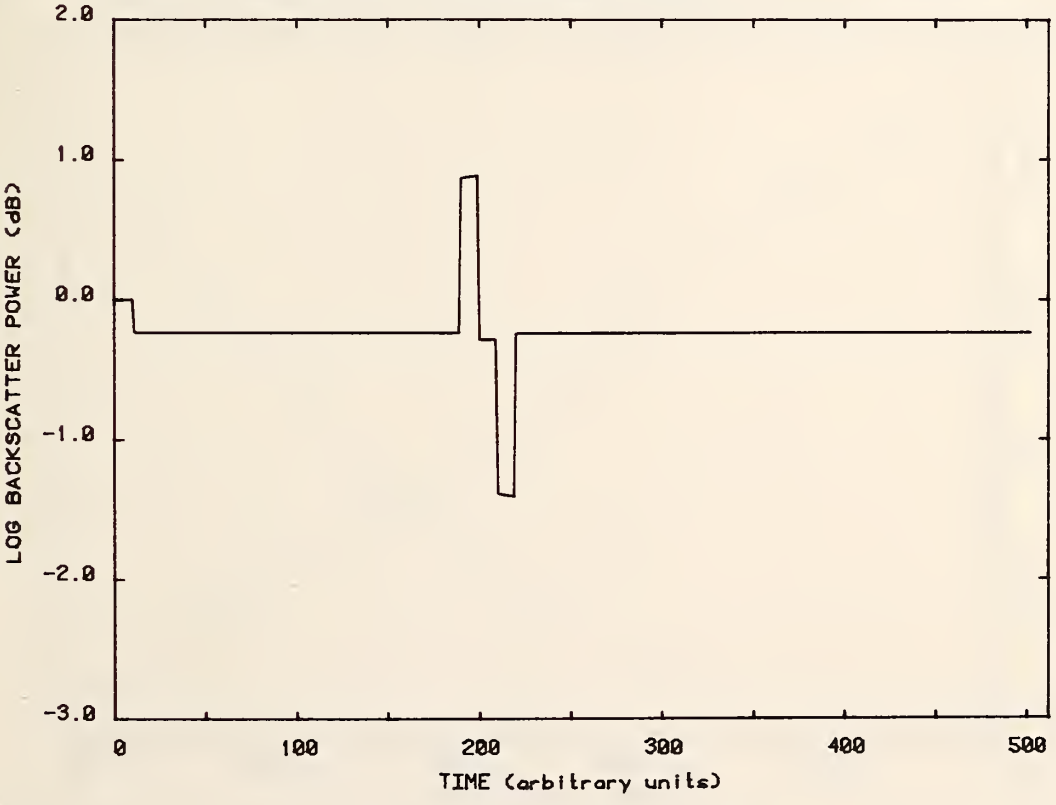

Figure 3-120. Scatter-like imperfections; rectangular probe pulse of width 10 time units; delay 10 time units. Differential display.

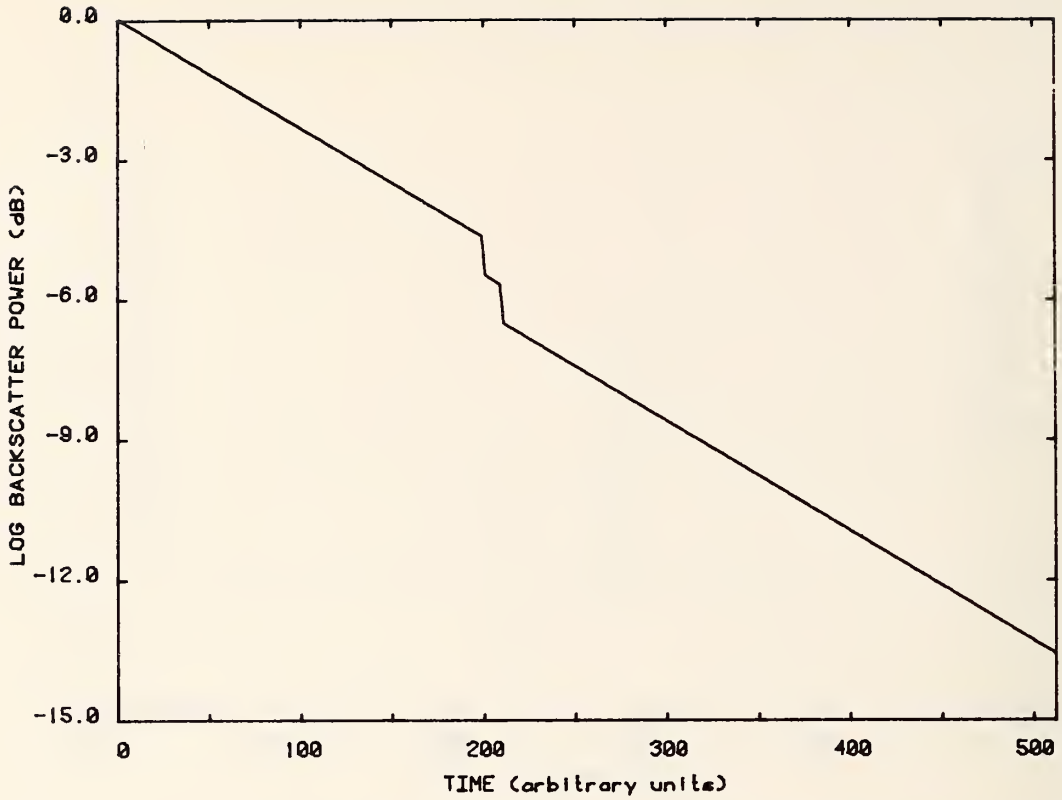

Figure 3-121. The impulse response for two absoption-like imperfections. Logarithmic display.

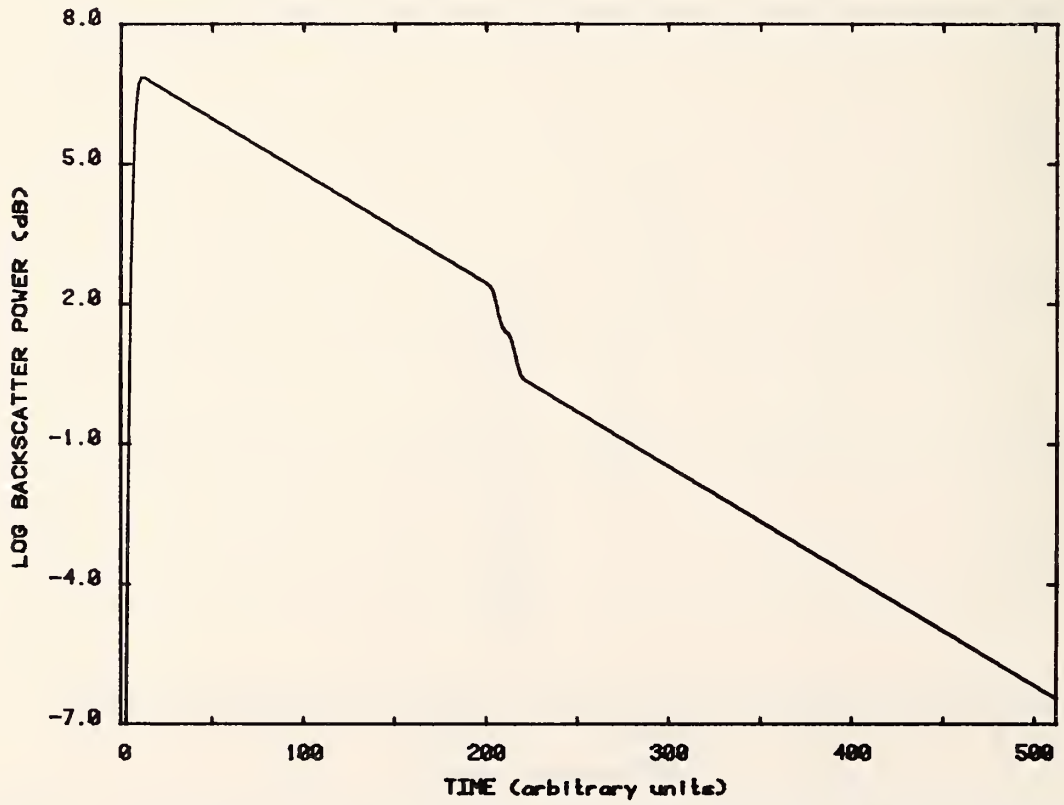

Figure 3-122. Absorption-like imperfections; Gaussian probe pulse; equivalent rectangular width 5 time units. Logarithmic display.

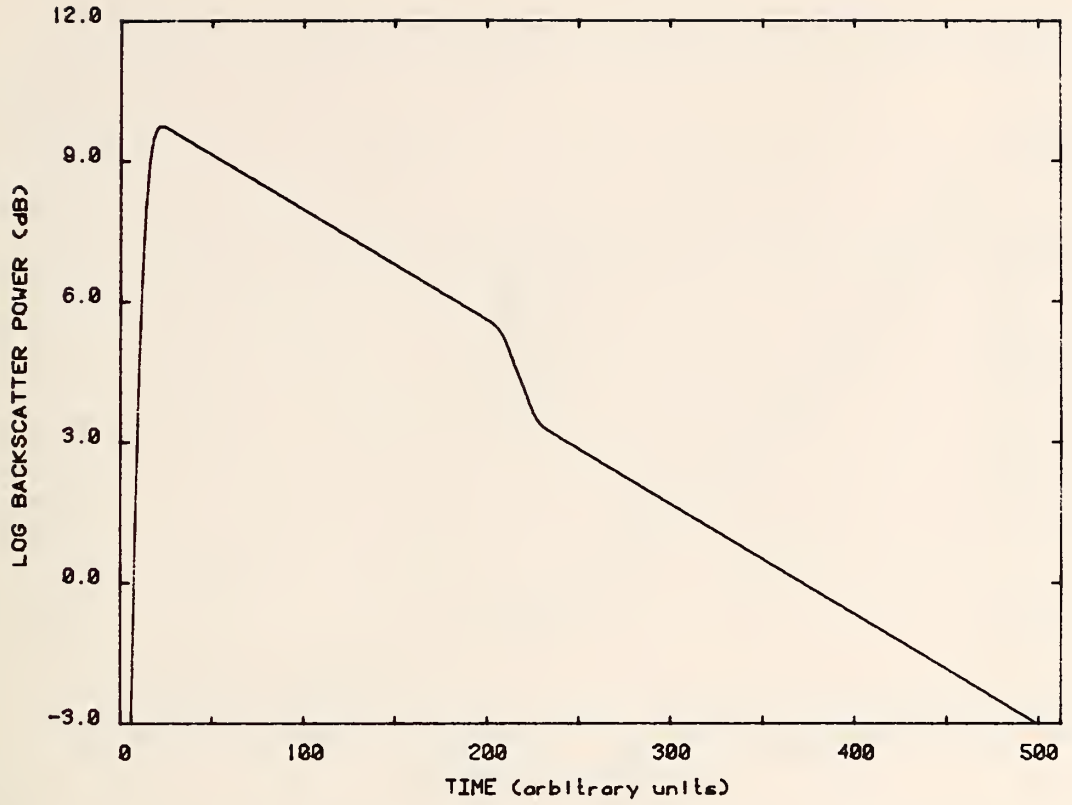

Figure 3-123. Absorption-like imperfections; Gaussian probe pulse; equivalent rectangular width 10 time units. Logarithmic display.

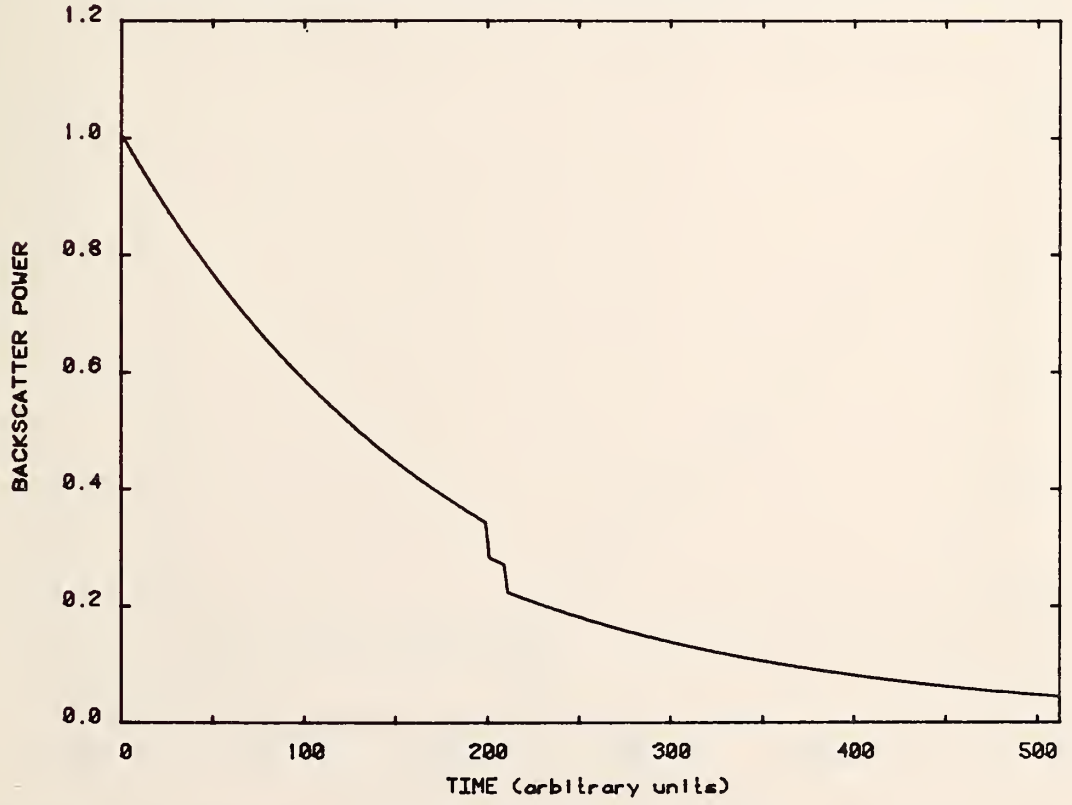

Figure 3-124. The impulse response for the two absorption-like imperfections. Liner display.

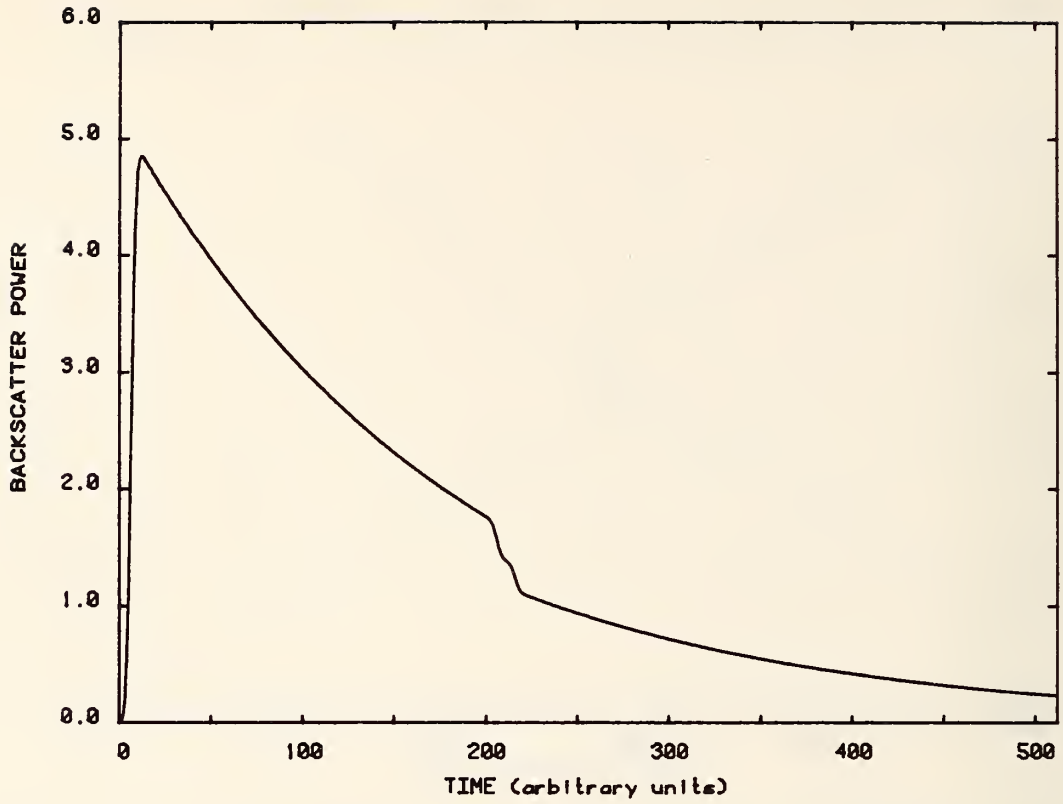

Figure 3-125. Absorption-like imperfections; Gaussian probe pulse; equivalent rectangular width 5 time units. Linear display.

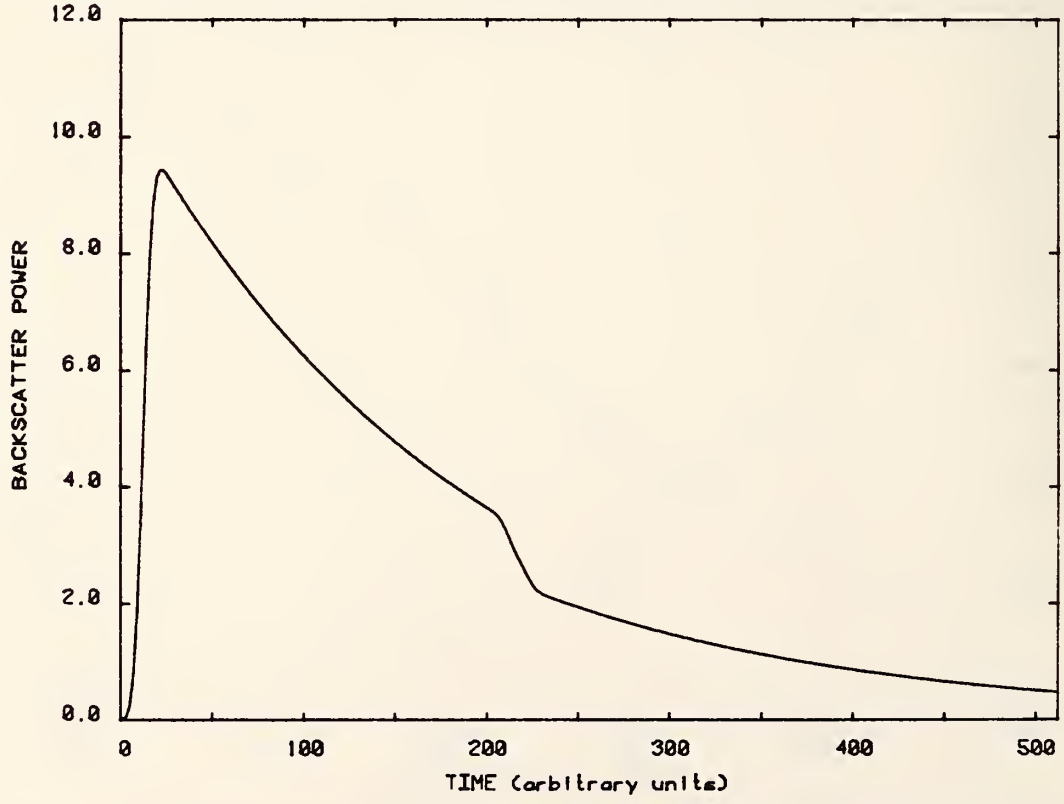

Figure 3-126. Absorption-like imperfections; Gaussian probe pulse; equivalent rectangular width 10 time units. Linear display.

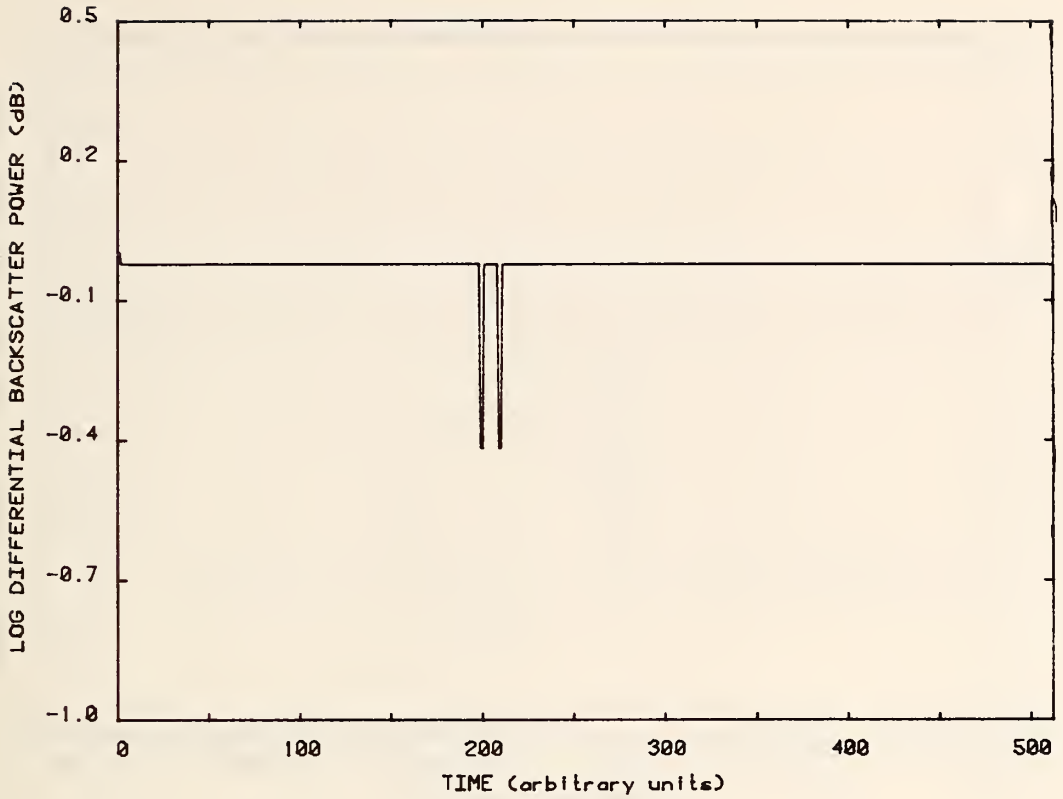

Figure 3-127. The impulse response for the two absorption-like imperfections; delay 1 time unit. Differential display.

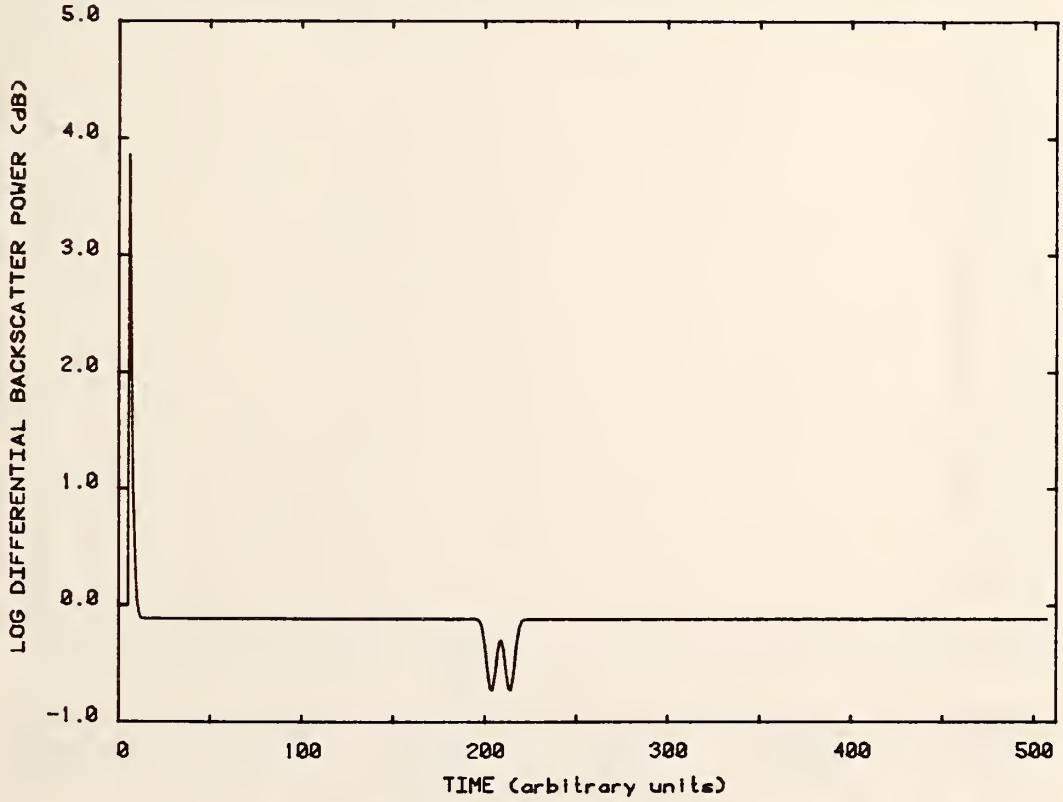

Figure 3-128. Absorption-like imperfections; Gaussian probe pulse; equivalent rectangular width 5 time units, delay 5 time units. Differential display.

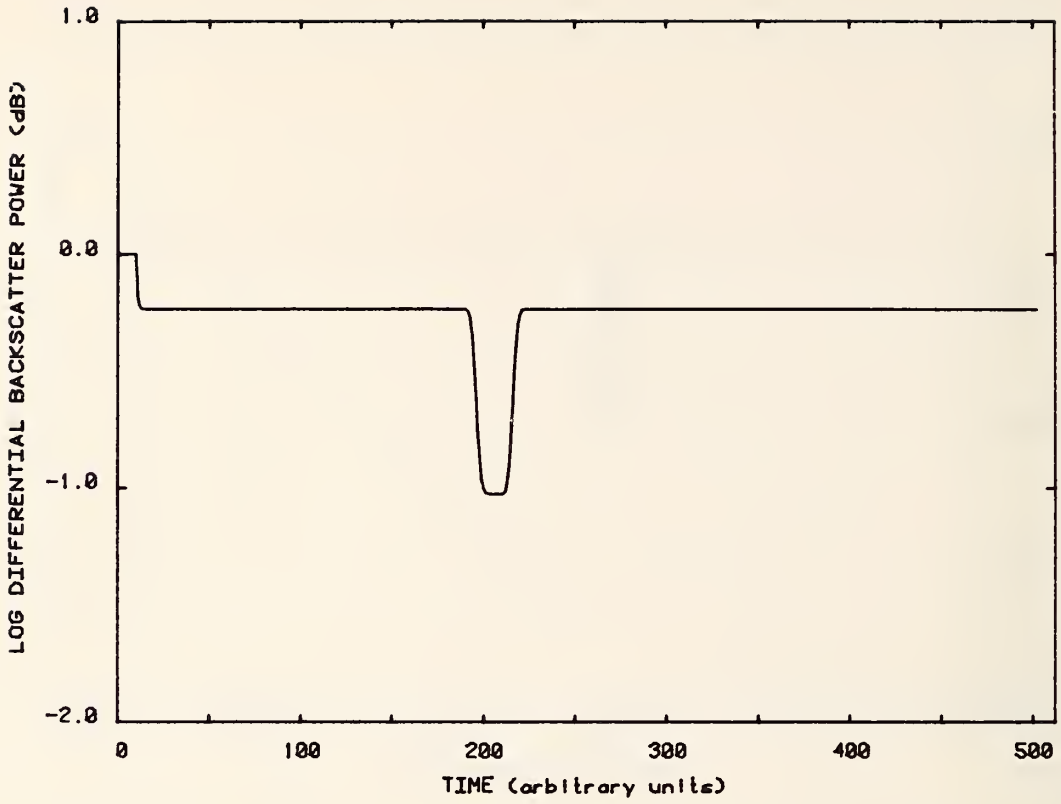

Figure 3-129. Absorption-like imperfections; Gaussian probe pulse; equivalent rectangular width 5 time units, delay 10 time units. Differential display.

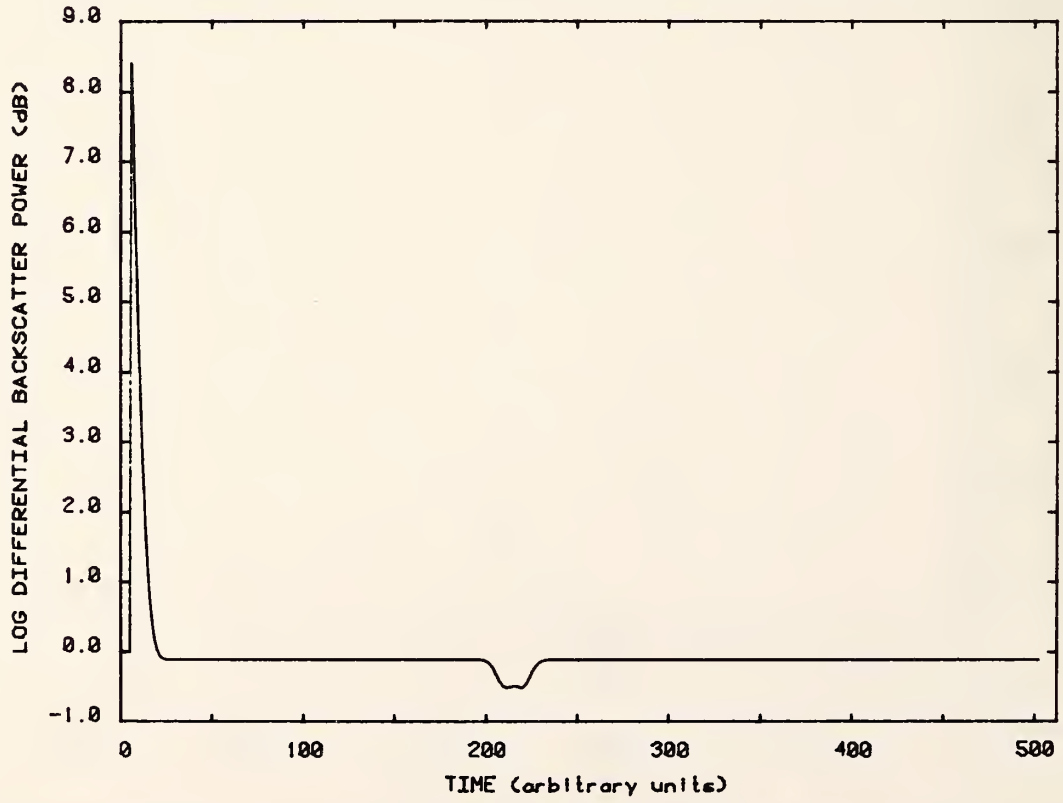

Figure 3-130. Absorption-like imperfections; Gaussian probe pulse; equivalent rectangular width 10 time units, delay 5 time units. Differential display.

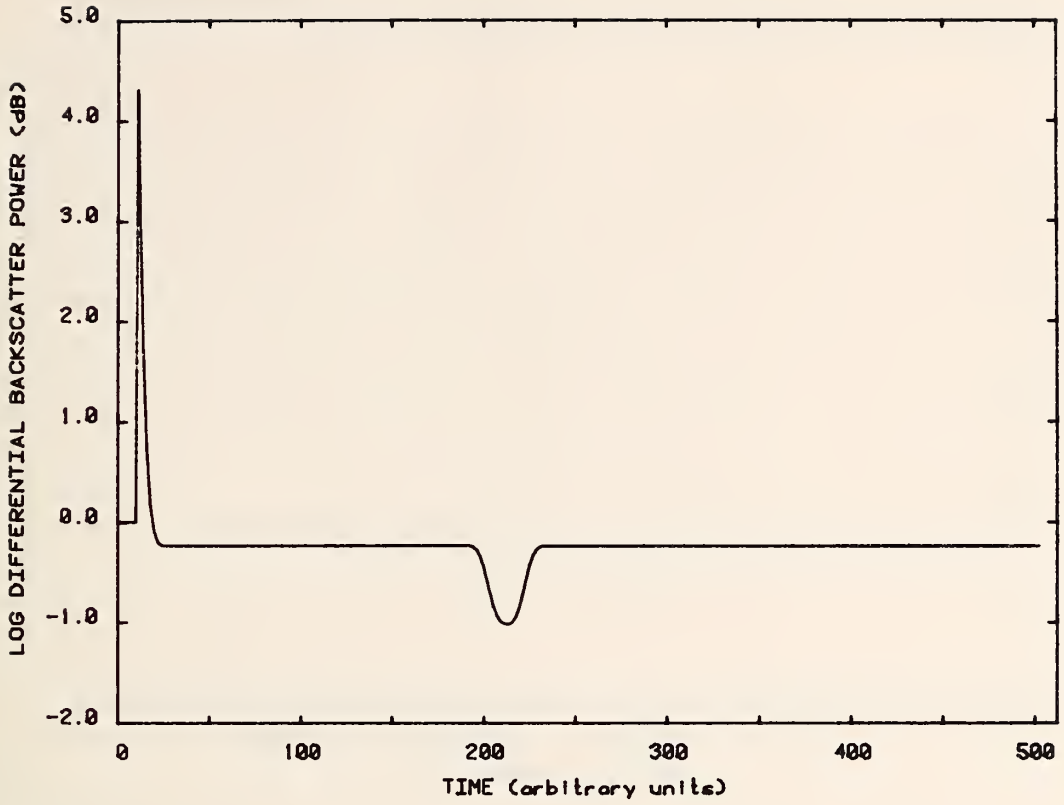

Figure 3-131. Absorption-like imperfections; Gaussian probe pulse; equivalent rectangular width 10 time units, delay 10 time units. Differential display.

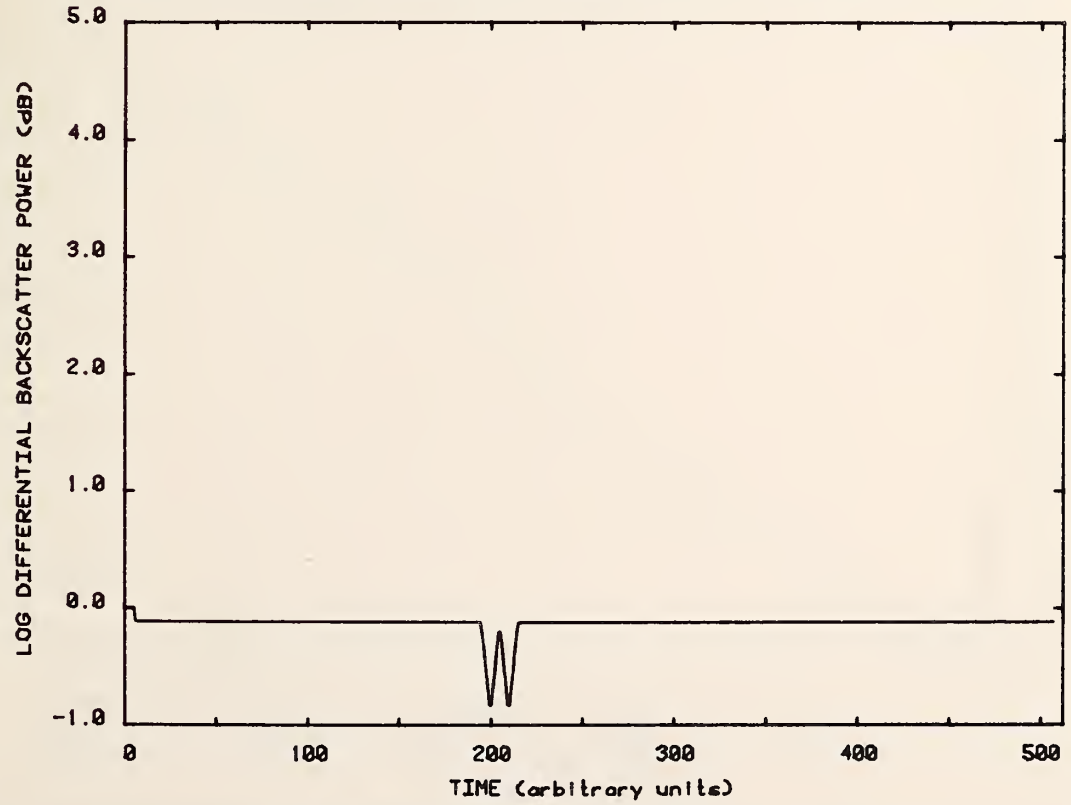

Figure 3-132. Absorption-like imperfections; rectangular probe pulse of width 5 time units; delay 5 time units. Differential display.

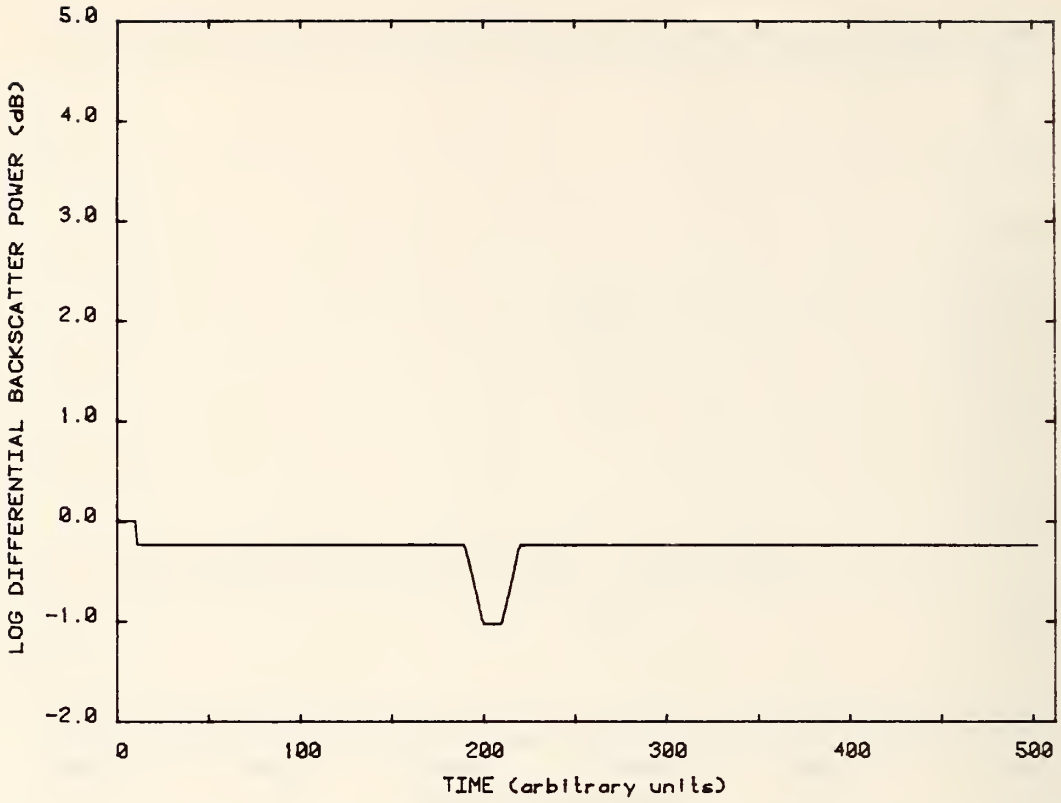

Figure 3-133. Absorption-like imperfections; rectangular probe pulse of width 5 time units; delay 10 time units. Differential display.

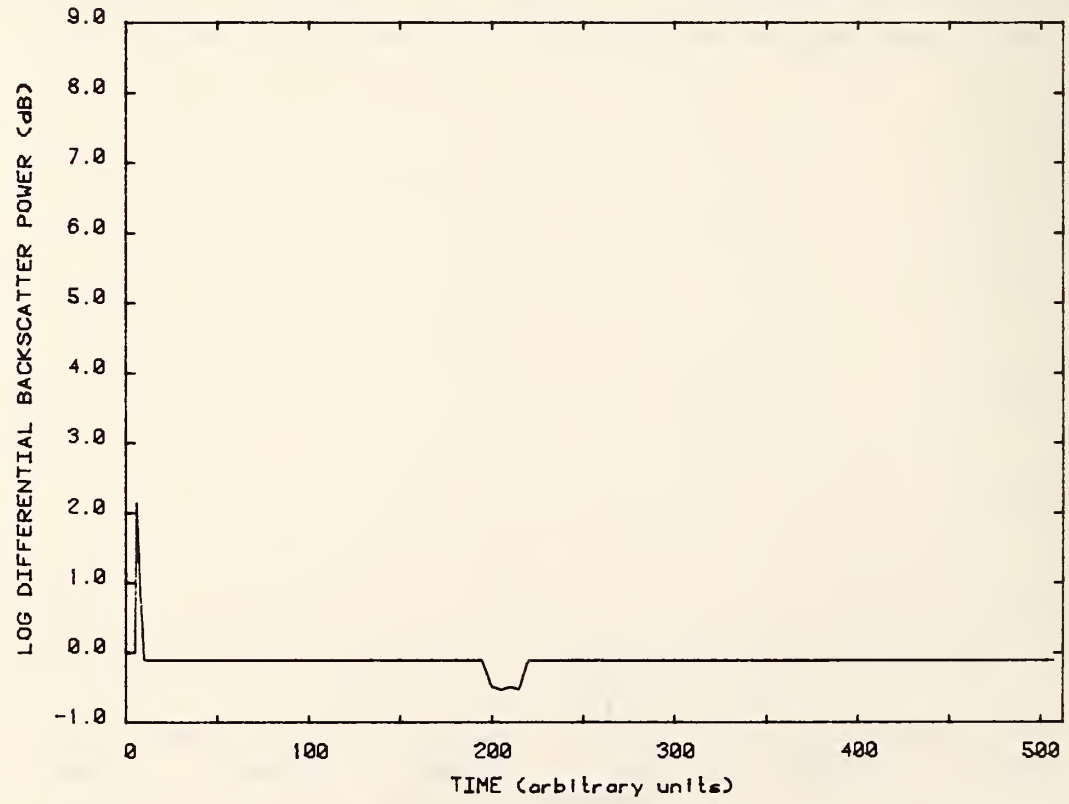

Figure 3-134. Absorption-like imperfections; rectangular probe pulse of width 10 time units; delay 5 time units. Differential display.

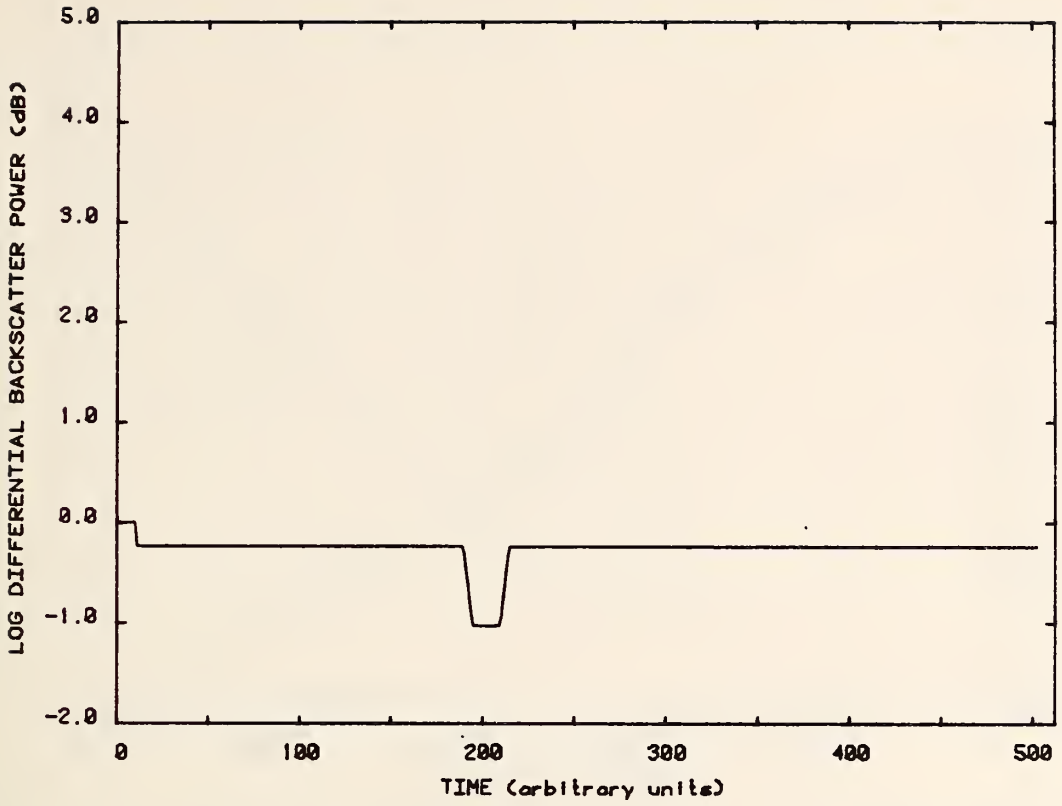

Figure 3-135. Absorption-like imperfections; rectangular probe pulse of width 10 time units; delay 10 time units. Differential display.

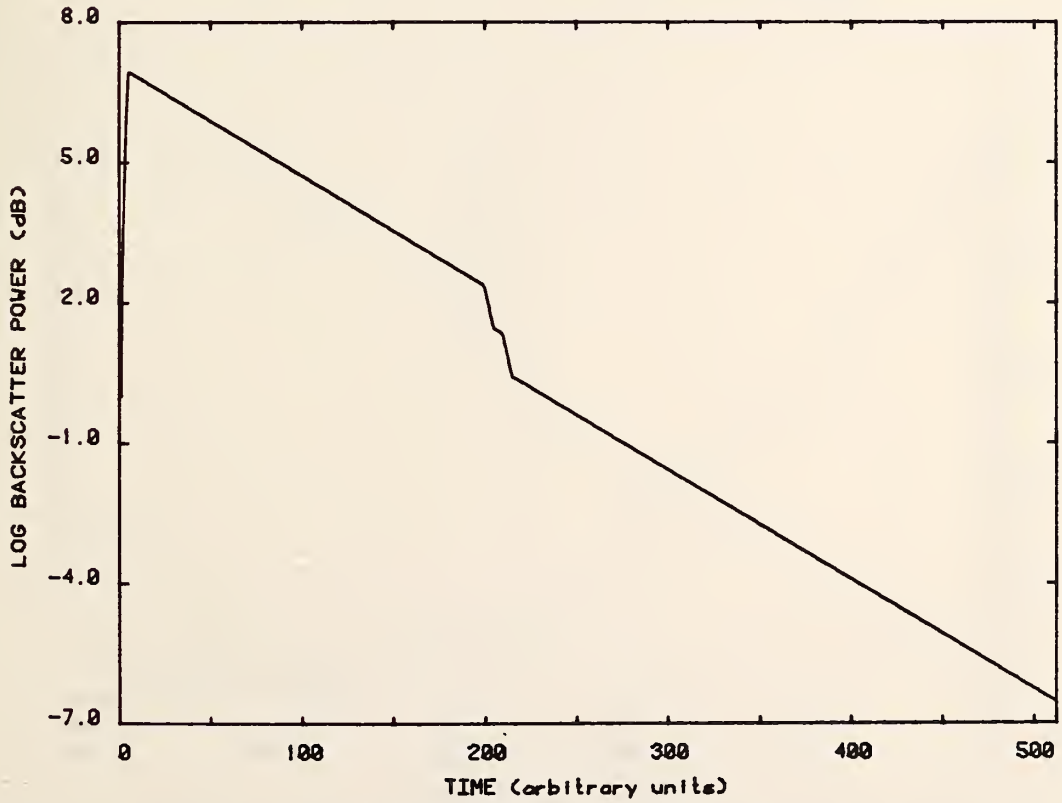

Figure 3-136. Absorption-like imperfections; rectangular probe pulse of width 5 time units. Logarithmic display.

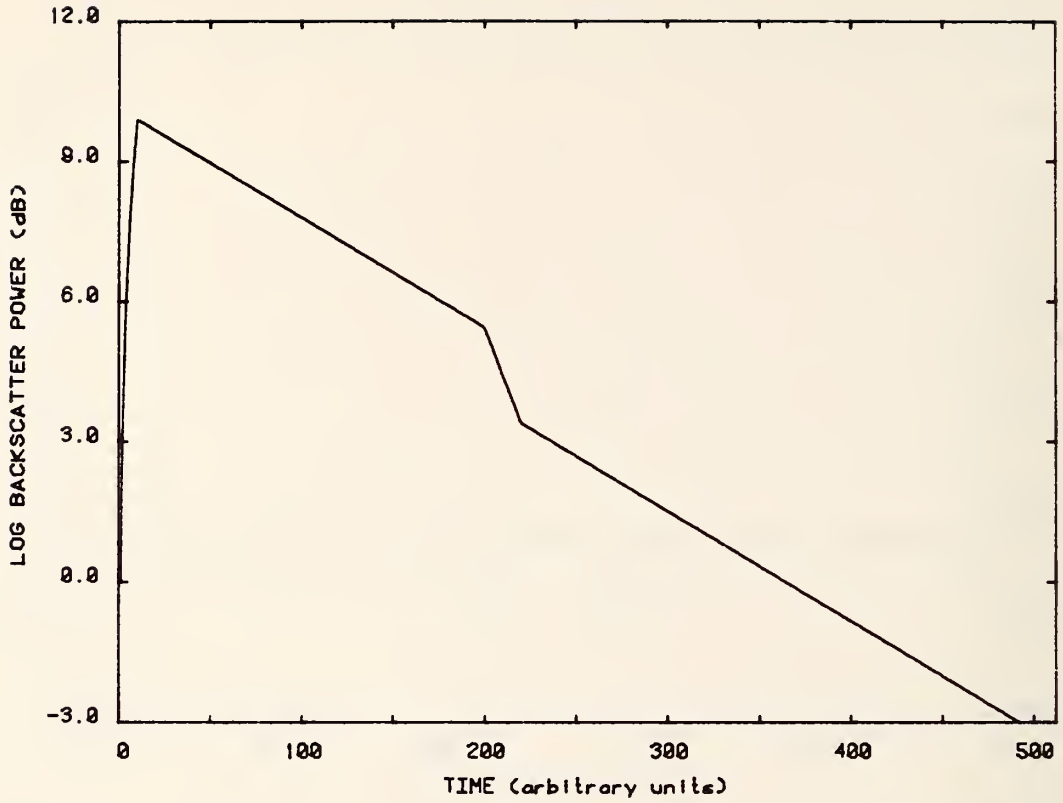

Figure 3-137. Absorption-like imperfections; rectangular probe pulse of width 10 time units. Logarithmic display.

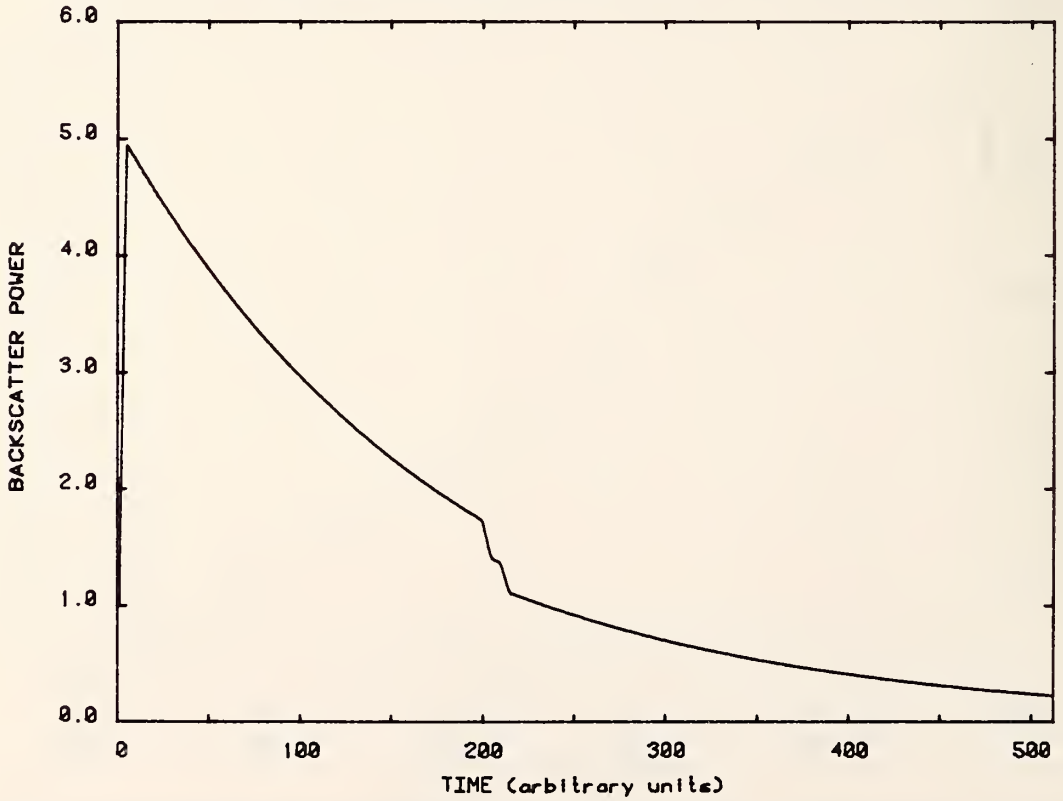

Figure 3-138. Absorption-like imperfections; rectangular probe pulse of width 5 time units. Linear display.

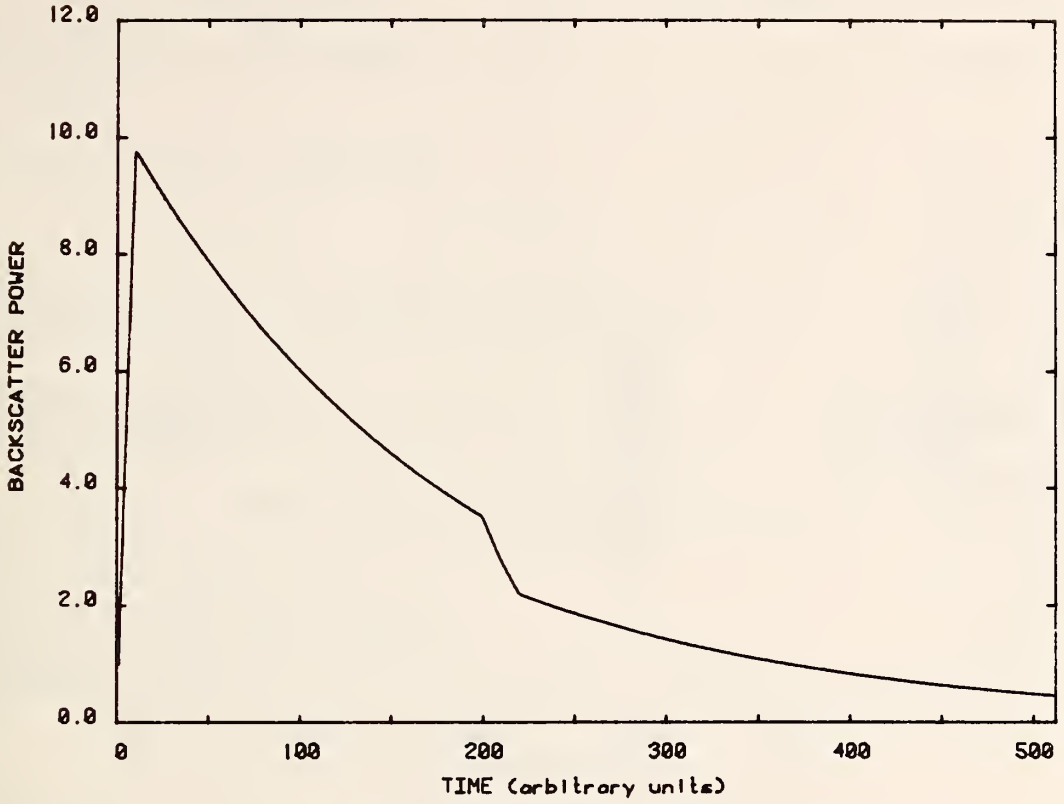

Figure 3-139. Absorption-like imperfections; rectangular probe pulse of width 10 time units. Linear display.

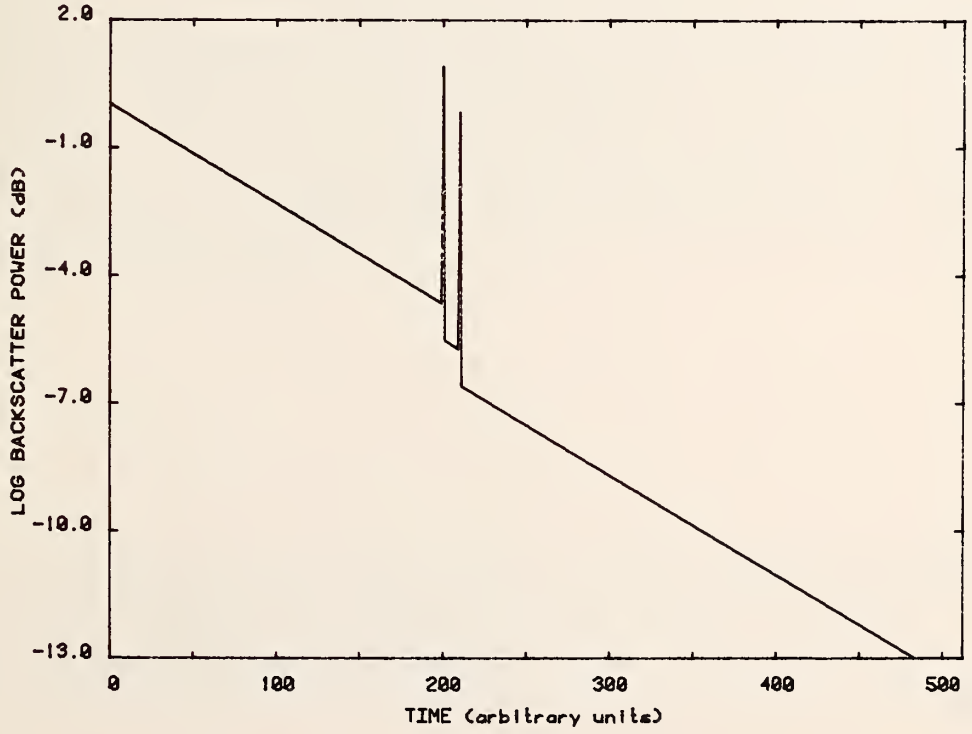

Figure 3-140. Impulse response of two composite imperfections separated by 100 time units. Logarithmic display.

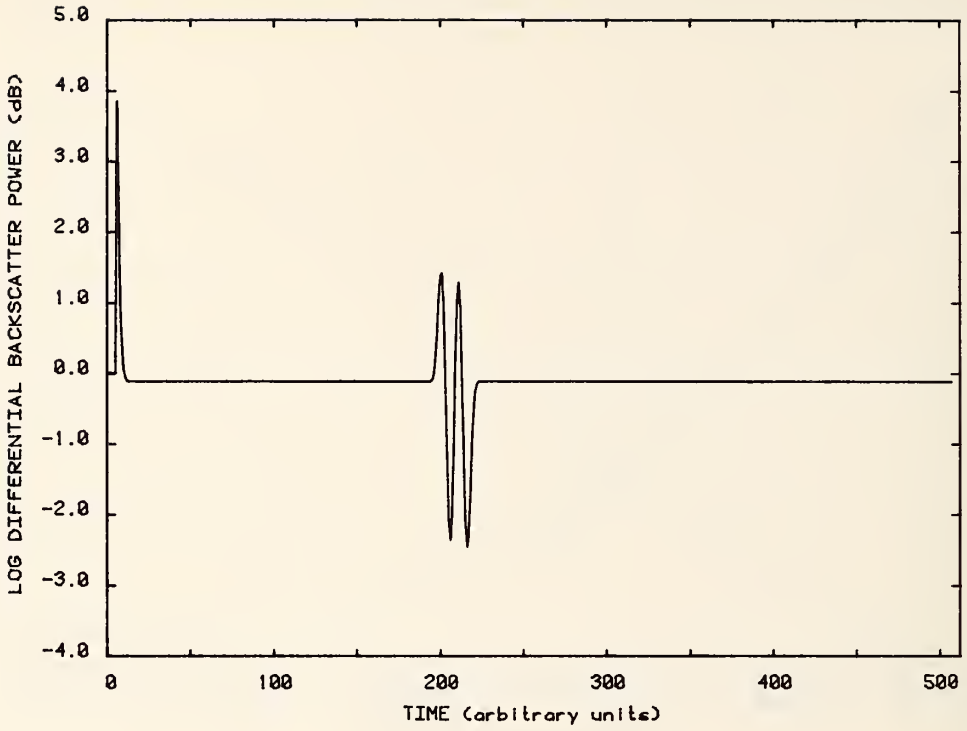

Figure 3-141. Composite imperfections; Gaussian probe pulse; equivalent rectangular width 5 time units, delay 5 time units. Differential display.

NBS-114A (REV. 2-8C)

U.S. DEPT. OF COMM. BIBLIOGRAPHIC DATA SHEET (See instructions)	1. PUBLICATION OR REPORT NO. NBS TN-1050	2. Performing Organ. Report No.	3. Publication Date December 1981

4. TITLE AND SUBTITLE

Backscatter Signature Simulations

5. AUTHOR(S)

B. L. Danielson

6. PERFORMING ORGANIZATION (If joint or other than NBS, see instructions)

NATIONAL BUREAU OF STANDARDS
DEPARTMENT OF COMMERCE
WASHINGTON, D.C. 20234

7. Contract/Grant No.

8. Type of Report & Period Covered
Final
10/1/80 - 10/1/81

9. SPONSORING ORGANIZATION NAME AND COMPLETE ADDRESS (Street, City, State, ZIP)

Communications Systems Center
U.S. Army Communications R&D Command
Fort Monmouth, New Jersey 07703

10. SUPPLEMENTARY NOTES

☐ Document describes a computer program; SF-185, FIPS Software Summary, is attached.

11. ABSTRACT (A 200-word or less factual summary of most significant information. If document includes a significant bibliography or literature survey, mention it here)

This report presents a collection of computer-generated backscatter signatures which represent realistic replicas of signals that can be encountered in optical time-domain reflectometer (OTDR) systems. Emphasis is placed on illustrating the appearance of backscatter signatures originating from localized and distributed imperfections which are superimposed on an otherwise uniform optical fiber. The details of these signatures are shown to be a function of the particular type of fiber perturbation, experimental parameters, and data reduction methods. This compilation of simulated responses is intended to facilitate the correct interpretation of OTDR signals as well as to point out sources of error which can arise in the characterization of optical fibers using backscatter techniques.

12. KEY WORDS (Six to twelve entries; alphabetical order; capitalize only proper names; and separate key words by semicolons)

backscattering; backscatter signatures; optical fiber scattering; optical time-domain reflectometer; OTDR

13. AVAILABILITY

☒ Unlimited
☐ For Official Distribution. Do Not Release to NTIS
☐ Order From Superintendent of Documents, U.S. Government Printing Office, Washington, D.C. 20402.
☒ Order From National Technical Information Service (NTIS), Springfield, VA. 22161

14. NO. OF PRINTED PAGES
100

15. Price
$9.50

USCOMM-DC 6043-P80

☆U.S. GOVERNMENT PRINTING OFFICE:1982—577-325 / 108

U.S. DEPARTMENT OF COMMERCE
National Bureau of Standards
Washington, D.C. 20234

OFFICIAL BUSINESS

Penalty for Private Use, $300

POSTAGE AND FEES PAID
U.S. DEPARTMENT OF COMMERCE
COM-215

SPECIAL FOURTH-CLASS RATE
BOOK